January 2013

Theoretical Studies of Co Based Catalysts on CO Hydrogenation and Oxidation

Nianthrini Balakrishnan
University of South Florida, nianthrini@gmail.com

Theoretical Studies of Co Based Catalysts on CO Hydrogenation and Oxidation

by

Nianthrini Balakrishnan

A dissertation submitted in partial fulfillment
of the requirements for the degree of
Doctor of Philosophy
Department of Chemical and Biomedical Engineering
College of Engineering
University of South Florida

Co-Major Professor: Babu Joseph, Ph.D.
Co-Major Professor: Venkat R. Bhethanabotla, Ph.D.
Vinay Gupta, Ph.D.
John Kuhn, Ph.D.
Srinivas Katkoori, Ph.D.
Ivan Oleynik, Ph.D.

Date of Approval:
April 4, 2013

Keywords: Density functional theory, Fischer Tropsch synthesis, promoted catalyst, deactivation, reaction mechanisms

DEDICATION

To my parents, brother and my husband.

ACKNOWLEDGMENTS

I would like to thank my advisors Dr. Babu Joseph and Dr. Venkat R. Bhethanabotla for their constant guidance, support and encouragement throughout my Ph.D. I would like to thank the committee members Dr. Vinay Gupta, Dr. John Kuhn, Dr. Srinivas Katkoori and Dr. Ivan Oleynik, and the Chair of my doctoral defense, Dr. Brian Space, for their valuable time and suggestions. I thank my labmates and friends: Pabitra, Sanchari, Bijith, Debosruti, Chita, Ali and Kassie for helping and supporting me during my research. I also extend my thanks to my family especially my husband for his patience. Finally, I would like to thank USF research computing, National Energy Research Scientific Computing Center and Extreme Science and Engineering Discovery Environment (formerly Teragrid) for their computing resources. I also acknowledge the funding from the Florida Energy Systems Consortium through the state of Florida and the department of Chemical Engineering at University of South Florida.

TABLE OF CONTENTS

LIST OF TABLES

LIST OF FIGURES

LIST OF SCHEMES

ABSTRACT

CO hydrogenation and CO oxidation are two important processes addressing the energy and environmental issues of great interest. Both processes are carried out using metallic catalysts. The objective of this dissertation is to study the catalytic processes that govern these two reactions from a molecular perspective using quantum mechanical calculations. Density Functional Theory (DFT) has proven to be a valuable tool to study adsorption, dissociation, chain growth, reaction pathways etc., on well-defined surfaces. DFT was used to study the CO reduction reactions on promoted cobalt catalyst surfaces and CO oxidation mechanisms on cobalt surfaces.

CO hydrogenation via Fischer-Tropsch Synthesis (FTS) is a process used to produce liquid fuels from synthesis gas. The economics of the Fischer-Tropsch process strongly depends on the performance of the catalyst used. The desired properties of a catalyst include selectivity towards middle distillate products such as diesel and jet fuel, higher activity and longer catalyst life. Catalysts are often modified by adding promoters to obtain these desirable properties. Promoters can influence the reaction pathways, reducibility, dispersion, activity and selectivity. In FTS, understanding the effect of promoters in the molecular scale would help in tailoring catalysts with higher activity and desired selectivity. Preventing deactivation of catalyst is important in FTS to increase the catalyst life. Deactivation of Co catalyst can occur by reoxidation, C deposition,

sintering, formation of cobalt-support compounds etc. Designing catalyst with resistance to deactivation by the use of promoters is explored in this dissertation. The influence of promoters on the initiation pathways of CO hydrogenation is also explored as a first step towards determining the selectivity of promoted catalyst.

The influence of Pt promoter on O removal from the surface of Co catalyst showed that Pt promoter reduced the activation barrier for the removal of O on both flat and stepped Co surfaces. An approximate kinetic model was developed and a volcano plot was established. The turn-over frequency (TOF) calculated based on the activation barriers showed that Pt promoted Co surface had a higher rate than unpromoted Co surface. The effect of Pt and Ru promoters on various pathways of C deposition on Co catalyst was studied to gain a mechanistic understanding. The promoters did not affect the subsurface C formation but they increased the barriers for C-C and C-C-C formation and also decreased the barriers for C-H formation. The promoters also influence the stabilities of C compounds on the Co surface suggesting that Pt and Ru promoters would decrease C deposition on Co catalysts. The effect of Pt promoter on unassisted and H-assisted CO activation pathways on Co catalyst was studied. Pt promoted Co surface followed H-assisted CO activation. Pt promoter decreased the activation barriers for CO activation pathways on Co catalyst thereby increasing the activity of Co catalyst.

CO oxidation is a process used to prevent poisoning of fuel cell catalysts and reduce pollution of the atmosphere through exhaust gases containing CO. Expensive catalysts like Pt are widely used for CO oxidation which significantly increases the cost of the process and hence it is necessary to search for alternative lower cost catalysts. Understanding the mechanism of a reaction is the first step towards designing better and

efficient catalyst. DFT is helpful in determining the basic mechanism and intermediates of reactions.

The mechanism of CO oxidation on CoO catalyst was explored. Four possible mechanisms for CO oxidation on CoO catalyst were studied to determine the most likely mechanism. The mechanism was found to be a two-step process with activation barrier for formation of CO_2 larger than the barrier for formation of the intermediate species.

CHAPTER 1:

INTRODUCTION

1.1. Motivation

1.1.1. CO Hydrogenation

The increased use of fossil fuels caused by population growth and industrialization has led to growing concern over greenhouse gas emissions and global warming effects. Biomass can be converted to liquid fuels by gasification to produce a mixture of CO and H_2 (syngas) followed by Fischer-Tropsch Synthesis (FTS). The process for converting syngas to liquids was developed by Franz Fischer and Hans Tropsch in the 1920s. It converts a mixture of CO and H_2 into long chain hydrocarbons suitable for liquid transportation fuels. The first four production plants were commissioned in Germany in 1936 with a production capacity of 200 000 tons per year. However, the discovery of oil reserves in 1950s declined the interest in FTS process. The energy crisis in 1970's and the limited oil reserves renewed the interest in FTS. The various reactions producing different products are given below:

$$\text{Paraffins: } (2n+1)\ H_2 + n\ CO \rightarrow C_nH_{2n+2} + n\ H_2O \quad (1.1)$$

$$\text{Olefins: } 2n\ H_2 + n\ CO \rightarrow C_nH_{2n} + n\ H_2O \quad (1.2)$$

$$\text{Alcohols: } 2n\ H_2 + n\ CO \rightarrow C_nH_{2n+1}\ OH \quad (1.3)$$

In addition, side reactions like WGS and Boudouard reactions could also occur.

$$\text{WGS reaction: } CO + H_2O \rightarrow CO_2 + H_2 \quad (1.4)$$

$$\text{Boudouard reaction: } 2CO \rightarrow C + CO_2 \quad (1.5)$$

FTS process is operated at temperatures ranging from 150-300 °C. Higher temperature leads to higher conversion and favors methane formation and higher pressures leads to higher conversion and favors the formation of long chained alkanes. Metal catalysts such as cobalt, iron and ruthenium have been found to be most suitable for CO hydrogenation.[1] Fe and Co are the catalysts of choice in industrial applications based on activity and cost. Cobalt-based catalysts exhibit high activity, high yields of long-chain paraffins, and low activity for the competing water gas shift reaction compared to Fe catalysts.

Activity is influenced by surface-ligand effect (modification of electronic structure on the surface caused by promoters) and lattice strain effect (modification caused by introduction of promoter atoms to the lattice).[2-5] Though the structure sensitivity of Co surfaces has been investigated,[6-7] the structure sensitivity of the promotional effect has not been accounted. Two types of promotional effects are observed, namely structural promotion and textural promotion.[8] Structural promoters increase the amount of active sites in promoted catalysts and textural promoters change the intrinsic properties of surface sites mainly by modifying electronic properties of the surface.

Heterogeneous catalysis involves adsorption of the reactants to the catalytic surface, reaction and desorption from the surface. The catalyst should bind the adsorbates strong enough that the reactants stick to the catalyst surface yet weak enough to form the products. Catalysts help by changing the kinetics of the reaction, thereby allowing the reaction to take place at milder conditions compared to the reaction in the absence of a catalyst. Thus, binding energy plays an important role in catalysis. Addition of promoters change the binding energy of the reactants and hence adding the right promoter can yield a catalyst with higher activity.

1.1.2. CO Oxidation

CO oxidation is a process to reduce the emission of toxic CO gas from automobile exhaust and also to prevent poisoning of fuel cell catalysts.[9-13] CO oxidation is often used as a probe reaction to study catalysis.[14-15] CO oxidation reaction involves CO adsorption, O_2 adsorption/dissociation, reaction between CO and O_2 (or dissociated O) and desorption of CO_2. [16-18] Commonly used catalysts for this reaction are noble metals like Pt, Ru, Rh, Pd, etc. Recent studies indicate these catalysts oxidize under O_2 rich atmosphere.[19-20] These oxidized catalyst had lower barriers for CO oxidation compared to their unoxidized form thereby increasing the catalyst activity which was attributed to the surface geometric effect.[21] The fundamental step in catalysis is to understand the reaction mechanism at the molecular level.

1.2. Objectives

The aim of this research is to explore CO oxidation and reduction mechanisms on Co based catalysts using Density Functional Theory (DFT) based modeling tools. Due to

the complex nature of the reaction mechanisms in heterogeneous systems, experimental studies alone are not sufficient to understand reaction mechanisms. Quantum chemical calculations can be used to yield crucial insights into the nature of active sites and individual reaction steps during the reaction. DFT studies have been successfully used to identify and screen catalysts for various applications.[22-26] There is a good agreement between theoretical results and experiments.[22, 24-26]

The specific objectives of this doctoral research are the following:

i. Investigate the role of Pt promoter on the oxygen removal from cobalt surfaces during FTS reaction. It has been experimentally suggested that Pt assists in the removal of O through water formation. [27-28] The main objective here is to determine if Pt present as a promoter lowers the activation barrier for the removal of O from Co surface.

ii. Study the effect of Ru and Pt promoters on the deactivation of Co catalyst during FTS reactions. Catalyst life is shortened due to deactivation caused by carbidization. Certain promoters modify the properties of catalyst making them less prone to C deposition. The goal is to check if Ru and Pt as promoters aid in preventing the deactivation of CO catalyst due to carbidization.

iii. Study the influence of Pt promoter on CO activation pathways of Co catalysts during FTS. The aim is to determine if Pt promoters lower the activation barriers for CO activation thereby increasing the catalyst activity as suggested by previous experimental studies.

iv. Study the CO oxidation reaction mechanism on CoO catalysts. The goal is to explain observed experimental data from in-situ surface reaction studies of Mankidy[29] that CO oxidation on CoO catalyst is a 2-step process.

The reaction pathways and activation energies were calculated using Climbing Image Nudged Elastic Band (CI-NEB) as implemented in VASP (Vienna Ab Initio Simulation package) [30-32] code. A reaction pathway with the lowest activation energy was calculated. A kinetic model was established to determine the activity or the reaction mechanism will be established. The schematic representation of the approach used is given in Figure 1.1.

1.3. Significance of the Work

1.3.1. CO Hydrogenation

Desired catalyst properties for FTS include better catalyst life, higher activity and better selectivity. Deactivation of catalysts can occur by reoxidation, C deposition, sintering, formation of support-catalyst compounds and poisons. Deactivation can render the catalyst inactive by blocking the active sites. Introduction of promoters to the catalyst surface can alter the catalyst surface to resist deactivation thereby increasing the catalyst life. Promoters can also influence the activity and selectivity of catalyst by changing the activation barriers or/and reaction pathways. DFT can be used to study various pathways for deactivation of catalyst which would be rather difficult and time consuming using experiments. This dissertation discusses in detail the influence of Pt or/and Ru promoters on deactivation (reoxidation, C deposition) and activity (CO activation pathways) on Co catalyst. The effect of promoter on activation barriers of each reaction that can contribute

to O removal, C deposition and CO activation was explored to assess if adding a particular promoter would decrease the deactivation and increase the activity of catalyst. Modifying a catalyst to have decreased deactivation rate and increased activity would be the first step towards the design of better catalyst.

1.3.2. CO Oxidation

Alternatives for the expensive Pt catalyst are being explored to reduce the cost of catalyst used for CO oxidation. CoO catalyst were explored to determine the reaction mechanism and activation barrier for CO oxidation. It is difficult to determine the reaction mechanism and intermediates using experiments due to the complexity of the reaction, efficiency of equipment used and time consumption. DFT can identify the intermediates in a reaction and elucidate the reaction mechanism. The activation barriers can then be used to assess the feasibility of catalyst for CO oxidation.

1.4. Outline of the Dissertation

This proposal is organized as follows:

- Chapter 2 describes the methods and techniques used in our DFT studies including a brief overview of DFT.
- Chapter 3 discusses the effect of Pt promoter for the reduction of Co catalyst using DFT.
- Chapter 4 describes the effect of Pt and Ru promoter on deactivation due to C deposition on Co catalyst using DFT.
- Chapter 5 discusses the effect of Pt promoter on CO activation pathways of Co catalyst using DFT.

- Chapter 6 discusses the mechanism behind CO oxidation reaction on CoO catalyst using DFT.
- Chapter 7 summarizes the research and describes the future work.

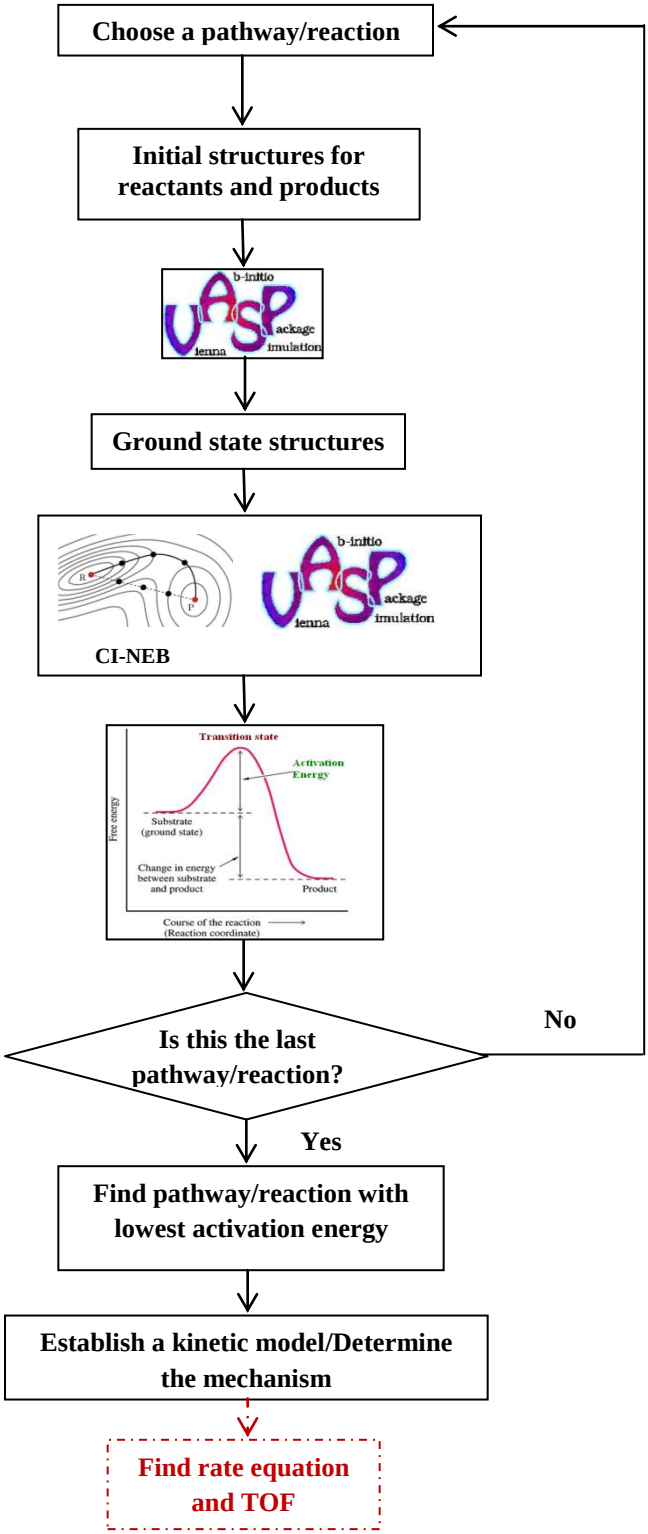

Figure 1.1. Schematic to represent the approach used

CHAPTER 2:

METHODS

In this chapter, the basics of DFT are first discussed. Then the software used for these calculations and other methods used such as CI-NEB and Bader analysis are explained.

2.1. Density Functional Theory

DFT is used to investigate the electronic structure of many-body systems. The Hamiltonian for system of electrons and nuclei is,

$$\hat{H} = -\frac{\hbar^2}{2m_e}\sum_i \nabla_i^2 - \sum_{i,I}\frac{Z_I e^2}{|r_i - R_I|} + \frac{1}{2}\sum_{i\neq j}\frac{e^2}{|r_i - r_j|} - \sum_I \frac{\hbar^2}{2M_I}\nabla_I^2 + \frac{1}{2}\sum_{I\neq J}\frac{Z_I Z_J e^2}{|R_I - R_J|} \quad (2.1)$$

where the first term is the kinetic energy of the electrons, second term is the potential energy arising from electron-nuclei coulombic attraction, third term is the potential energy from nuclei-nuclei coulombic repulsions, fourth term is the kinetic energy of the nuclei and the last term is the potential energy from electron-electron coulombic repulsions.

Hohenberg and Kohn[33] in 1964 proved that the properties of the ground state can be determined from the ground state electron density but did not provide a guidance to compute the ground state density. Kohn and Sham[34] in 1965 provided a way to calculate

the ground state density by solving a set of equations involving a single electron. The difficult many-body terms are incorporated into an exchange-correlation function which is approximated using local density approximation (LDA)[35] and various generalized gradient approximations (GGA).[36] LDA uses the exchange-correlation potential of an electron gas with the electron density at that point. But LDA does not solve the exact Schrodinger equation as the exchange-correlation function is not truly represented by this approximation. GGA uses both the local electron density as well as the gradient of electron density to represent the functional. Perdew-Wang functional (PW91)[36] and Perdew-Burke-Ernzerhof functional (PBE)[37] are the commonly used functionals under GGA.

2.1.1. Thomas-Fermi-Dirac Approximation

A semiclassical model was introduced by Thomas[38] and Fermi[39] in 1927 based on electron density. This model was based on an approximate functional for kinetic energy of a homogeneous gas with density equal to that of density at a point. The exchange and correlation energy was neglected in this formulation. The approximation for exchange energy was included by Dirac.[40]

The energy functional is given by

$$E_{TF}[n] = C_1 \int d^3r\, n(r)^{\left[\frac{5}{3}\right]} + \int d^3r\, V_{ext}(r)n(r) + C_2 \int d^3r\, n(r)^{\left[\frac{4}{3}\right]} + \frac{1}{2}\int d^3r\; d^3r'\; \frac{n(r)n(r')}{|r-r'|} \qquad (2.2)$$

where the first term is the kinetic energy approximation, second term is the external potential, third is the local exchange and the last term is the Hartree energy. This model uses crude approximations and hence does not provide a good description of electrons. The ground state energy and density can then be found by the minimization of the functional with the following constraint on the number of electrons

$$\int d^3r\, n(r) = N. \tag{2.3}$$

2.1.2. Hohenberg-Kohn Theorem

This formulation applies to any system under the influence of an external potential including any system of electrons and fixed nuclei. The Hamiltonian is given by

$$\hat{\mathrm{H}} = -\frac{\hbar^2}{2m_e}\sum_i \nabla_i^2 + \sum_i V_{ext}(r_i) + \frac{1}{2}\sum_{i\neq j}\frac{e^2}{|r_i - r_j|} \tag{2.4}$$

There are two theorems established by Hohenberg and Kohn[33]. They are,

i. Ground state density of a particle $n_o(r)$ uniquely defines the external potential $V_{ext}(r)$ under the influence of which the particle is present. Hence, the Hamiltonian and the many-body wavefunction for all the states are determined. All the properties of a particle can then be found from the knowledge of ground state density $n_o(r)$.

ii. Given an external potential, the density n(r) which minimizes the energy of the functional is the exact ground state density $n_o(r)$ and the energy corresponding to that ground state energy is the ground state energy.

The ground state energy and the ground state properties can be determined from this theorem but the properties or energy of excited states cannot be found.

2.1.3. Self-Consistent Kohn-Sham Equation

Kohn-Sham[34] equation was formulated to replace the many-body system with a system that can be solved easily. The Kohn-Sham ansatz assumes the ground state density of the original interacting system to be equal to that of some non-interacting system which can be exactly solved. All the difficult many-body terms are included in the exchange and correlation functional of the density and thus the accuracy of the ground state energy and density of the original system depends on the exchange and correlation approximations.

This ansatz is based on two assumptions, namely:

i. The ground state density of the auxiliary system of non-interacting particles represents the exact ground state density.
ii. The auxiliary Hamiltonian is assumed to have a kinetic energy and an effective potential $V_{eff}^{\sigma}(r)$ acting on an electron of spin σ at point r and thus is spin dependent however, the external potential $\hat{V}_{ext}$ is spin independent.

The ground state energy functional according to Kohn-Sham approach is given by,

$$E_{KS} = T_s[n] + \int drV_{ext}(r)n(r) + E_{Hartree}[n] + E_{11} + E_{xc}[n]. \qquad (2.5)$$

where T is the kinetic energy, $V_{ext}(r)$ is the external potential due to the nuclei and any other external fields (assumed to be independent of spin), $E_{Hartree}$ is the Hartree energy, E_{11} is the interaction between the nuclei and E_{xc} is the exchange correlation energy.

2.1.4. Exchange and Correlations Functionals Approximations

The exchange and correlation can be assumed to be a local or nearly local functional of the density and is expressed as

$$E_{xc}[n] = \int dr\, n(r)\epsilon_{xc}([n], r) \tag{2.6}$$

where $\varepsilon_{xc}([n], r)$ is the energy per electron at point that depends only upon the density *n*(r, σ) in some neighborhood point of r. In LDA, the exchange energy of the homogeneous gas is given by a simple analytic form,

$$\epsilon_x^\sigma = \frac{E_x^\sigma}{N^\sigma} = -\frac{3}{4\pi} k_F^\sigma = -\frac{3}{4}\left(\frac{6}{\pi} n^\sigma\right)^{\frac{1}{3}} \tag{2.7}$$

and the correlation energy is calculated using Monte Carlo methods.[41-42] This approximation is the most accurate for solids close to a homogeneous gas and inaccurate for inhomogeneous systems. Improved functionals like GGA were then developed which were accurate for many systems and has improved agreement with experiments. GGA functional is given by,

$$E_{xc}^{GGA}[n^\uparrow, n^\downarrow =$$
$$\int d^3r\, n(r)\epsilon_{xc}\left(n^\uparrow, n^\downarrow, \left|\nabla n^\uparrow\right|, \left|\nabla n^\downarrow\right|, \ldots.\right) \equiv$$
$$\int d^3r\, n(r)\epsilon_x^{hom}(n) F_{xc}\left(n^\uparrow, n^\downarrow, \left|\nabla n^\uparrow\right|, \left|\nabla n^\downarrow\right|, \ldots.\right) \tag{2.8}$$

where, F_{xc} is dimensionless and $\epsilon_x^{hom}(n)$ is the exchange energy of the unpolarized gas. Widely used forms of GGA are Becke (B88),[43] Perdew and Wang (PW91)[36] and Perdew, Burke and Enzerhof (PBE).[37] Correlation is treated using the Lee-Yang-Parr (LYP)[44] functional derived for He atom and extended to atoms with more electrons.

2.1.5. Pseudopotentials and Projector Augmented Wave Method

The chemical bonding and other physical characteristics of the materials are not influenced by the core electrons but are dominated by the valence electrons. Pseudopotentials replace the coulombic potential of the nucleus and the effects of tightly bound core electrons by an effective ionic potential acting on the valence electrons.[45-46] This reduces the computational cost as the number of plane waves in a calculation is reduced. Pseudopotentials with low cutoff energy are soft and those requiring higher cutoff energy are hard. Further ultrasoft pseudopotentials (US-PP)[47] were developed which required even lower cutoff energies. US-PP is expressed as a sum of a smooth part and rapidly varying function localized around each ion core.

Projector augmented wave (PAW)[48] method was introduced to overcome the disadvantage of empirical parameters to be specified for US-PP. PAW potentials represent the entire set of all-electron core functions along with smooth parts of valence functions. However, the matrix elements involving the core functions are treated using muffin-tin spheres in addition to maintaining the ease of calculation of pseudopotentials. PAW method gives reliable results for materials with strong magnetic moments or large differences in electronegativity.

2.2. Vienna Ab Initio Simulation Package

Vienna Ab Initio Simulation package (VASP)[30-32] is a software tool used to perform ab-initio quantum mechanical molecular dynamics at finite temperature. It uses plane wave basis set and ultrasoft pseudopotentials (US-PP)[47] or projector-augmented wave (PAW)[48] method to describe the interaction between ions and electrons. The code was developed in the group led by Jürgen Hafner by Georg Kresse and Jürgen Furthmüller. It is a DFT based tool developed to solve a system with periodic boundary conditions. The ions can be moved to find the instantaneous ground state of the system and the ground state energy. The minimization algorithm used in VASP involves an outer loop to evaluate the charge density and an inner loop to evaluate the wavefunctions. An initial charge density is used to calculate the Hamiltonian and the wavefunction is optimized. The optimized wavefunction is used to calculate the new charge density and it is mixed with the old charge density and the iteration is repeated. The energies obtained must be converged with respect to the cutoff energy and k-point sampling for accurate results.

2.3. Climbing Image Nudged Elastic Band

CI-NEB method developed by Jonsson and co-workers[49-51] is implemented in VASP. This is a method to find the transition state and the reaction pathway from stable initial and final states. A string of images connected by spring forces are relaxed to minimize the energy of the images and the pathway is converged to a minimum energy path (MEP). The initial sets of images are found by interpolation between the initial and final states. Different optimization algorithms like velocity Verlet, quick-min, steepest

descent etc., can be used to move the string of images. However, the highest energy image is not affected by the spring forces but it is moved such that the energy is maximum along the bands and minimum in all other directions. The difference between the energy of the highest image in the MEP and the energy of the initial state gives the activation barrier for the reaction. Normal mode frequencies can be calculated for the transition state and only a single imaginary frequency would be present for a true transition state.

2.4. Bader Analysis

Bader analysis[52-54] is used to identify the charges associated with individual atoms in molecules. The charge distribution is based on zero flux surfaces where the charge density perpendicular to the surface is a minimum. The charge density is a minimum between the atoms and is used to divide the atoms into Bader volumes. A grid based method is used to divide the atomic surfaces and hence the charges have to be optimized with the grid size to ascertain the actual charges associated with the atomic surface. This analysis is independent of the basis set used and can be used with calculations based on plane wave basis as well as atomic basis. A steepest ascent path is followed from a grid point and the path ends at a point of maximum charge density. This path analysis is repeated from each unassigned grid point and all the grid points ending in the same maxima belong to the same Bader volume. The charges over the grid points in a Bader volume are then summed up to get the total charge within that volume. This analysis can be used to determine the charge transfer that occurs within a molecule by comparing the original charge distribution and the charge distribution for the molecule.

CHAPTER 3[1]:

EFFECT OF PLATINUM PROMOTERS ON THE REMOVAL OF O FROM THE SURFACE OF COBALT CATALYSTS: A DFT STUDY

This chapter summarizes the study on the role of platinum promoter in the removal of oxygen from the cobalt surface. Cobalt is one of the commonly used catalysts in Fischer-Tropsch Synthesis (FTS). Small amounts of Pt are often added to cobalt to prevent deactivation and improve activity during FTS.[55] Removal of oxygen from the cobalt surface is one of the final steps in FTS mechanism. We investigate the role of the surface platinum promoter in the removal of oxygen from the cobalt surface using density functional theory (DFT) calculations. The activation barriers and transition states on both flat and stepped Co(0001) surfaces for the removal of oxygen from the cobalt surface with and without the presence of platinum were calculated using the Climbing Image Nudged Elastic Band (CI-NEB) method.[49-51]

[1] These results have been previously published (Nianthrini Balakrishnan, Babu Joseph, Venkat R. Bhethanabotla**,** Effect of platinum promoters on the removal of O from the surface of cobalt catalysts: A DFT study, Surf. Sci., 606, 2012, 634-643) and are utilized with permission of the publisher. Refer to Appendix B-1 for copyright information to use published manuscript. Nianthrini Balakrishnan: Performed the calculations and wrote the manuscript. Babu Joseph: Directed the research and edited the manuscript. Venkat R. Bhethanabotla: Directed the research and edited the manuscript.

3.1. Introduction

FTS is a process for converting syngas into long chain hydrocarbons. It provides a promising solution for meeting the increasing demand of such fuels from natural gas and biomass sources. Metal catalysts such as cobalt, iron and ruthenium have been found to be most suitable for FTS.[1] Fe and Co are the catalysts of choice in industrial applications based on activity and cost. Cobalt-based catalysts exhibit high activity, high yields of long-chain paraffins and lower activity for the competing water gas shift reaction compared to Fe catalysts.

The removal of O is important in 3 stages of FTS: (1) reduction of cobalt oxide precursor formed during the preparation of catalyst, (2) removal of O formed during the dissociation of CO which can reoxidize cobalt to cobalt oxide and (3) removal of O formed by the reoxidation of cobalt by water. CO adsorption and dissociation is recognized as one of the first steps in FTS reaction mechanism. Two pathways for CO dissociation have been proposed in the literature, namely, unassisted CO dissociation and H-assisted CO dissociation. [56] Unassisted CO dissociation involves the dissociation of the adsorbed CO into C and O while H-assisted dissociation starts with the addition of H to the adsorbed CO molecule as shown in Table 3.1.

Ojeda *et al*.[56] found that H-assisted dissociation is the most favorable mechanism on Co catalysts. However C deposition and subsequent graphene formation occur on the cobalt catalyst during the FTS[57] and hence O deposition can also occur. O from CO dissociation can deactivate the catalyst by blocking the active sites. DFT studies by Huo *et al*.[58] showed that 1/4 ML O pre-covered Co(0001) surface raises the CO dissociation

barrier, favors the formation of CO_2, as well as raises the energy barrier of the CH/CH coupling thereby decreasing the FTS activity. Thus, it is important to examine the role of promoters in the removal of O.

Catalysts can be deactivated by oxidation, carbidization, formation of catalyst-support compounds and poisons. There are discrepancies in the reports of deactivation of Co catalyst during FTS. Most of the studies indicate that oxidation of Co catalyst as an important deactivation mechanism.[59-62] Schanke *et al.*[59] in their study on cobalt catalysts observed significant deactivation when water was added to the feed and bulk cobalt reoxidation in the absence of H_2. The extent of reoxidation reduced in the presence of H_2 and surface oxidation or oxidation of highly dispersed cobalt phases was concluded to be responsible for the observed deactivation. Van Berge *et al.*[60] observed the oxidation of reduced cobalt catalysts under realistic FTS conditions and also found the oxidation to be dependent on the P_{H2}/P_{H2O} ratio. Van Steen *et al.*[62] found that spherical cobalt crystallites were oxidized under FTS synthesis conditions. Saib *et al.*[63] concluded that oxidation is not a deactivation mechanism during FTS for supported Co catalysts with crystallite size in excess of 2 nm. In another experimental work,[64] they concluded that the oxidation of spherical Co/SiO_2 model catalysts with water is difficult and is size-dependent.

Promoters are often added to FTS catalysts to enhance activity, selectivity and catalyst life. The commonly used promoters in FTS are transition metals (Zr, Mn, Re, Ru, Rh, Ir, Ni, Pd, Pt, Cu, Ag and Au) and alkali metals (e.g. Li, K, Na, Cs). Promoters can increase reducibility, dispersion of catalyst thereby improving the activity and/or selectivity.[3-4, 65-67] They can also prevent the deactivation of catalysts caused by oxidation [68-70] or carbidization.[71-73] Noble metal promoters modify the structure of cobalt catalysts

which affects cobalt reducibility, dispersion, formation of barely reducible cobalt support mixed compounds and decomposition of cobalt precursors.[74] Some of these promoters increase the dispersion of catalyst, which increases the activity of the catalyst.[75-76] Addition of metal oxides (B, La, K, and Zr),[77] CaO[78] and metals like Cu, Ag, Au [79] were found to decrease the reducibility of the catalyst, by increasing the metal active site densities, thereby affecting the CO conversion levels. Das *et al*.[27] observed that Pt promotion increased the reducibility of cobalt but did not alter the dispersion. This was attributed to the catalyzing effect of Pt which increases the fraction of cobalt that was reduced to the metal. Jacobs *et al*.[28] observed that the addition of platinum metal to cobalt/alumina-based FTS catalysts increased the extent of cobalt reduction by a factor of two.

One view of Pt promotion is that the reducibility of Co oxides is enhanced by the formation of the Co-Pt bimetallic bonds. It is speculated that Pt provides electrons to Co, thus, enhancing the H_2 activation ability of Co.[80] Another view is that hydrogen dissociates on a Pt site and spills over to reduce cobalt. This would increase the dispersion and the average cobalt particle diameter would become smaller than in the un-promoted catalyst if it is assumed that the major fraction of the cobalt that is reduced in the un-promoted catalyst exists as CoO particles.[27, 81] Spillover effects are not considered in the current study.

In this work, the effect of Pt promoter on the removal of O was studied using surface alloy models where the promoter metal was dispersed on the top surface of the catalyst. We considered the removal of O from an oxygen covered cobalt surface and compared that to oxygen removal from a Co surface with some Pt atoms present on the

surface. The activation barriers for the reaction, O + 2H → OH + H and OH + H → H_2O on promoted and un-promoted Co(0001) surface were calculated on both flat and stepped surfaces.

Pt atoms were found to segregate to the first two layers when cobalt atoms were deposited on Pt(111) surface under inert atmosphere.[82] Pt-Co alloy surface prepared at 425°C contained about 85% of Pt in the first layer and LEED experiments on the Pt-Co surface annealed at 470°C exhibited a structure with most of the Pt occupying the first ten layers under inert atmosphere.[83-84] Pt has a tendency to occupy the near-surface or surface sites but a complete segregation to a core – shell structure is not observed.[85] So, surface alloy models were used in this study.

3.2. Computational Details and Methodology

In this work, VASP (Vienna Ab Initio Simulation package) code[30-32] was used with Perdew–Burke–Ernzerhof (PBE) form of the generalized gradient approximation (GGA)[86] functional for the exchange and correlation functional. The electron-ion interaction was modeled by the projector-augmented wave (PAW)[48] method. The plane-wave cutoff energy was set to 500 eV and spin polarized calculations were included to account for the ferromagnetic nature of Co. The convergence criterion for structure optimization was set to an energy tolerance of about 0.01 eV/ Å. The lattice constant of bulk cobalt was found to be 2.528 Å and c/a ratio was found to be 1.622 in agreement with the experimental values (a= 2.503 Å and c/a= 1.62).[87] The magnetic moment of bulk cobalt was found to be 1.59 μB which is also in agreement with the experimental value (1.58 μB).[88]

Flat and stepped Co(0001) surface were simulated using a slab supercell approach with periodic boundary conditions. Calculations were carried out on a 2x2 supercell of Co(0001) slab for the flat surface with about 4 layers of atoms consisting of about 16 atoms and 4x2 surface of Co(0001) for the stepped surface with about 4 layers of atoms consisting of about 28 atoms. For the reactions occurring on the step edge and lower terrace, the stepped surface was modeled by removing two of the four rows of cobalt atoms on the top layer. Among the 4 layers of metal atoms, the bottom two layers were frozen and top 2 metal layers and the adsorbates were allowed to relax. The energy difference between 5 layers of atoms and 4 layers of atoms on stepped surface were found to be less than 0.02 eV (Appendix C-1) and hence 4 layers of atoms were studied.

Pt atoms replaced Co atoms on the surface for the planar model and for the stepped surface, Co atoms on the edges were replaced by Pt atoms. One of the atoms on the slab surface was replaced by platinum making it $Co_3Pt(0001)$ surface as shown (Figure 3.1). Surface Monkhorst[89] Pack meshes of 5x5x1 and 5x2x1 k-point sampling in the surface Brillouin zone were used for flat and stepped surfaces respectively. The vacuum region between the slabs was set to about 10 Å to reduce interactions. We used a one-sided slab approach in our calculations.

On the flat surface, 0.25 ML oxygen pre-covered surface of Co(0001) was considered as it is thermodynamically more stable than any other coverage.[58] High hydrogen coverage of 0.5 ML which would be present under real FTS conditions was considered. On the stepped surface, 0.25 ML oxygen pre-covered upper terrace and 0.5 ML hydrogen-covered lower terrace was used. Only the reactions occurring on the step edges were considered for the stepped surfaces.

The binding energies of O, H, OH, OH + H, H_2O were determined using the formula, $E_b = E_{tot} - E_{slab} - E_A$, where E_{tot} is the total energy of the slab with adsorbate A, E_{slab} is the energy of the clean metal surface and E_A is the energy of isolated adsorbate A. Having determined the initial and final states, different pathways for the reactions, O + 2H → OH + H and OH + H → H_2O were determined using the CI-NEB method developed by Jonsson and co-workers[49-51] and the minimum energy path (MEP) was identified. Normal mode harmonic frequencies were calculated to confirm the transition states. The activation barriers for the removal of O on the Co_3Pt slab were compared to the clean Co slab.

3.3. Results

Removal of O on the close packed Co(0001) and Co_3Pt(0001) surfaces were examined and the activation barriers for the reactions were calculated. O is removed from the Co catalyst surface in two steps,

$$O + H \leftrightarrow OH \quad (3.1)$$

$$OH + H \leftrightarrow H_2O \quad (3.2)$$

0.25 ML oxygen pre-covered surface was considered at the most favorable site for O adsorption (hcp site). On the pre-covered surface, 0.5 ML dissociated hydrogen was adsorbed. Due to the repulsions from the pre-covered oxygen, dissociated hydrogen atoms tend to occupy sites which would lower their repulsion. These repulsions change the most favorable site for H adsorption from fcc to hcp on the flat surface. A number of

pathways were examined for each step in the reaction and the pathway with the least activation energy was found.

3.3.1. Removal of O on Flat Co(0001)

Binding energies of co-adsorbed species O-H-H, OH-H and H_2O were calculated and the most stable sites were identified. The most favorable adsorption state for O-H-H configuration (O-hcp H-hcp H-hcp) was considered as the initial state for the reaction pathway. For the first reaction step, different OH adsorption sites such as top, bridge, hcp and fcc were considered and the most favorable was found to be fcc hollow site. For the second reaction step, H_2O adsorption sites such as top, hcp and fcc were considered and the most favorable site was found to be a top site. However, the pathway with the lowest barrier was not for the OH adsorption site with the strongest adsorption energy. For the first step, the pathway with the lowest barrier was with OH on bridge site and for the second step was with H_2O on a top site. In the transition state (Figure 3.2(c) and 3.3(c)), the O atom is on the hcp hollow site and the H atom is activated to the bridge site with a O-H distance of about 1.330 Å in the first step of the reaction and OH is on top site and H is slightly displaced from the hcp site with O-H distances of about 0.98 Å and 1.465 Å in the second step of the reaction.

3.3.2. Removal of O on Flat $Co_3Pt(0001)$

The most favorable adsorption state for O-H-H configuration (O-hcp H-hcp H-hcp) was similar to that found on the Co(0001) surface and considered as the initial state for the reaction pathway. Different OH and H_2O adsorption sites were considered as before and the most favorable site for OH was hcp hollow site and was top site for H_2O.

The favorable adsorption site was changed from fcc on Co(0001) to hcp on the promoted surface. The pathway with the lowest barrier for the first step was with OH on hcp site which is the OH adsorption site with the strongest adsorption energy and for the second step was with H_2O on a top site. In the transition state (Figure 3.2(f) and 3.3(f)), the O atom is on the hcp hollow site and the H atom is activated to the bridge site with a O-H distance of about 1.390 Å in the first step which is similar to that on the un-promoted surface and OH is on top site and H is activated to the bridge site with O-H distances of about 0.98 Å and 1.549 Å in the second step. Thus, the O-H distance in the transition state are longer in the promoted surfaces and is attributed to the change in electronic structure of the surface.

3.3.3. Removal of O on Stepped Co(0001)

Similar to the flat surface, the most favorable adsorption state for O-H-H configuration on the stepped surface was O-hcp H-hcp H-hcp and considered as the initial state for the reaction pathway. For the first reaction step, the pathway with the lowest activation barrier was the one with OH on the edge bridge site and was the most favorable adsorption site. For the second reaction step, H_2O adsorption on a top site inclined at an angle towards the step was found to be the most favorable similar to that on the flat surface. The pathway with the lowest barrier was for H_2O adsorbed on top site. In the transition state (Figure 3.4(c) and 3.5(c)), the O atom is activated to an edge bridge site and the H atom is slightly displaced from the hcp site in the terrace below with a O-H distance of about 1.465 Å in the first step of the reaction and OH is on top site and H is on a top site in the terrace below with O-H distances of about 0.98 Å and 1.447 Å in the second step of the reaction.

3.3.4. Removal of O on Stepped $Co_3Pt(0001)$

The most favorable adsorption state for O-H-H configuration, similar to that on the stepped Co(0001) surface was O-hcp H-hcp H-hcp and considered as the initial state for the reaction pathway. For the first reaction step, the pathway with the lowest activation barrier was the one with OH on the edge bridge site and was the most favorable adsorption site. For the second reaction step, H_2O adsorption on a top site inclined at an angle towards the step was found to be the most favorable similar to that on the flat surface. The pathway with the lowest barrier was for H_2O adsorbed on top site. In the transition state (Figure 3.4(f) and 3.5(f)), the O atom is activated to an edge bridge site and the H atom is slightly displaced from the hcp site in the terrace below with a O-H distance of about 1.478 Å in the first step of the reaction and OH is on top site and H is on a bridge site in the terrace below with O-H distances of about 0.98 Å and 1.487 Å in the second step of the reaction which is different from that found on the stepped Co(0001) surface.

3.4. Discussion

3.4.1. Comparison of Barriers on Flat and Stepped Surfaces

The barrier for the first step in the removal of O on the flat Co(0001) surface is about 0.992 eV whereas it is reduced to 0.664 eV on the promoted surface. The barriers for the reverse reaction in the first reaction step are 0.858 eV and 0.864 eV on the un-promoted and promoted surfaces. The barrier for the second step on the flat Co(0001) surface is about 1.136 eV and is reduced to 0.792 eV on the promoted surface. For the reverse reaction, the barrier is about 0.880 eV on both promoted and un-promoted

surface. This shows that when water is present in the reaction conditions, it will oxidize both the promoted and un-promoted surface to the same extent, however the surface oxygen formed can be easily removed on the Pt promoted surface than on an unpromoted surface and the water would desorb as the desorption energy of water is less than 0.26 eV on both the promoted and unpromoted surfaces. The reduced barriers on the promoted surface is due to the presence of platinum promoter which changes the electronic structure of the surface resulting in different transition states for the two surfaces.

For the stepped surface, the barrier for the first step in the removal of O is about 0.806 eV on the un-promoted surface and is reduced to just 0.194 eV on the promoted surface. For the reverse reaction, the barriers are about 0.922 eV and 0.610 eV on the un-promoted and promoted surfaces respectively making the reoxidation of the surface by H_2O easier on the promoted surface. This is different from that found on the flat surface where both the promoted and un-promoted surfaces showed the same barriers for reoxidation. This is in agreement with the fact that the catalyst for forward reaction is also a good catalyst for the reverse reaction. The easy reoxidation of Pt-promoted surface by water was also found experimentally by Viljoen and Steen.[90] They found that platinum did not enhance the rate of oxidation in the range of degrees of reduction between 10 and 50% but the oxidation of the last 10% of metallic cobalt was faster in the promoted catalyst. For the second step on the stepped surface, the barriers on the un-promoted and promoted surfaces are 1.772 eV and 1.378 eV which are larger than those found on the flat surface. The reverse reaction has barriers of 1.051 eV and 0.756 eV on the un-promoted and promoted surfaces, respectively. This result is similar to the first reaction

step where the promoted surface can be oxidized easily and the desorption energy of water is less than 0.5 eV on both the promoted and unpromoted surfaces.

These results suggest that the reaction barrier for the first reaction step in the removal of O is reduced on the stepped surface but the barrier for the second reaction step is increased on both the promoted and un-promoted stepped surfaces making the second reaction step difficult than that on the flat surface. This is in agreement with the results of Gong *et al*.[91] who reported the removal of O by H_2 to be facile on the flat surface than on the stepped surfaces. They found that the reaction O+H→OH, is not feasible on flat Co(0001) due to high barrier, however, it is feasible on steps where the barrier is reduced and the barrier for the reaction OH+H→H_2O, is higher on steps than that on the flat surface.

3.4.2. Charge Transfer between Pt and Co

To verify the hypothesis that electron transfer occurs between Pt and Co, Bader analysis[52-53, 92] on the charge density grid was done to determine the charge transfer between the atoms. It was found that about 0.728 electrons were transferred from Co to Pt as expected. This has also been experimentally observed on Co-Pt bimetallic catalyst where electron transfer from Co to Pt were observed for a similar crystal configuration.[93] This is in agreement with the fact that charge will flow from the metal with a higher Fermi level to the lower or from the metal with a lower to a higher electronegativity.[94]

3.4.3. Electronic Structure and Charge Redistribution

Alloying of metal surface changes its electronic properties by lattice strain effect and ligand effect. The average lattice constant of Co surface after relaxation is 2.51 Å and that of Pt promoted surface is 2.55 Å. Lattice strain is about 1.6% on the promoted surface. There is no change in the lattice structure compared to a surface or subsurface alloy where layers of alloying metal is used. The ligand effect is the change in the electronic properties of the surface due to the presence of the other metal. The electronic properties affect the adsorption energy and catalytic activity of the adsorbates. Hammer and Norskov[95] introduced a reactivity measure which is influenced by 3 factors namely: (1) position of bonding and anti-bonding states relative to the d-bands, (2) coupling matrix and (3) filling of anti-bonding states given by the position of Fermi level. The position of d-bands is a parameter which determines the shift of bonding and anti-bonding states, coupling matrix and degree of filling and is used to describe the reactivity. If the d-bands are shifted up, the anti-bonding states are shifted above the Fermi level and becomes empty leading to stronger interaction and if the d-bands are shifted down, the anti-bonding states are shifted below the Fermi level and becomes filled leading to weaker interaction.

The total d-band center (Appendix C-2) was found for the configurations [O, H, H] and [OH, H]. The d-band center is shifted by about 0.26 eV and 0.12 eV, respectively on the flat surfaces and 0.06 eV and 0.04 eV, respectively on the stepped surfaces, for the species considered (Figure 3.6 and 3.7). The d-band center for the surface atoms involved in bonding with the absorbates (Appendix C-3) were shifted by 0.58 eV and 0.44 eV on the flat surface and 0.12 eV and 0.14 eV on the stepped surfaces respectively. The shift in

the d-band center towards lower energy for the promoted surface is in agreement with the weak adsorption energy of the adsorbates on the promoted surface compared to un-promoted Co surface as shown in Tables 3.4 and 3.5. Pt promoter when added to Co shifts the d-band to lower energies due to the d-band broadening caused by the hybridization of 3d states of Co with the 5d states of Pt. This broadening of d-band is compensated by the downshift of d-band center leading to weaker adsorption. Thus the d-band is narrowed due to both the lattice strain and the presence of Pt 5d orbitals. Similar downshift of the d-band center was found for a Pt surface alloyed with excess of Co and was attributed to lattice mismatch and electronic interaction between Co and Pt atoms.[96]

As it can be seen in Table 3.6, the charge on the O atom and the net charge on the OH atom are higher on the unpromoted surface compared to the Pt promoted surface. This reduced charge on the O and OH atoms of the promoted surface lower the barrier for the formation of OH and H_2O respectively. This is in agreement with the work by Wilke *et al.*[97] where a reduced charge transfer to O adatom favored lower barrier heights. Similar to the results from d-band center, the difference in charge transfer on the stepped surface is not substantial. On the stepped surface, the lower activation barrier of transition states in the Pt promoted surface is due to the lower binding energy of electron-deficit Co in the promoted surface which makes the OH bond formation easier. On the flat surface, the electron deficiency in combination with geometric effects (direct contact of the transition state with Pt) influences the binding energy as the Pt atoms increases the distance between the surface and the adsorbate. This weak adsorption energy leads to weak interaction between the reactants and the surface and to a lower barrier for the formation of products. However, the shift in d-band center on the stepped surface is

smaller than that on the flat surface. The small shifts in the d-band center on the stepped surfaces could be due to the small amount of Pt in the supercell as compared to the supercell used for flat surfaces. Small increase in DOS (Density of states) giving rise to a few percent increase in the adsorption energy were reported in few studies.[98-100] Thus, even small shifts in the d-band center could show a large effect on the reaction barriers.

3.4.4. Micro-Kinetic Model

To investigate the influence of the catalyst on the reaction rate, we developed a micro- kinetic model for the reactions shown in Scheme 3.1. following the approximate procedure outlined by Bligaard *et al.*[1] and Cheng *et al.*[101] The rate equations were derived as a function of net enthalpy change (ΔH_R). An equilibrium coverage of O (Θ_o = ¼ ML) was considered since O was assumed to be pre-adsorbed on the catalyst surface prior to H_2 adsorption. Bronsted- Evans – Polanyi (BEP) relation for H_2O dissociation on stepped surface was used (E_P^{dis} = 0.27 ΔH_P + 0.52). Enthalpy change for formation of water at T = 500 K (ΔH = -2.5 eV), entropies (S_{H2} = 145.7 J/Kmol, S_{H2O} =206.5 J/Kmol) and pressures (P_{H2} = 1 bar and P_{H2O} = 0.01 bar) were used in the calculations. The energy profiles are shown in Figure 3.8.

Two rate equations were derived, one considering desorption as the rate determining step and adsorption of H_2 in quasi-equilibrium and the other with adsorption of H_2 as the rate determining step and desorption in quasi-equilibrium. The highest activation barrier in the multistep water formation i.e. OH*(ads) + H*(ads)→H_2O*(ads) is considered as the activation barrier for the desorption step. An equilibrium coverage of

O was considered and was assumed to be a constant ($\Theta_O = ¼$) for derivation purposes. A detailed description of the derivation of the rate equations is given in Appendix C-5.

The rate with desorption as rate determining step is,

$$Rate_{des} = \frac{9k_2\left(1-\frac{4P_{H_2O}}{P_{H_2}K_{eq}}\right)}{64\left(1+\frac{1}{\sqrt{P_{H_2}K_1}}\right)^2} \tag{3.3}$$

The rate with adsorption as rate determining step is,

$$Rate_{ads} = \frac{9k_1P_{H_2}\left(1-\frac{4P_{H_2O}}{P_{H_2}K_{eq}}\right)}{8\left(1+\sqrt{\frac{4P_{H_2O}}{K_2}}\right)^2} \tag{3.4}$$

where

$k_1 = \frac{K_BT}{h}e^{\frac{-S_{H_2}}{R}}e^{\frac{-E_1}{RT}}$ is the rate constant for adsorption

$k_2 = \frac{K_BT}{h}e^{\frac{-E_2}{RT}}$ is the rate constant for desorption

$K_1 = e^{\frac{-S_{H_2}}{R}}e^{\frac{-\Delta H_R}{RT}}$ is the standard equilibrium constant for adsorption

$K_2 = e^{\frac{S_{H_2O}}{R}}e^{\frac{\Delta H_P}{RT}}$ is the standard equilibrium constant for desorption

$K_{eq} = e^{\frac{-S_{H_2}+S_{H_2O}}{R}}e^{\frac{-\Delta H}{RT}}$ is the overall standard equilibrium constant

K_B is Boltzmann constant, T is the temperature, h is Planck's constant, R is gas constant, S_{H_2} and S_{H_2O} are the entropies of hydrogen and water in their gaseous phase respectively.

Substituting the rate constants we have the final rate equations,

$$Rate_{des} = \frac{9K_BTe^{\frac{-E_2}{RT}}\left(1-\frac{4P_{H_2O}}{P_{H_2}K_{eq}}\right)}{64h\left(1+\frac{1}{\sqrt{P_{H_2}e^{\frac{-S_{H_2}}{R}}e^{\frac{-\Delta H_R}{RT}}}}\right)^2} \quad (3.5)$$

$$Rate_{ads} = \frac{9K_BT\frac{-S_{H_2}}{R}e^{\frac{-E_1}{RT}}P_{H_2}\left(1-\frac{4P_{H_2O}}{P_{H_2}K_{eq}}\right)}{8h\left(1+\sqrt{\frac{4P_{H_2O}}{e^{\frac{S_{H_2O}}{R}}e^{\frac{\Delta H_P}{RT}}}}\right)^2}. \quad (3.6)$$

A volcano curve was obtained by plotting the TOF against the heat of reaction of the reactant and the corresponding TOF for the promoted and un-promoted catalyst are shown (Figure 3.9). The volcano curve shows that the promoted Co surface has a higher activity for the removal of O compared to un-promoted surface and that there may be other promoters which can enhance this rate further.

3.5. Conclusions

The activation energy for the removal of O on flat and stepped $Co_3Pt(0001)$ surface is reduced compared to that on the Co(0001) surface. The pathway with the lowest barrier on the flat surface changes from OH bridge on Co(0001) to OH hcp hollow site on $Co_3Pt(0001)$, whereas for the stepped surfaces the pathway with the lowest barrier are similar on both the stepped surfaces except for the transition state in the second step of O removal. Thus, the removal of O is easier on the Pt promoted surface which forms

H_2O easily which could be beneficial for FTS. This lowering of the activation barrier is due to the change in the electronic structure of the cobalt surface induced by the Pt promoter. The change in the electronic structure also changes the most favorable sites on the promoted surface. An approximate micro-kinetic model of the reaction kinetics suggests an increase in the turn-over frequency for the reduction reaction when Pt is present.

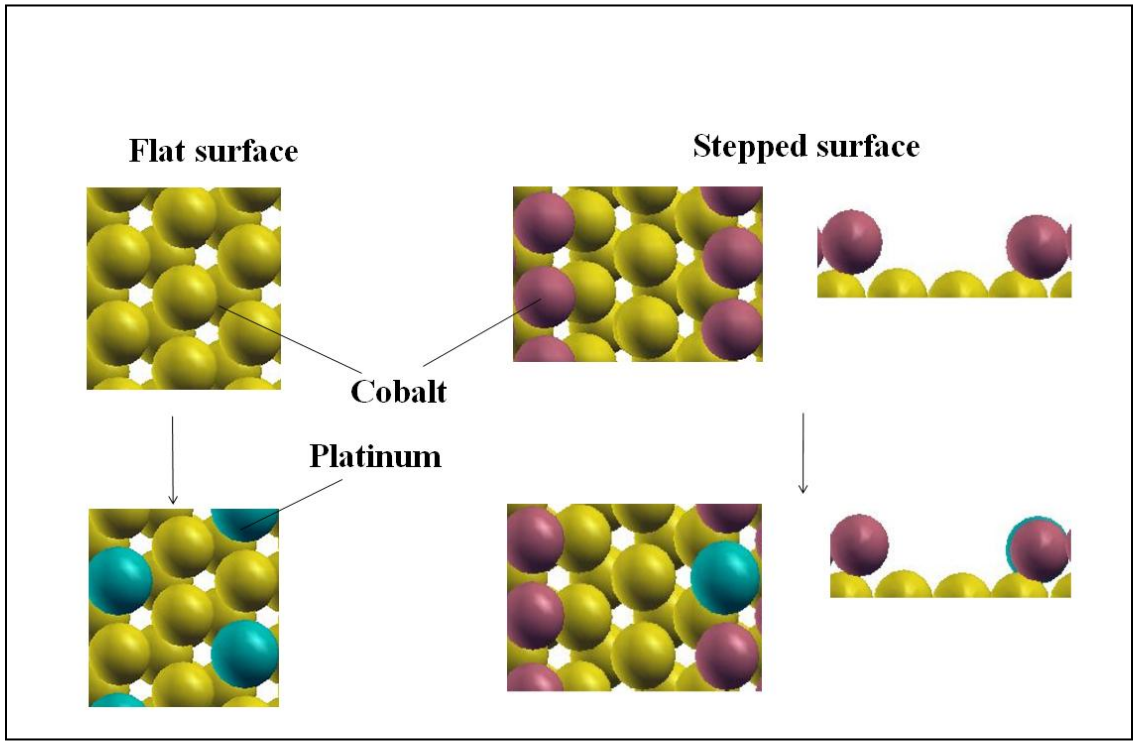

Figure 3.1. Models showing the flat and stepped Co(0001) and Co_3Pt(0001) surface.

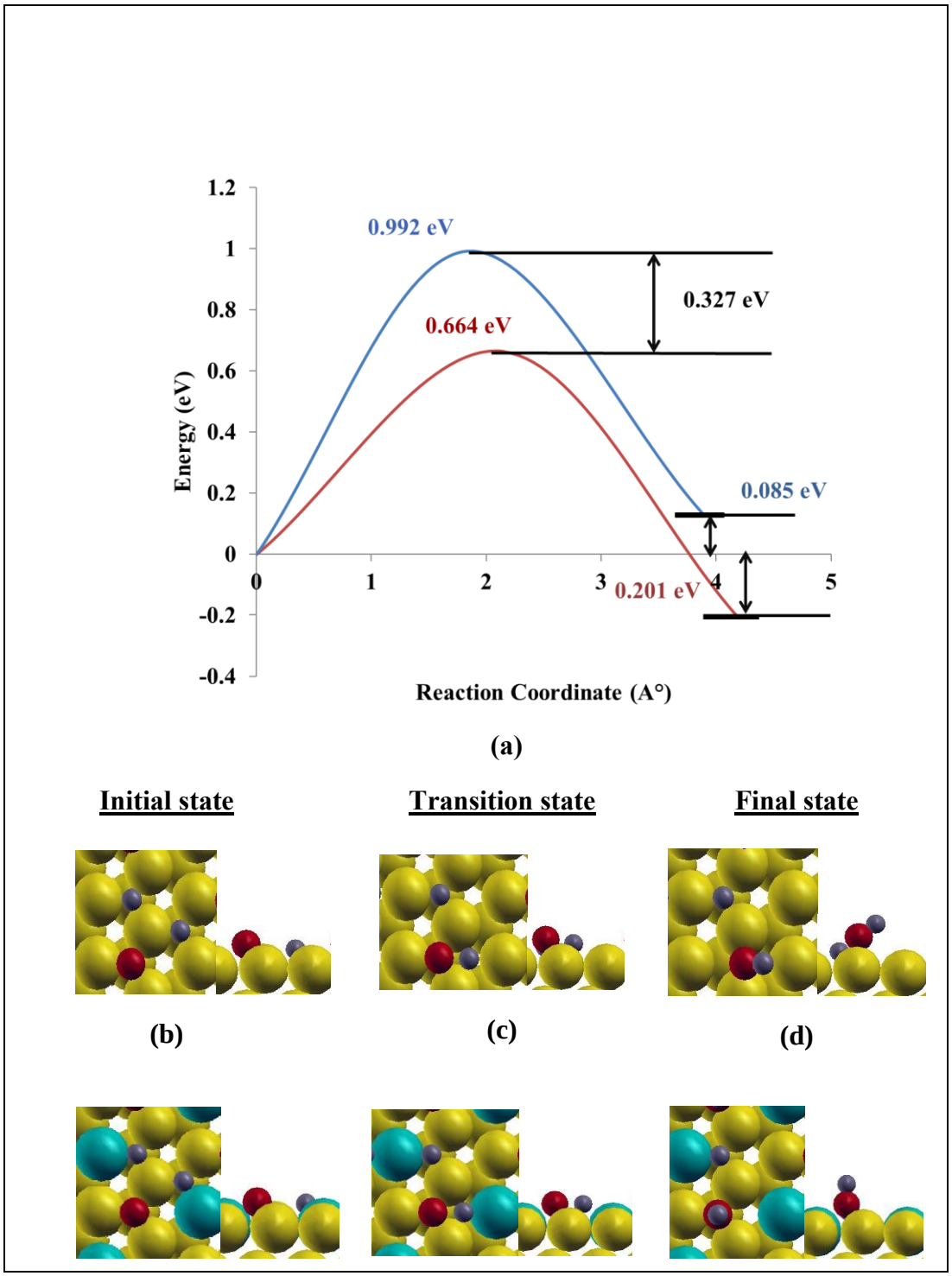

Figure 3.2. (a) Activation barrier for the reaction O + 2H → OH + H on flat Co(0001) surface (blue) and $Co_3Pt(0001)$ surface (red) and (b)-(g) top and side views for various Co(0001) and $Co_3Pt(0001)$ surface (Grey – H atoms, Red – O atoms).

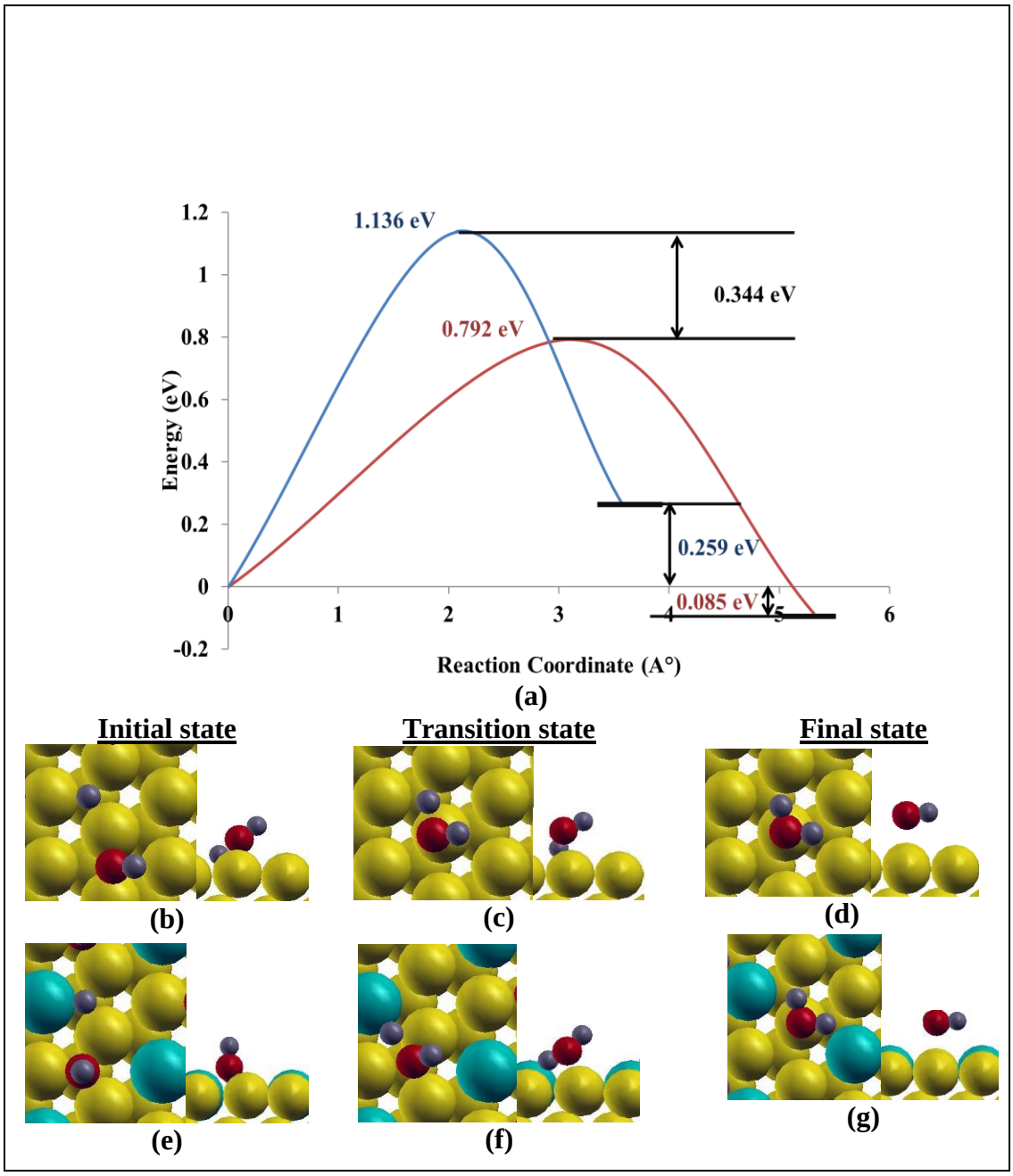

Figure 3.3. (a) Activation barrier for the reaction OH + H → H_2O on flat Co(0001) surface (blue) and Co_3Pt(0001) surface (red) and (b)-(g) top and side views for various Co(0001) and Co_3Pt(0001) surface (Grey – H atoms, Red – O atoms).

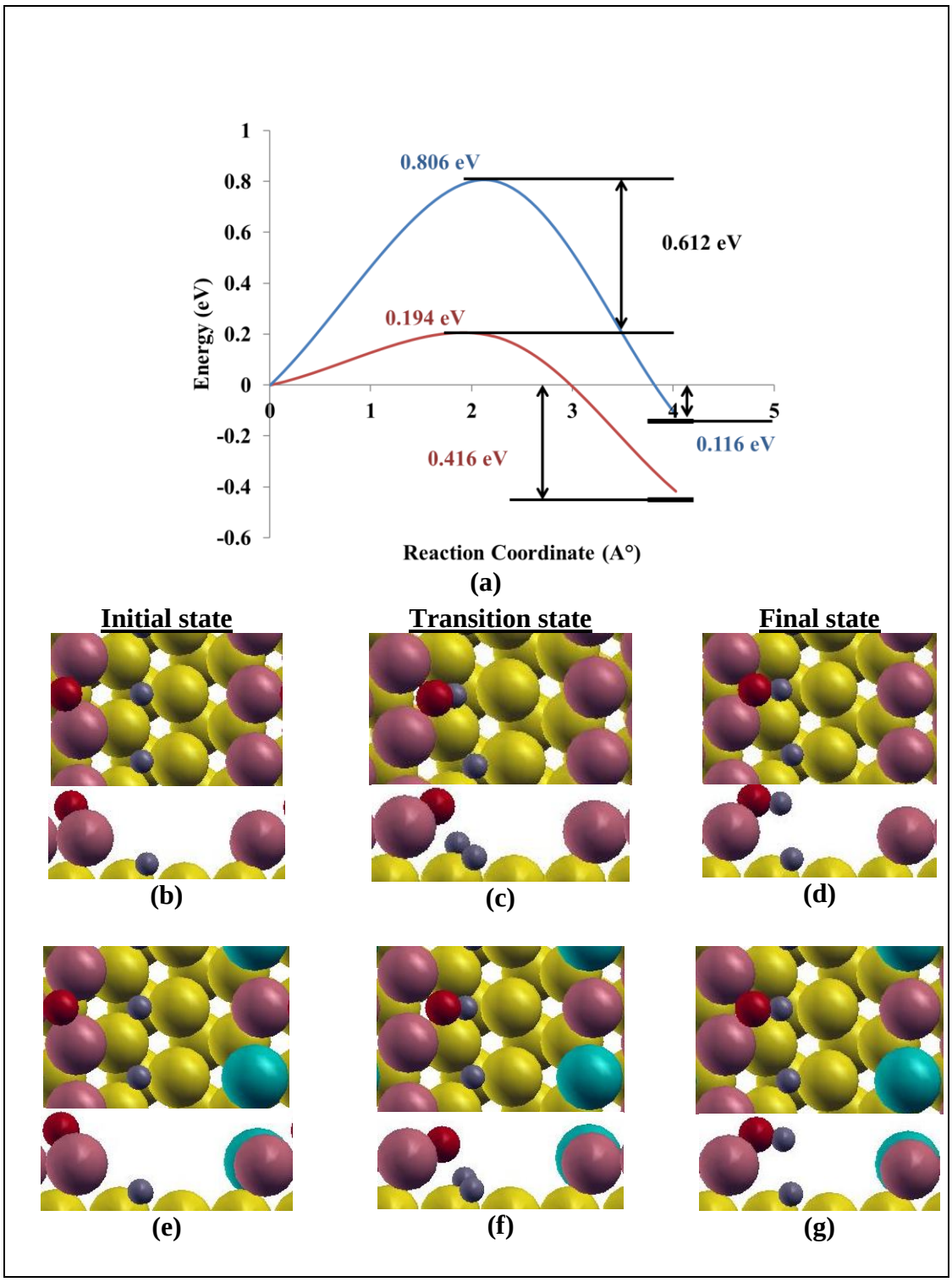

Figure 3.4. (a) Activation barrier for the reaction O + 2H → OH + H on stepped Co(0001) surface (blue) and Co_3Pt(0001) surface (red and (b)-(g) top and side views for various Co(0001) and Co_3Pt(0001) surface (Grey – H atoms, Red – O atoms).

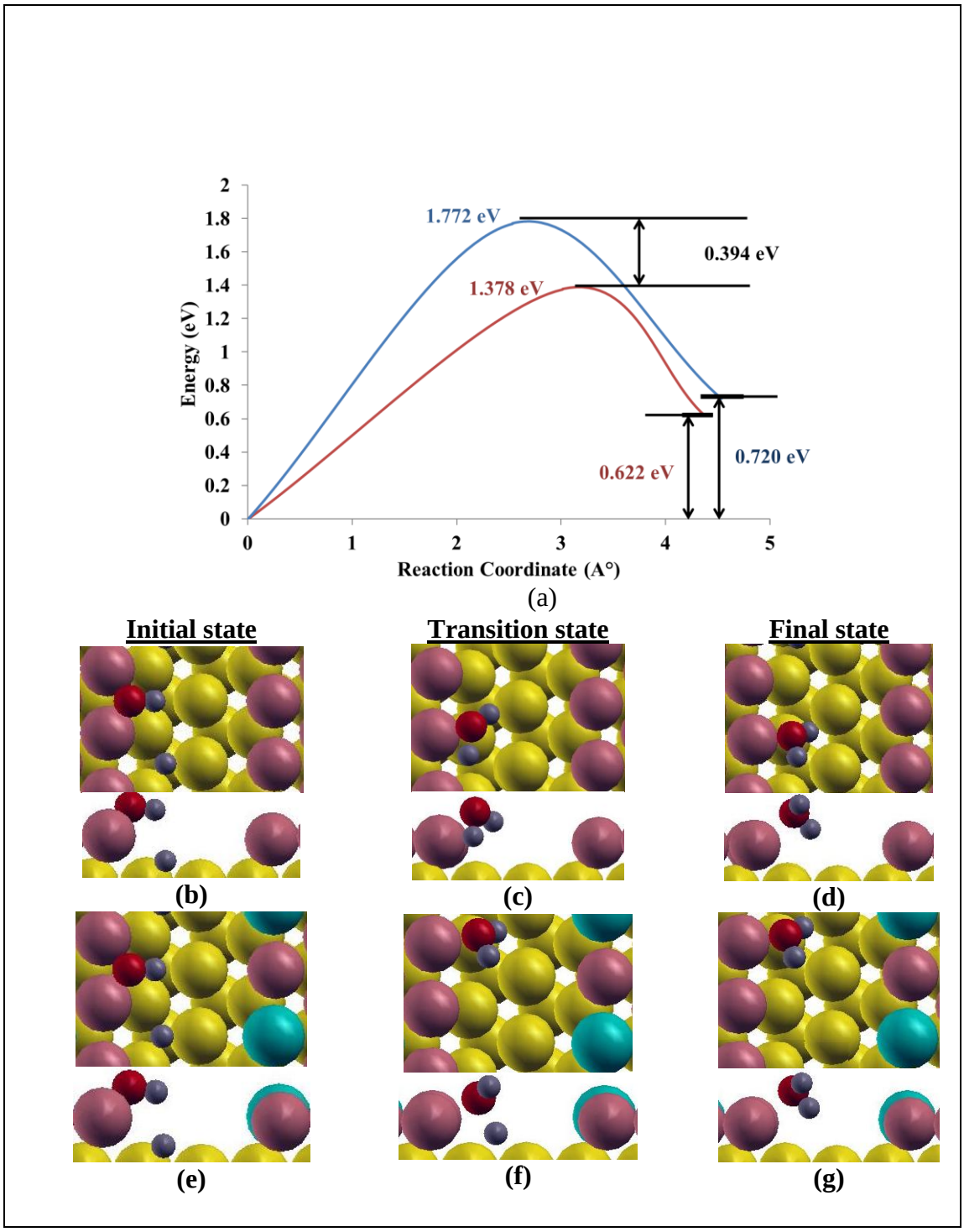

Figure 3.5. (a) Activation barrier for the reaction OH + H → H_2O on stepped Co(0001) surface (blue) and Co_3Pt(0001) surface (red) and (b)-(g) top and side views for various Co(0001) and Co_3Pt(0001) surface (Grey – H atoms, Red – O atoms).

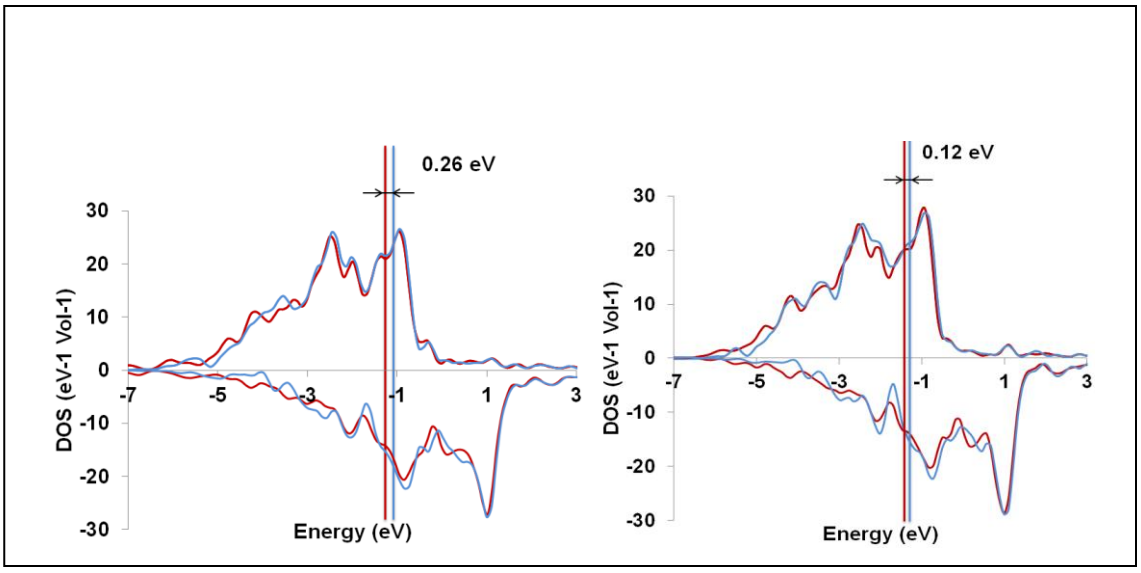

Figure 3.6. The d-band center for O hcp H hcp Hhcp (left) and OH brid/hcp Hhcp (right) on flat Co(0001) (Blue curve) and $Co_3Pt(0001)$ (Red curve). (0 eV corresponds to the Fermi level).

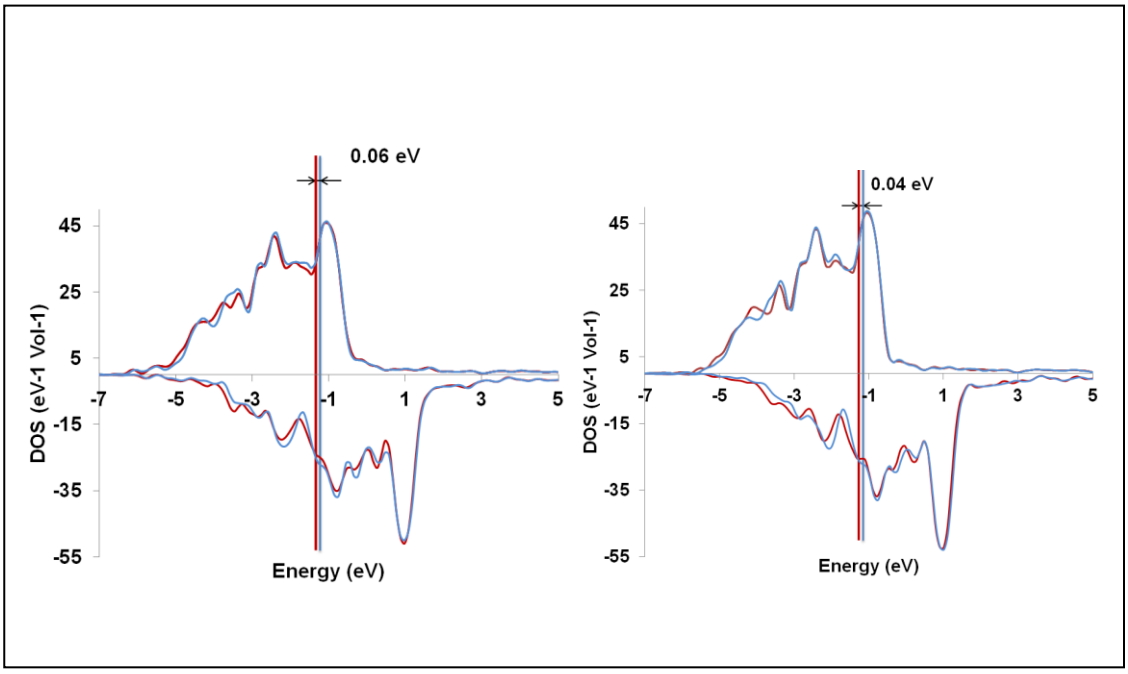

Figure 3.7. The d-band center for O hcp H hcp Hhcp (left) and OH edge brid Hhcp (right) on stepped Co(0001) (Blue curve) and $Co_3Pt(0001)$ (Red curve). (0 eV corresponds to the Fermi level).

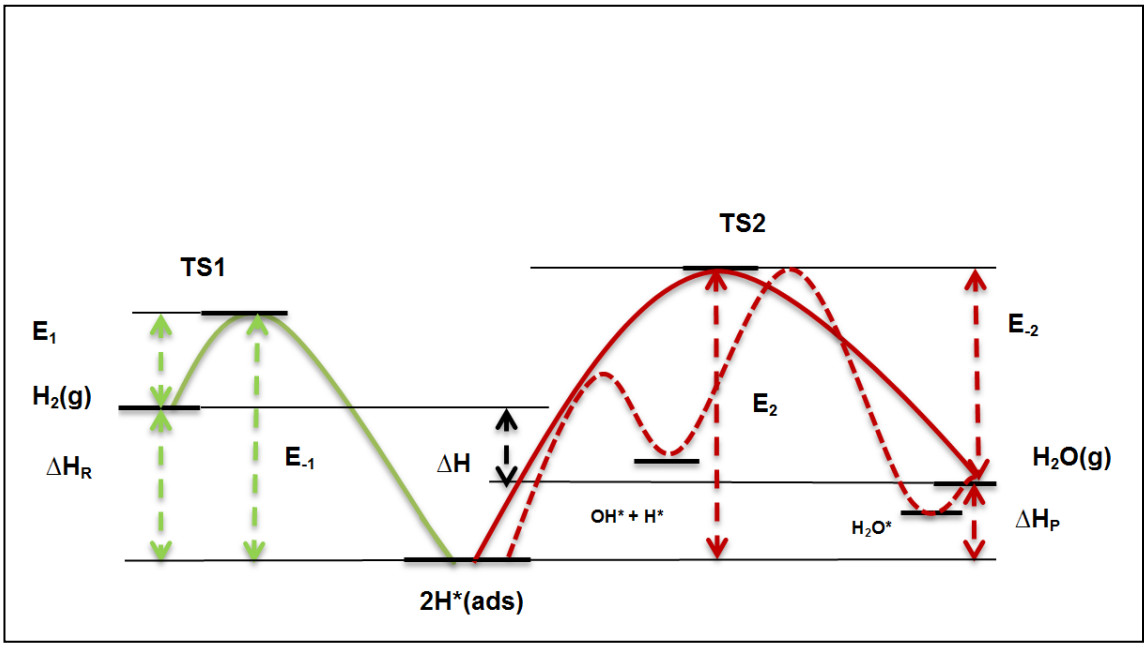

Figure 3.8. Energy profiles showing the approximate and actual scheme for the removal of O as H_2O. ΔH, ΔH_R and ΔH_P are the enthalpy changes for the overall reaction, adsorption and desorption processes. E_1 and E_{-1} are the barriers for the adsorption and its reverse reaction and E_2 and E_{-2} are the barriers for desorption and its reverse reaction respectively. TS1 and TS2 are the transition states for the adsorption and desorption processes respectively.

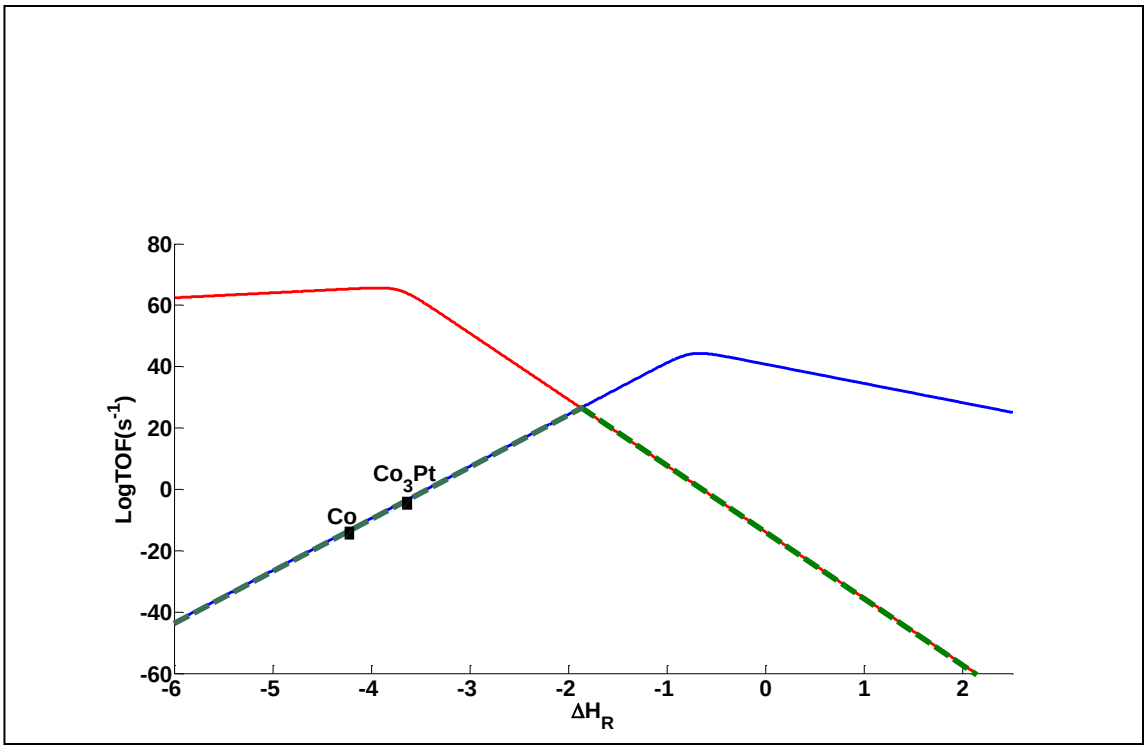

Figure 3.9. Plot of logTOF Vs. ΔH_R. Blue curve corresponds to desorption as rate determining step, red curve corresponds to adsorption as rate-determining step and green curve corresponds to combined rate.

Table 3.1. Pathways for unassisted and H-assisted CO dissociation.

Unassisted CO dissociation	H-assisted CO dissociation
CO* → C* + O*	CO* + H* → HCO*
C* + H* → CH*	HCO* + H* → HCOH*
O* + H* → OH*	HCOH* → CH* + OH*
OH* + H* → H_2O*	OH* + H* → H_2O*

Table 3.2. Initial and final states and barriers for forward and backward reactions in the two steps of removal of O on the flat surface. E_{bf} is the barrier for the forward reaction and E_{bb} is the barrier for the backward reaction.

	Co(0001)	**Co_3Pt(0001)**	**Co(0001)**	**Co_3Pt(0001)**
	O + 2H →OH + H		**OH + H → H_2O**	
Initial	O hcp H hcp H hcp	O hcp H hcp H hcp	OH bridge H hcp	OH hcp H hcp
Final	OH bridge H hcp	OH hcp H hcp	H_2O top	H_2O top
E_{bf}	0.992 eV	0.664 eV	1.136 eV	0.792 eV
E_{bb}	0.858 eV	0.864 eV	0.880 eV	0.880 eV

Table 3.3. Initial and final states and barriers for forward and backward reactions in the two steps of removal of O on the stepped surface. E_{bf} is the barrier for the forward reaction and E_{bb} is the barrier for the backward reaction.

	Co(0001)	**Co_3Pt(0001)**	**Co(0001)**	**Co_3Pt(0001)**
	O + 2H →OH + H		**OH + H → H_2O**	
Initial	O hcp H hcp H hcp	O hcp H hcp H hcp	OH edge brid Hhcp	OH edge brid Hhcp
Final	OH edge brid H hcp	OH edge brid H hcp	H_2O top	H_2O top
E_{bf}	0.806 eV	0.194 eV	1.772 eV	1.378 eV
E_{bb}	0.922 eV	0.610 eV	1.051 eV	0.756 eV

Table 3.4. Adsorption energies (Appendix C-4) of various species on flat Co(0001) and Co_3Pt(0001) surface.

	H (fcc) (eV)	**O (hcp) (eV)**	**OH (hcp) (eV)**	**CO (hcp) (eV)**
Co(0001)	2.852	5.421	3.446	1.719
Co_3Pt(0001)	2.704	5.050	3.129	1.462

Table 3.5. Adsorption energies of various species on stepped Co(0001) and $Co_3Pt(0001)$ surface.

	H (near-edge hcp) (eV)	**O (near-edge hcp) (eV)**	**OH (edge-bridge) (eV)**	**CO (step-corner) (eV)**
Co(0001)	2.792	5.612	3.958	1.943
$Co_3Pt(0001)$	2.686 (step-corner)	5.249	3.816	1.856

Table 3.6. Charge transfer for the species on flat and stepped Co(0001) and $Co_3Pt(0001)$ surface.

Species	**Flat Co(0001)**	**Flat $Co_3Pt(0001)$**	**Stepped Co(0001)**	**Stepped $Co_3Pt(0001)$**
O	-0.836	-0.814	-0.910	-0.900
OH	-0.526	-0.438	-0.528	-0.521

Multistep desorption

$O^*(ads) + 2H^*(ads) \leftrightarrow OH^*(ads) + H^*(ads) + *$

$OH^*(ads) + H^*(ads) \leftrightarrow H_2O^*(ads) + *$

$H_2O^* \leftrightarrow H_2O + *$

Single desorption step

$O^*(ads) + 2H^*(ads) \leftrightarrow H_2O(g) + *$

$H_2(g) + * \leftrightarrow 2H^*(ads)$

$O^*(ads) + 2H^*(ads) \leftrightarrow H_2O(g) + *$

Scheme 3.1. Kinetic model for the removal of O from the catalyst surface. *stands for free surface site.

CHAPTER 4:

EFFECT OF PLATINUM AND RUTHENIUM PROMOTERS ON DEACTIVATION OF COBALT CATALYSTS BY C DEPOSITION DURING FISCHER-TROPSCH SYNTHESIS: A DFT STUDY

In this chapter the effect of Pt and Ru promoters on the deactivation of Co catalyst by carbon deposition during CO hydrogenation is investigated using Density Functional Theory (DFT). The barriers for diffusion of C on the catalyst surface were calculated on the promoted and unpromoted surfaces. The barriers for subsurface C diffusion were also calculated on both the surface to determine the ease of formation of carbidic compounds. Then the barriers for C-C/C-H and C-C-C/C-C-H formation were calculated to determine the effect of promoters on C chain growth. In addition, the stabilities of various C compounds that could be formed on Co surface during FTS were also calculated to determine the influence of promoters on stabilities of C compounds. These results give insights into effects of Pt and Ru promoters on deactivation processes that could occur on Co catalysts during FTS reactions.

4.1. Introduction

Fischer-Tropsch Synthesis (FTS) is used to convert a mixture of CO and H_2 (syngas) to liquid hydrocarbon fuels. This process has become industrially significant as it provides a route for producing renewable liquid hydrocarbon fuels from biomass. It

also provides a route to produce liquid fuels from more plentiful natural gas sources. Cobalt catalysts used in Fischer-Tropsch synthesis deactivates over time for a variety of reasons. These include pore blocking due to wax deposition,[102] poisoning by sulphur, chlorine and nitrogen containing compounds (irreversible blocking of active sites),[103] oxidation of cobalt active sites (to form CoO),[104] formation of surface carbon species,[105] carbidization,[105] surface reconstruction[106] and sintering of cobalt crystallites.[107] Addition of other transition metals such as Pt and Ru has been suggested as a way to mitigate deactivation processes.[105, 108] In this work, we focus on the effect of adding Pt and Ru promoters on deactivation processes occurring through C deposition.

Prior studies have shown that FTS mechanism could follow H assisted CO dissociation or unassisted CO dissociation. H assisted CO dissociation was shown to be favored on Co catalysts where CH or CH_2 and O would be formed.[56, 109-110] However C deposition and subsequent graphene formation occur on the cobalt catalyst during the FTS[57, 63, 111-114] possibly by the Boudouard reaction ($2CO \leftrightarrow CO_2 + C$), or by dehydrogenation of hydrocarbons. Ideally we want the C deposited on the surface to form hydrocarbons and desorb. At low C coverages, Co surface can be transformed to cobalt carbide by atomic C.[111] At high coverages, various C species such as cyclic carbon chains, graphene or coke can be formed on the surface.[112] Moodley *et al.*[113] showed that the polymeric carbon on the metal is a cause for longer term catalyst deactivation. Tan *et al*.[114] detected carbidic and polyaromatic carbon species on Co catalyst and also observed a reduction of CO conversion by 30% after 200 h.

C deposition on catalysts can be reduced by tuning the surface sites, catalyst properties or operating conditions. It has been suggested that selective poisoning of steps

would prevent C deposition.[115-116] Additives like potassium, sulfur, and gold are known to block the step sites which are highly active towards the nucleation of graphite.[117] However, CH_x species can diffuse from the step sites to the flat surface and undergo dehydrogenation increasing the C deposition on flat surfaces.[118] Also, C-C bond formation on Co flat surfaces takes place more easily than on stepped surfaces.[118] Recent studies on Co flat surfaces indicate that larger carbon clusters and graphene are stable under FTS conditions and hence selective poisoning will not inhibit C deposition.[119] This study focuses on the coupling barriers and the various C compounds that could be formed on promoted and unpromoted flat cobalt surfaces.

Promoters can influence the catalyst by changing the activation barriers for the desired and undesired reaction steps during CO hydrogenation. Promoters have been shown to improve activity and/or selectivity,[3-4, 65-66, 120] and prevent oxidation,[69-70, 121-122] carbidization[71, 108, 123] and formation of cobalt support compounds.[74] In our previous work,[121] we found that Pt aids in the removal of O from the Co surface thus hindering oxidation of Co surface. Promoters like Sn, K, S, B, Au, Pt, Rh etc. have been suggested as a way to retard the deactivation of catalysts caused by C deposition.[105, 108, 117, 124-126] However, experimental and theoretical studies on the effect of promoters on carbon deposition and growth on Co catalysts are limited. B promoter reduce C deposition on Co catalyst by preferentially blocking the adsorption sites of C.[125] Ru and Pt promoted Co catalysts have higher resistance towards carbon deposition than unpromoted Co catalyst thereby enhancing catalyst stability.[105] Park *et al.*[108] observed that Pt promoted Co catalyst had higher catalytic stability than Ru promoted Co catalyst where large amounts of polymeric carbons were deposited on the surface. In this study, we explore the effect

of promoters on C deposition and growth on flat Co surfaces using Density Functional Theory (DFT). The objective is to understand the stability of C on the surface, compare barriers for C-C coupling and understand the differences from an electronic structure perspective.

Pt[85] and Ru[127] promoters in Co have the tendency to segregate to the surface layers. EXAFS measurement of Pt-Co bimetallic catalyst indicated no observable Pt-Pt bonds but showed Pt-Co bonds suggesting high dispersion of Pt.[93, 128] Similar studies on Ru-Co bimetallic catalyst showed finite miscibility between Co and Ru at low Ru concentrations with most of the Ru near the outer crystalline surface.[129] Hence surface alloy models were used in this study.

We explore the various pathways in which C can react to form various compounds on the surface to gain a mechanistic understanding. The activation barriers for C-H/C-C and C-C-C/C-C-H coupling were calculated to determine if the promoters inhibit or enhance the coupling reactions thereby preventing or facilitating the deactivation of the catalyst surface by the formation of various C compounds. The thermodynamic stability of various carbon species like monomers, dimers, trimers, tetramers (linear, branch), ring structures, infinite structures and graphene was investigated using the formation energy per carbon atom of such species.

4.2. Computational Details

VASP (Vienna Ab Initio Simulation package) code[30-32] was used with Perdew–Burke–Ernzerhof (PBE) form of the generalized gradient approximation (GGA)[86] for the exchange and correlation functional. The electron-ion interaction was modeled by the

projector-augmented wave (PAW)[48] method. The plane-wave cutoff energy was set to 500 eV and spin polarized calculations were included to account for the ferromagnetic nature of Co. The convergence criterions for structure optimization and transition state search were set to an energy tolerance of 0.01 eV/ Å and 0.05 eV/ Å respectively. The settings and the accuracy of the calculations were tested earlier.[121]

Flat Co (0001) surface was simulated using a slab supercell approach with periodic boundary conditions. For all the calculations, slabs with 4 layers of atoms were considered. Among the 4 layers of metal atoms, the bottom two layers were frozen and top 2 metal layers and the adsorbates were allowed to relax. The carbon clusters were named according to the number of carbon atoms, the site of adsorption and the type of carbon clusters. The name of the carbon cluster was followed by X, Y or Z if the adsorption site was associated with a promoter atom. Monomers were named according to the site of adsorption hcp, fcc, top. Dimers and trimers of carbon were named after the first letter of the site of adsorption as hf (hcp-fcc), bb (bridge-bridge), hfh (hcp-fcc-hcp) and fhf (fcc-hcp-fcc). Compounds with more than 3 C atoms were named with the type of cluster followed by the number of carbon atoms (linear-4C, branch-4C, ring-5C, ring-6C, etc.). Infinite clusters were named with the type of infinite cluster (Inf-chain, Inf-branch) along with number of C atoms in the ring if any (Inf-ring-5C, Inf-ring-6C). Infinite clusters with complete ring structures were named with the number of rings in the finite direction and the type of site at the center of the ring (Inf-1-ring-bri, Inf-2-ring-bri, etc.). Surface Monkhorst[89] Pack meshes were used for sampling the K-points in the surface Brillouin zone. The supercells used for the various C compounds and the corresponding K-points are given in Appendix D (Table D-1).

For all the supercells, 1 Co atom on the surface was replaced by either Pt or Ru for the promoted surfaces. The vacuum region between the slabs was set to about 15 Å to reduce interactions. We used a one-sided slab approach in our calculations. The formation energy of the carbon clusters from CO and H_2 yielding water as the byproduct is given in Figure 4.1. This energy can be found for each of these species to determine the stability of these species with respect to gaseous species (CO, H_2 and H_2O).[119] The activation barriers were determined using the CI-NEB (Climbing Image Nudged Elastic Band) method developed by Jonsson and co-workers[49-51] and the minimum energy path (MEP) was identified. Normal mode harmonic frequencies were calculated to confirm the transition states.

4.3. Results and Discussion

4.3.1. Adsorption of C Monomers

The formation energies of various C monomers per carbon atom on the promoted and un-promoted surfaces are given in Figure 4.2. These energies give the thermodynamic stability of the C species with respect to gaseous species (CO, H_2 and H_2O).[119] The formation energies do not take into account the presence of other gas species on the catalyst surface. Hcp is the most preferred adsorption site for single C atom on unpromoted Co. On Pt promoted Co surface, hcp site unassociated with Pt atom is the most preferred site whereas for Ru promoted surface, the hcp site associated with Ru atom (hcp_X) was more preferred. The trends of the adsorption energies (Figure 4.3) are in agreement with the formation energy per C atom (Figure 4.2).

C placed on a Co top site of unpromoted Co surface relaxed to an fcc site. Similarly, C placed on a Co top site of Pt promoted surface and Ru promoted surface relaxed to an fcc site associated with promoter (fcc_X). C placed on Pt-top and Ru-top sites had positive adsorption energies suggesting that these sites are not energetically preferable for C adsorption. The bridge site was not a stable adsorption site on the promoted and unpromoted surfaces and the C atom placed on bridge site relaxed to a hollow site associated with the promoter.

4.3.2. Diffusion Barrier for C to Move from Hcp to Fcc

The first step towards a buildup of carbon on the surface is the diffusion of an adsorbed C to a nearby site. If the diffusion barrier is increased by adding a promoter then we have reason to suspect that it will also inhibit C chain growth. Having established the stable adsorption sites for C, the diffusion of adsorbed C from 5 different sites were considered: Co hcp to Co fcc on unpromoted Co, Pt hcp (hcp_X) to Co fcc on Pt promoted Co, Co hcp to Pt fcc (fcc_X) on Pt promoted Co, Ru hcp (hcp_X) to Co fcc on Ru promoted Co and Co hcp to Ru fcc (fcc_X) on Ru promoted Co. The barrier for the movement of C atoms from hcp to fcc site is given in Figure 4.4.

Diffusion of C from Ru hcp site (hcp_X) was the most difficult as it is the most stable adsorption site for C among all the surfaces. The diffusion of C from Co hcp had the second highest barrier. The barriers for diffusion from other sites were lower due to the comparable stable adsorption energies on their respective fcc sites (Figure 4.3). The transition state for diffusion is a bridge site on all the surfaces, in agreement with the work of Swart *et al*.[119] But, this barrier alone is not a good measure for the coupling of C

atoms to form various C compounds. Hence it is necessary to determine the barriers for the formation of surface C-C coupling reactions.

4.3.3. Barrier for C to Move to Subsurface

Formation of cobalt carbides is one of the main modes of deactivation for cobalt catalyst [130-133]. While iron carbide is more active than metallic Fe for FTS reactions and has similar methane selectivity as Fe, Co carbide is less active than Co and has higher methane selectivity [134]. The barrier for the diffusion of carbon to the subsurface layer is an important factor to determine the ability of the catalyst to form carbides. Having established the stable adsorption sites for C, the diffusion of C to subsurface from 5 different sites were considered: Co fcc to Co subsurface on unpromoted Co, Pt fcc (fcc_X) to Pt subsurface (sub_X) on Pt promoted Co, Co fcc to Co subsurface on Pt promoted Co, Ru fcc (fcc_X) to Ru subsurface (sub_X) on Ru promoted Co and Co fcc to Co subsurface on Ru promoted Co. The barrier and transition state for the diffusion of carbon to subsurface for the promoted and unpromoted surfaces are shown in Figure 4.5.

The barrier for C diffusion to subsurface from a Co fcc site to the Co subsurface on all the surfaces is about 1.4 eV in agreement with the results on FCC Co(111) [119]. On the Pt fcc site, the C subsurface diffusion barrier is smaller as Pt showed the tendency to move to accommodate the subsurface C but this barrier is still higher (about 1 eV) than the barrier for C-C/C-C-C bond formation discussed in Section 4.3.4. The diffusion of C from the Ru fcc site has the highest barrier due to the similar stabilities of Ru fcc and subsurface site. This is similar to the results on Rh promoted Ni where the barrier for the diffusion of C was higher on Rh promoted Ni surface compared to unpromoted Ni.[126]

Though Ru promoted surface prevents the subsurface C diffusion when C is in contact with Ru, the C unassociated with Ru has lower barrier for subsurface diffusion than unpromoted Co surface. Similarly, Pt promoted surface has lower barriers for subsurface diffusion than unpromoted Co surface. Thus, Pt and Ru promoters would not significantly affect the subsurface C diffusion. These results suggest that formation of subsurface C could occur at low coverages of C in agreement with experiments.[111]

4.3.4. Barrier for C-C /C-H and C-C-C/C-C-H Coupling

These barriers were calculated to evaluate the possibility of C-C coupling in the presence of H vs. C-H coupling in the presence of C. These barriers would be a measure to understand if two C atoms would couple to deactivate the catalyst or if C combines with H to form FTS products. Similarly, the barriers were calculated to evaluate the possibility of C-C-C coupling in presence of H vs. C-C-H coupling in presence of C. Thus, these barriers would be a measure to understand if three C atoms would couple to further deactivate the catalyst or if C-C combines with H to form FTS products.

First, the barriers for 2 C atoms to couple to form C-C bond as opposed to a C and H atom to form C-H bond were calculated. The lowest barrier pathways and the transition states for the C-H and C-C coupling reactions are given in Table 4.1. The barriers for C-H formation are lower than for C-C formation on all the surfaces in agreement with the results of C coupling reactions on Co surfaces by Cheng *et al*.[118] The promoted surfaces have lower barrier for C-H formation and higher barrier for C-C formation than the unpromoted surface. Thus, C-H bond formation is more favorable on promoted surfaces than C-C bond formation and the barriers for C-C bond formation are increased on the

promoted surfaces. This is similar to the results on Rh promoted Ni[126] and Sn promoted Ni,[135] where the promoters increased the barrier for C-C bond formation.

C-C bond formation could also lead to the production of hydrocarbons as established by the calculations done by Cheng *et al.*[118] Hence it is important to consider the formation of larger C compounds. The reactions between the C-C structure and H or C atom were also considered to determine the barriers for the formation of C-C-C bond as opposed to the C-C-H bond. The lowest barrier pathways and the transition states for the C-C-H and C-C-C coupling reactions are given in Table 4.2. The barriers for C-C-H are much lower than those for C-C-C formation on all the surfaces. The promoted surfaces have higher barriers for C-C and C-C-C formation than on the unpromoted surface. The barrier for C-C-C coupling is lower than C-C coupling for Ru promoted surface due to the higher stability of C-C-C structure than C-C structure on Ru promoted surface. However, the barrier for C-H and C-C-H formation on all the surfaces were lower than the barrier for C-C and C-C-C formation suggesting that at high coverages of H_2, formation of hydrocarbons would be preferred.

4.3.5. Stability of Finite and Infinite C Compounds

The formation energies of finite C compounds per carbon atom are given in Figures 4.6-4.7. The structures of various finite and infinite C clusters are given in Appendix D (Figures D-1, D-2, D-3). Two carbon atoms placed on the bridge-bridge site relaxed to hcp-fcc site on all the three surfaces. It should be noted that for up to 4 C atoms, most of the C compounds adsorbed on a site unassociated with Pt and associated with Ru were more stable than other adsorption sites.

In case of 5 C atoms, the linear structures adsorbed on a site associated with Pt and Ru promoter are more stable. However, for branched 5 C structure the behavior is similar to that of structures with 1 to 4 C atoms. 5 C ring structures have 2 type of promoter sites, one in which the C is associated with the promoter (denoted X) and another in which the ring is directly above the promoter (denoted Y). For all the ring structures, the site with the ring center directly above the promoter atoms are the least stable. 5 C ring structures on a site associated with Pt and Ru promoter are the most stable. 6 C ring structures unassociated with Pt and associated with Ru are the most stable sites similar to that of structures with few C atoms. For most of the finite C structures, the energies follow the trend: Pt promoted Co < Ru promoted Co < unpromoted Co.

The formation energies per carbon atom of infinite C compounds are given in Figures 4.8-4.9. For the clusters infinite in 1 direction, branched structure away from promoter is more stable. Infinite ring-5C_X structure on Pt moves from closed ring on Pt top site to open ring on Pt whereas on Ru the closed ring stays on Ru top site. Similarly, infinite ring-6C_X structure moves from closed ring on Pt top site to a bridge site near Pt whereas on Ru the closed ring stays on Ru top site. Infinite ring-top site eventually converge to infinite ring-bridge sites on all the surfaces. The infinite multiple ring structures are arched at the center with the C atoms at the ends forming bonds with the surface. This is due to the stabilization of the structure with the tilting of the C atoms to fill the sp2-like orbitals with the surface atoms. The stability is higher for infinite structures than finite structures and infinite ring structures show higher stability than branched structures. The energies on the unpromoted Co surface are in agreement with the results on FCC Co (111).[119] The stability of the various clusters on promoted and

unpromoted surfaces of Co show that the presence of Pt promoter inhibits the formation of C compounds under FTS conditions. The stability of C compounds on Ru promoted surface is higher than Co surface for few of the C clusters. However, on Ru promoted surface, as the number of C atoms increase the C clusters have lower stability than unpromoted Co surface. Generally, the compounds at sites associated with Pt and those unassociated with Ru are less stable. The stability of the infinite clusters with large number of C atoms is very low on promoted surface than on the unpromoted surface.

4.3.6. Stability of Graphene

The energies of various graphene structures like ring top, ring fcc, ring hcp and ring bridge per carbon atom were calculated on the promoted and unpromoted surfaces and are given in Figure 4.10. Ring top graphene structure was found to be lifted off from all the surfaces. On the Ru promoted surface, ring bridge graphene eventually moved to form a ring hcp graphene structure and ring top graphene moved to ring bridge and lifted off the surface. Pt promoted surface have all the graphene structures lifted off the surface. For graphene, the energies followed the order Pt promoted Co < Ru promoted Co < unpromoted Co. Graphene was found to be the most stable of all C structures.

4.3.7. Electronic Structure

The charge density difference for the different surfaces was calculated as follows:

$$\Delta\rho = \rho_{C+surface} - \rho_{Surface} - \rho_{C} \quad (4.1)$$

where $\rho_{C+surface}$ is the charge density of the C adsorbed on the surface, $\rho_{Surface}$ is the charge density of the surface and ρ_{C} is the charge density of C.

The charge density difference isosurface of a single C atom on hcp hollow site for the promoted and unpromoted surfaces are shown in Figure 4.11. The isosurfaces show a distributed electron accumulation in the Π* molecular orbitals of C on the unpromoted and Ru promoted surface compared to the Pt promoted surface where there is a small charge accumulation in the Π* molecular orbitals of C between the C and Pt atoms. The charge accumulation increases the bonding strength of C with the surface in case of unpromoted and Ru promoted surface.

The effects of promoters on a catalyst surface include lattice strain and ligand effects. The average lattice constant of Co surface after relaxation is 2.51 Å and that of Ru and Pt promoted surface are 2.53 Å and 2.55 Å respectively. The strain in the lattice due to the introduction of promoter atoms is less than 1.6% which is not significant compared to the change in the lattice due to the introduction of layers/sub-layers of promoters in the catalyst surface. Reactivity of metal is measured by three factors[95] namely, (1) d band center, (2) coupling matrix and (3) d band filling. The d-band center is the main parameter which characterizes the ligand effect. The d-band shift to lower energies leads to weak adsorption energy as the anti-bonding states are shifted below the Fermi level and the d-band shift to higher energies leads to strong adsorption energy as the anti-bonding states are shifted above the Fermi level. Here, Pt 5d states (which are filled more than Co d states) broaden the 3d states of Co to maintain the same d-band filling, shifting the d band center to lower energies. Ru 4d states (which are filled less than Co d states) narrow the 3d states of Co to maintain the same d-band filling, shifting the d band center to higher energies as shown in Table 4.3. Thus, Pt would weaken the

adsorption of C and Ru would enhance the adsorption of C when Pt/Ru is involved in the bonding in agreement with the observed trend in formation energies.

The PDOS of C, the atoms involved in bonding and the Co atoms in the bulk are plotted in Figure 4.12 for the C at the hcp site. There is strong hybridization between the C p states and metal d states between -2.5 and -5 eV in both Ru promoted and unpromoted Co surface resulting in stronger adsorption energy in these surfaces. On the Pt promoted surface, there is widening of the d band states coupled with the weak hybridization of the C p states with the metal d states of the atoms involved in the bonding. There are additional states near -11 eV in all the surfaces due to the interaction of the p states of C with the metal which are absent in the bulk Co atoms.

Bader analysis[52-53, 92] on the charge density grid was done to determine the charge transfer between the atoms. It showed electron transfers to Pt and Ru atoms from Co which is in agreement with the fact that electrons transfer from less electronegative element to more electronegative element. About 0.73 electrons were transferred to Pt and 0.25 electrons were transferred to Ru. The charge on the individually adsorbed C and H atoms on the different surfaces are shown in Figure 4.13. The charge on the H and C atom correlates with the activation barrier for C-H bond formation. More the charge on H atom, higher is the activation barrier for C-H bond formation which is similar to our earlier study[121] where we found that higher charge on O and H leads to higher activation barrier for OH bond formation. However, there is no correlation between the charge on C atoms and the activation barrier for C-C bond formation. This could be due to the similar nature of the species involved in the bond and further analysis may be required which is beyond the scope of this work.

4.4. Conclusions

Pathways for the formation of carbon compounds on unpromoted and Pt and Ru promoted Co surfaces were studied to gain a mechanistic understanding of the effect of promoters on these reactions. The barriers for C-C and C-C-C coupling reactions were larger on Pt and Ru promoted Co surfaces than on the unpromoted Co surface indicating that C chain formation will be inhibited by these promoters. The promoters did not significantly alter the barrier for diffusion of C to the subsurface. In addition, most of the finite and infinite C structures on Pt promoted surface and the larger C structures on Ru promoted surface had lower stability than the C structures on the unpromoted surface. C structures on the Pt promoted surface were less stable than the C structures on the Ru promoted surface suggesting that Pt promoter would be better than Ru promoter to prevent C deposition on Co catalyst. These results suggest that Pt and Ru promoted Co surfaces would decrease C formation and C compound formation on the Co surface.

$$CO + H_2 \leftrightarrow \frac{C_n^*}{n} + H_2O$$

$$E_{ads-C} = \frac{(E_{C+Slab} + nE_{H_2O}) - (nE_{CO} + nE_{H_2} + E_{Slab})}{n} \text{ eV/C atom}$$

Figure 4.1. Reaction for the formation of C from CO and H_2 and the energy per C atom with respect to gaseous CO, H_2 and H_2O.

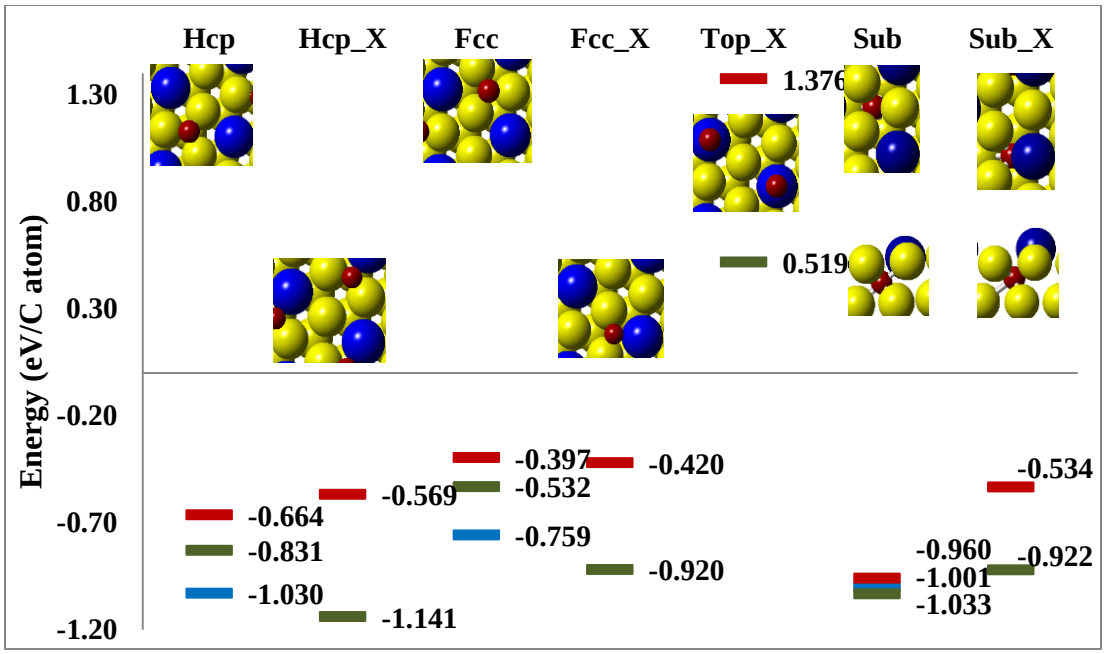

Figure 4.2. Formation energies of C on various promoted and un-promoted surface sites (Yellow – Co atom, Blue – Pt/Ru atom, Red – C atom; Blue bar – unpromoted Co surface, Red bar- Pt promoted surface, Green bar- Ru promoted surface).

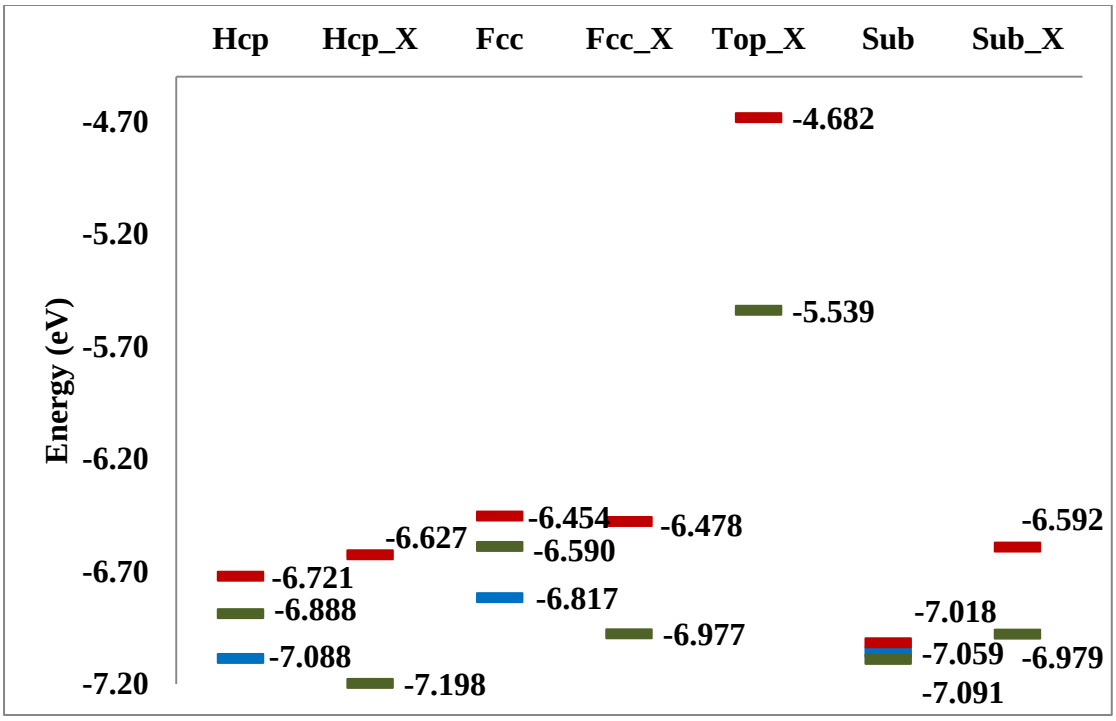

Figure 4.3. Adsorption energies of C on various promoted and un-promoted surface sites with respect to gaseous C (Blue bar – unpromoted Co surface, Red bar- Pt promoted surface, Green bar- Ru promoted surface).

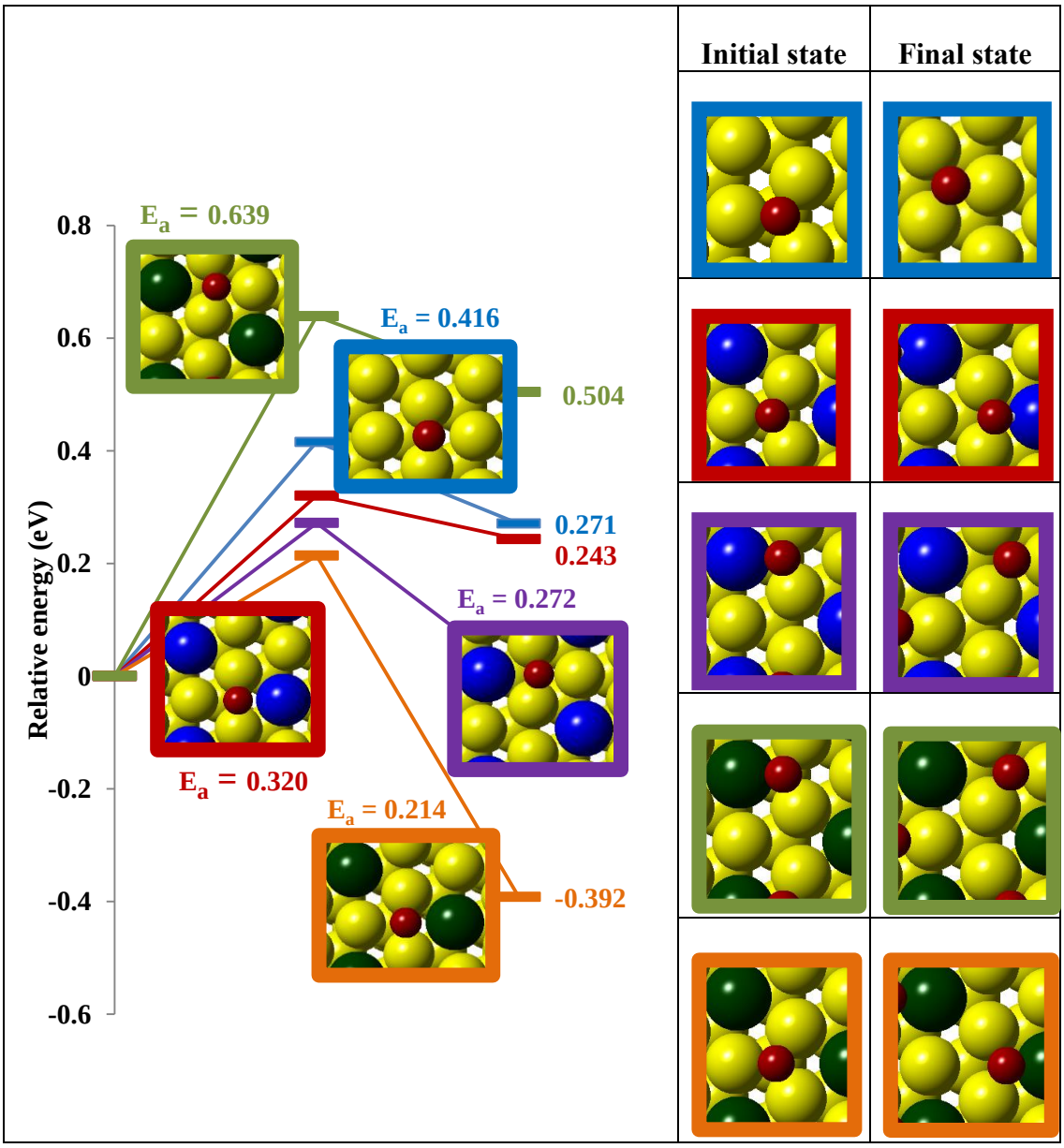

Figure 4.4. Figure showing the barriers, transition, initial and final states for the diffusion of C from an hcp site to fcc site on unpromoted, Pt promoted and Ru promoted Co surface (Yellow – Co atom, Blue – Pt atom, Green – Ru atom, Red – C atom).

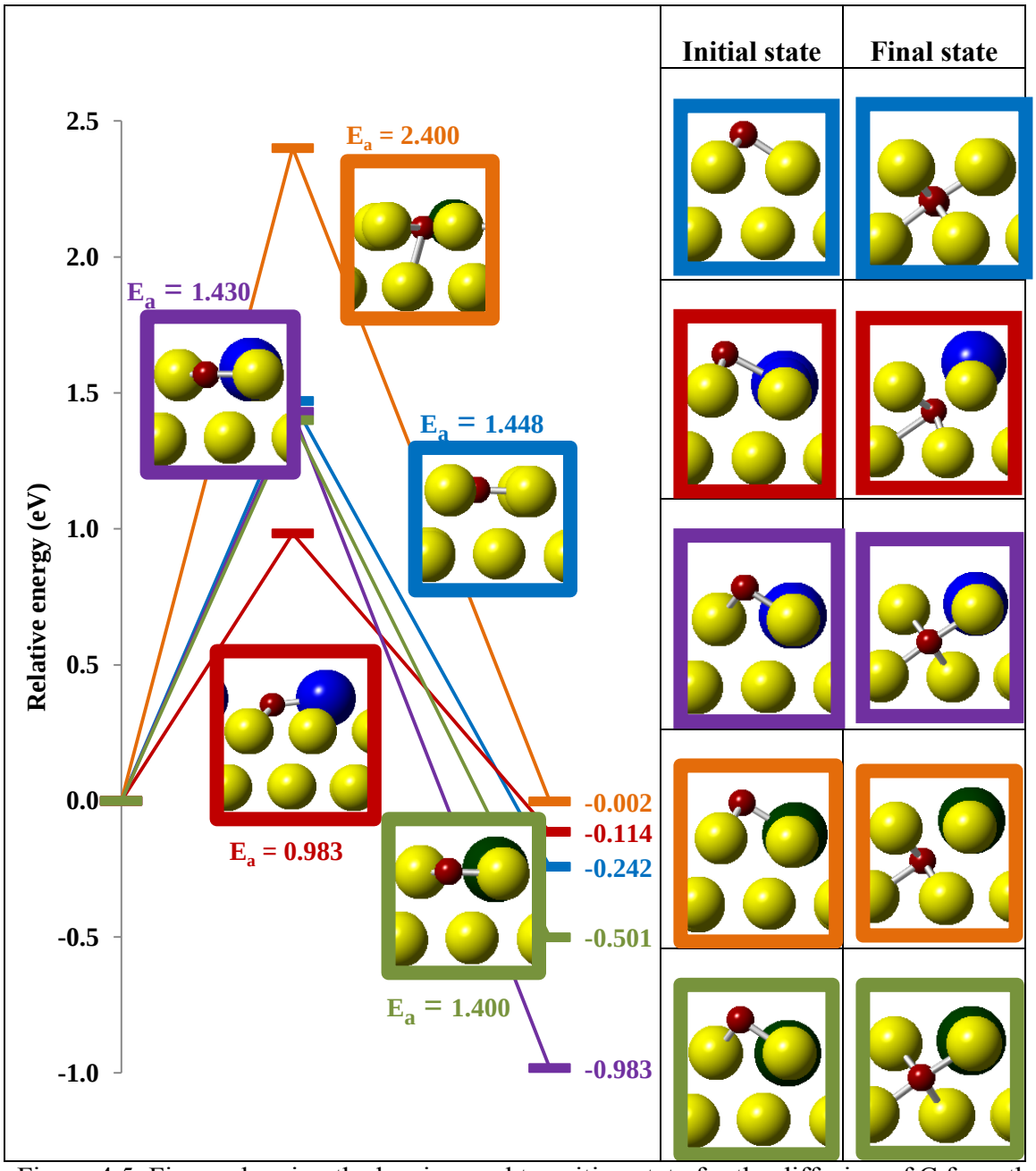

Figure 4.5. Figure showing the barriers and transition state for the diffusion of C from the surface to subsurface on unpromoted, Pt promoted and Ru promoted Co surface (Yellow – Co atom, Blue – Pt atom, Green – Ru atom, Red – C atom).

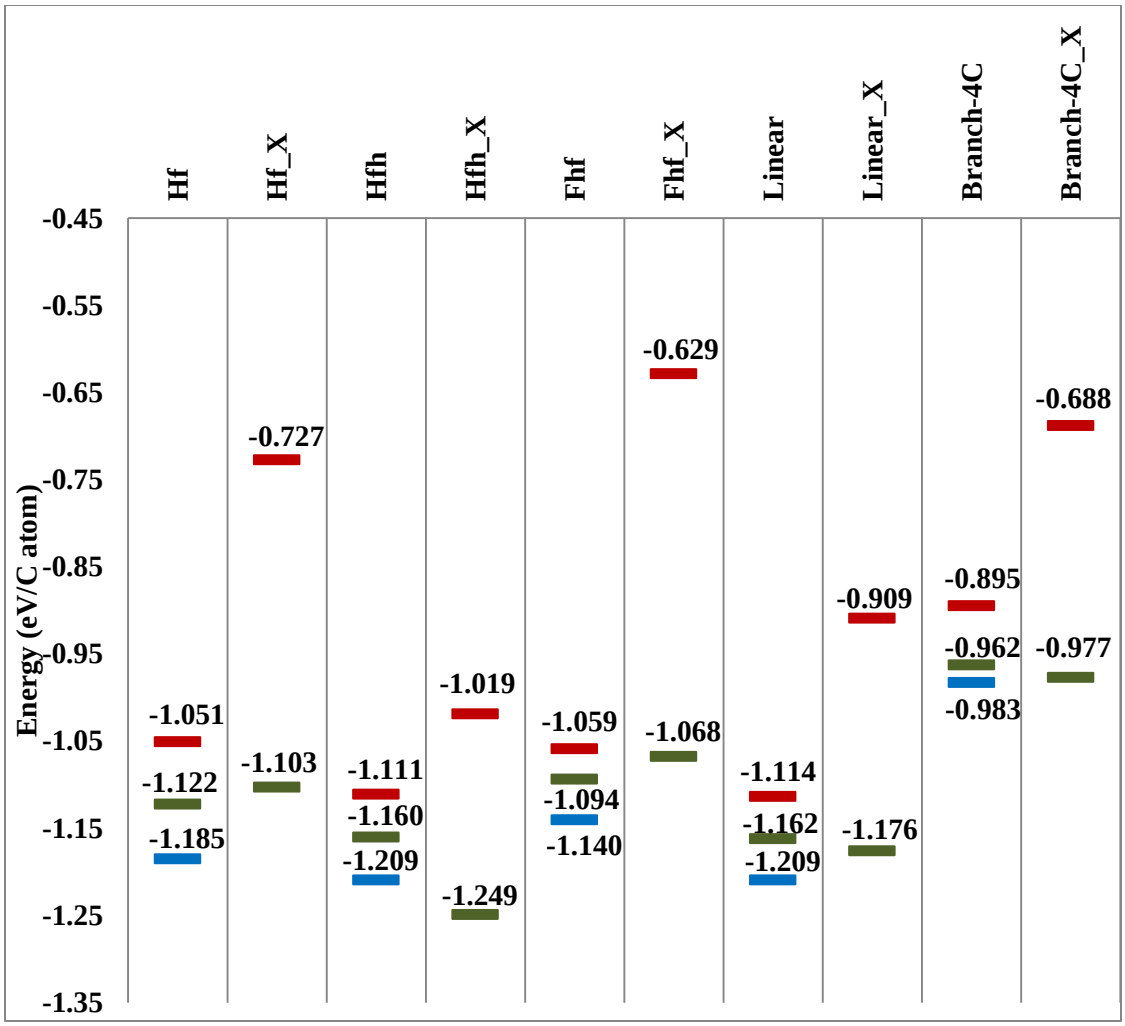

Figure 4.6. Formation energies of finite clusters of C with up to 4 C atoms on various promoted and un-promoted surface sites (Blue marker – unpromoted Co surface, Red marker- Pt promoted surface, Green marker- Ru promoted surface).

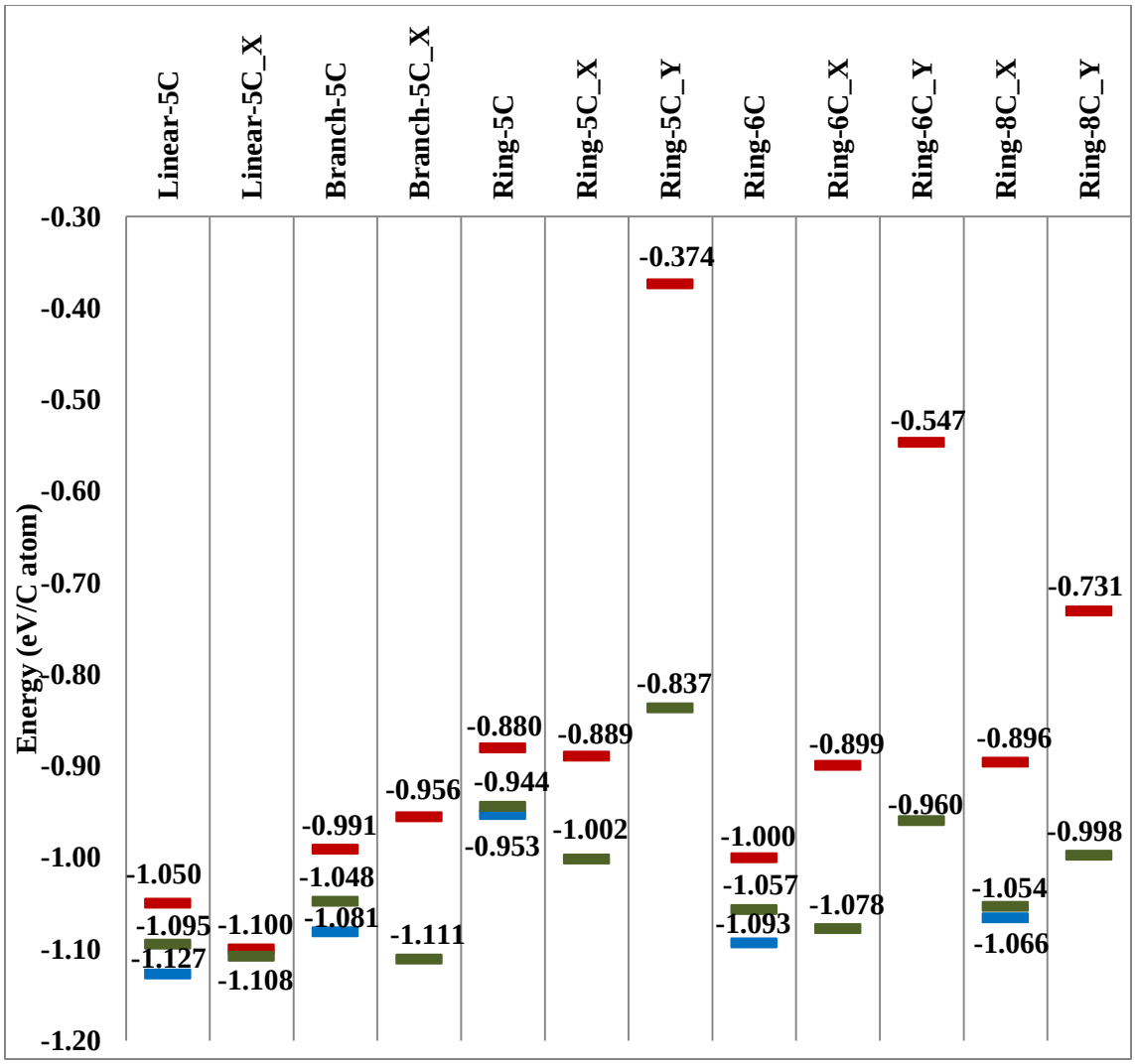

Figure 4.7. Formation energies of finite clusters of C with 4 to 8 C atoms on various promoted and un-promoted surface sites (Blue marker – unpromoted Co surface, Red marker- Pt promoted surface, Green marker- Ru promoted surface).

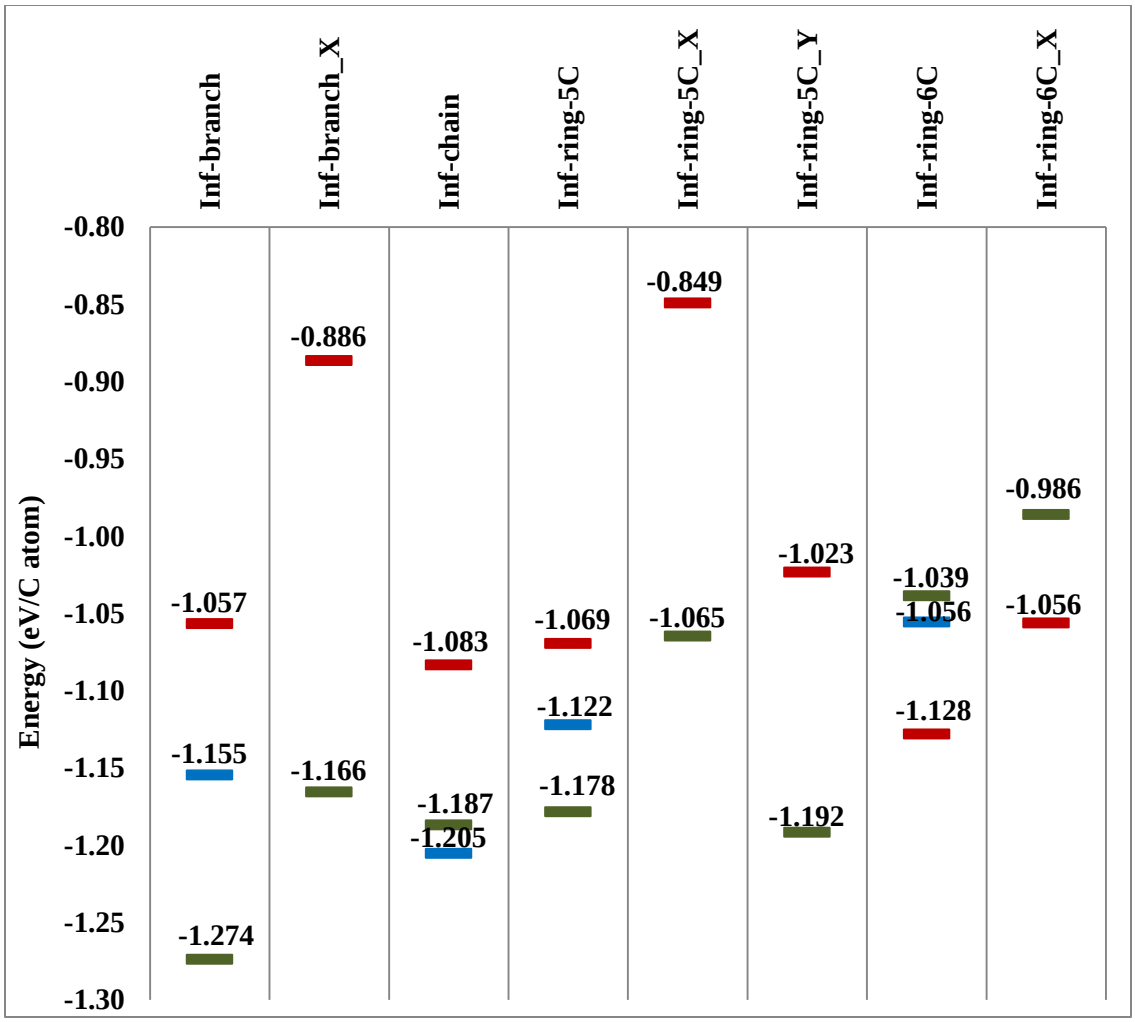

Figure 4.8. Formation energies of infinite clusters of C with up to six-C rings on various promoted and un-promoted surface sites (Blue marker – unpromoted Co surface, Red marker- Pt promoted surface, Green marker- Ru promoted surface).

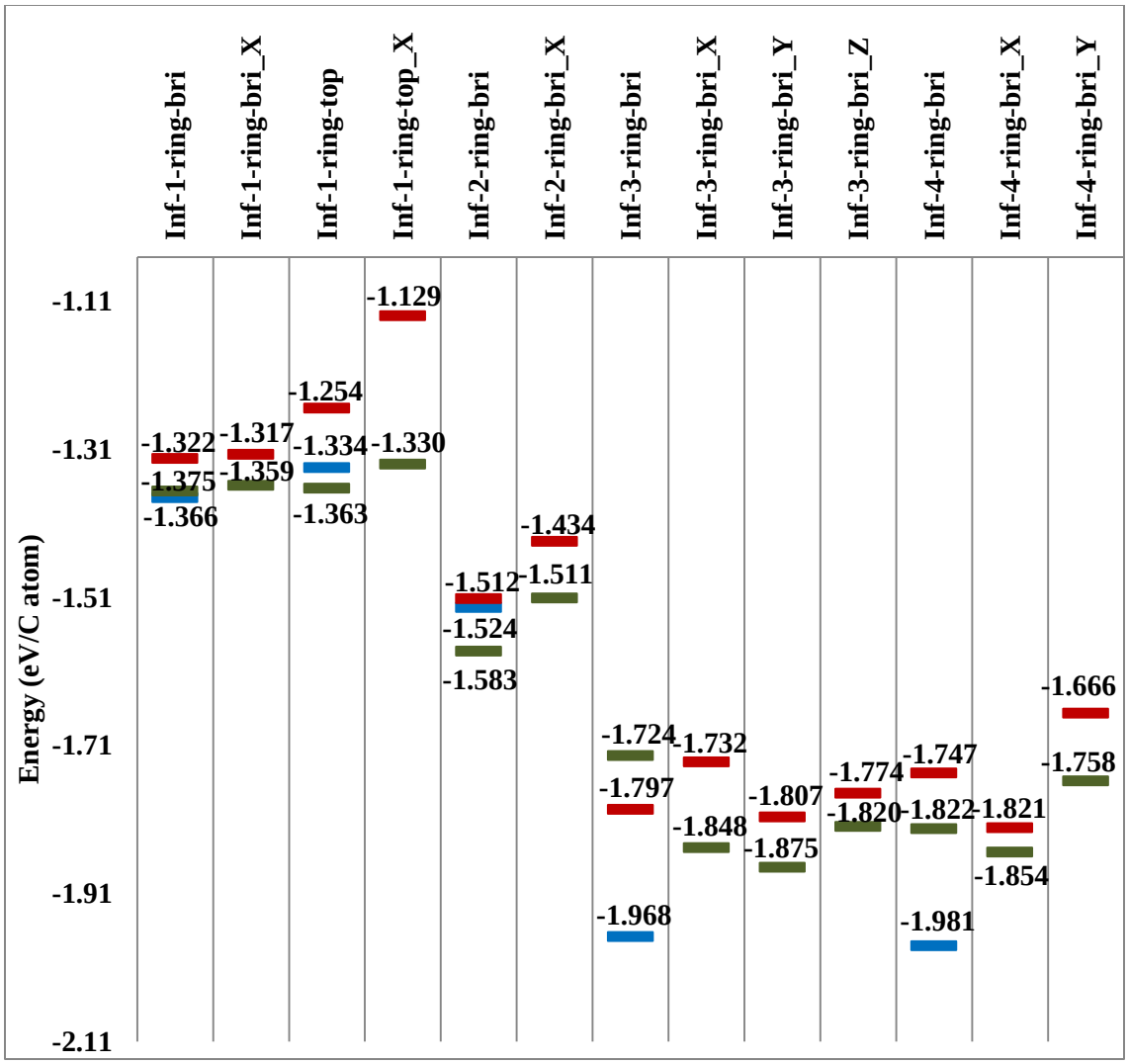

Figure 4.9**.** Formation energies of infinite clusters of C with 1 to 4 six-C rings on various promoted and un-promoted surface sites (Blue marker – unpromoted Co surface, Red marker- Pt promoted surface, Green marker- Ru promoted surface).

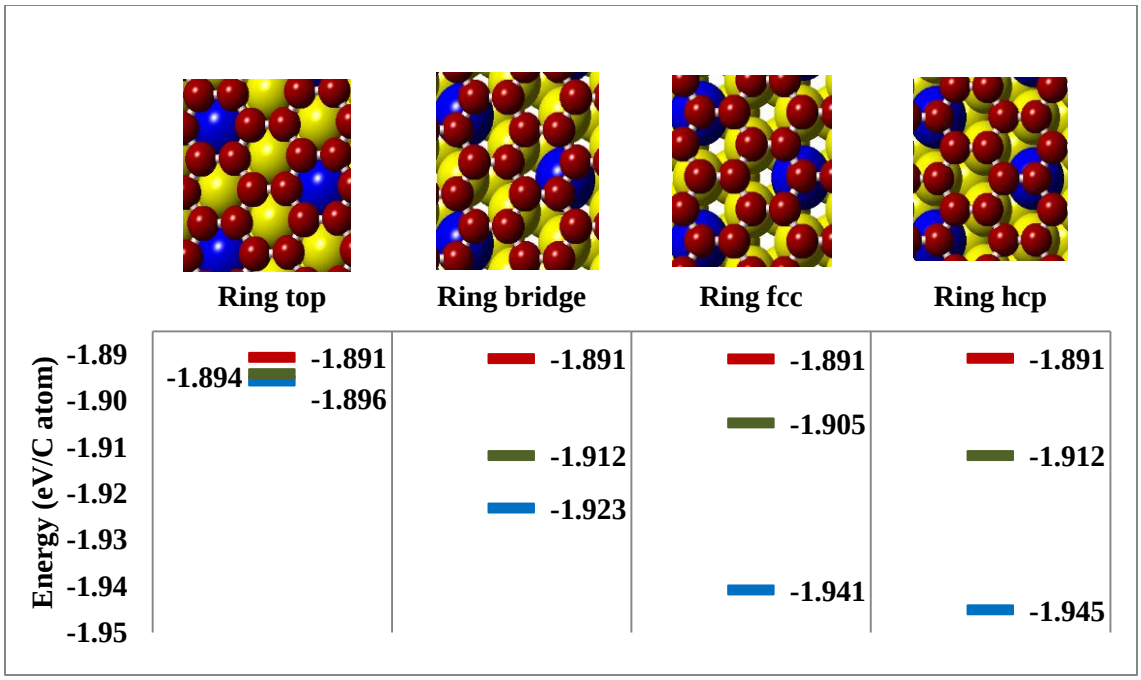

Figure 4.10. Formation energies of various graphene structures on promoted and un-promoted surface sites (Yellow – Co atom, Blue – Pt/Ru atom, Red – C atom; Blue marker – unpromoted Co surface, Red marker - Pt promoted surface, Green marker - Ru promoted surface).

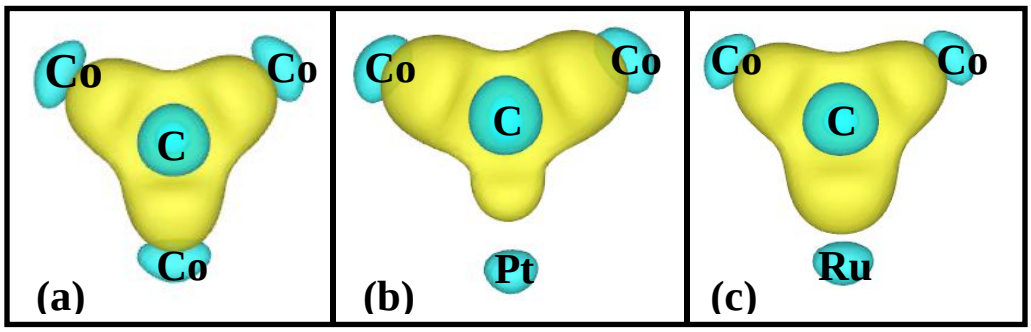

Figure 4.11. Isosurfaces of charge density difference at 0.02 e $Å^{-3}$ on (a) unpromoted Co surface (b) Pt promoted Co surface and (c) Ru promoted Co surface. Yellow and blue isosurfaces indicate charge accumulation and charge depletion respectively.

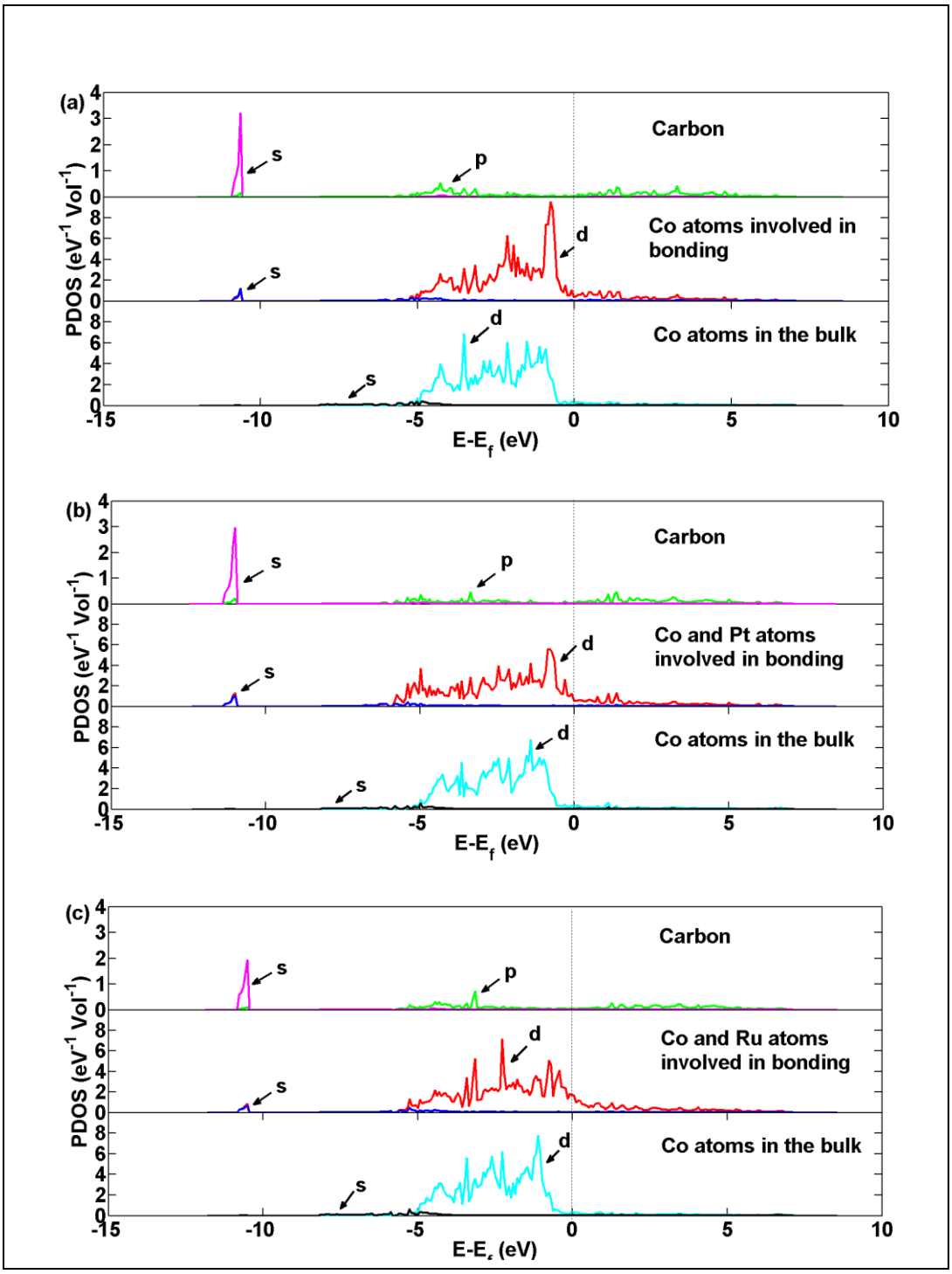

Figure 4.12. Spin up PDOS on (a) unpromoted Co surface (b) Pt promoted Co surface and (c) Ru promoted Co surface for a C atom adsorbed at hcp site. (0 eV corresponds to the Fermi level)

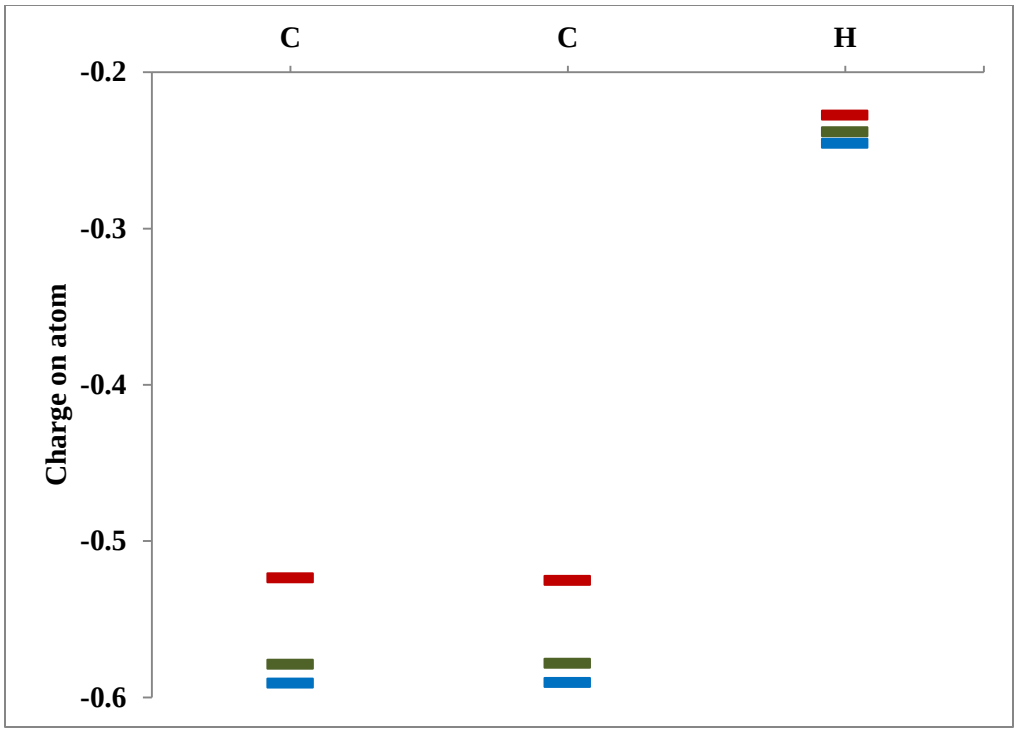

Figure 4.13. Charge on the individually adsorbed C and H atoms on promoted and un-promoted surfaces (Blue marker – unpromoted Co surface, Red marker- Pt promoted surface, Green marker- Ru promoted surface).

Table 4.1. Initial, transition, final states and activation barriers for forward and backward reactions for C-C coupling on unpromoted, Pt promoted and Ru promoted Co surface (Yellow – Co atom, Blue – Pt atom, Red – C atom).

Surface	Initial State	Activation barriers and transition State	Final State
H + C + C → CH + C			
Co	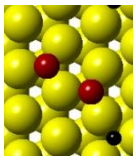	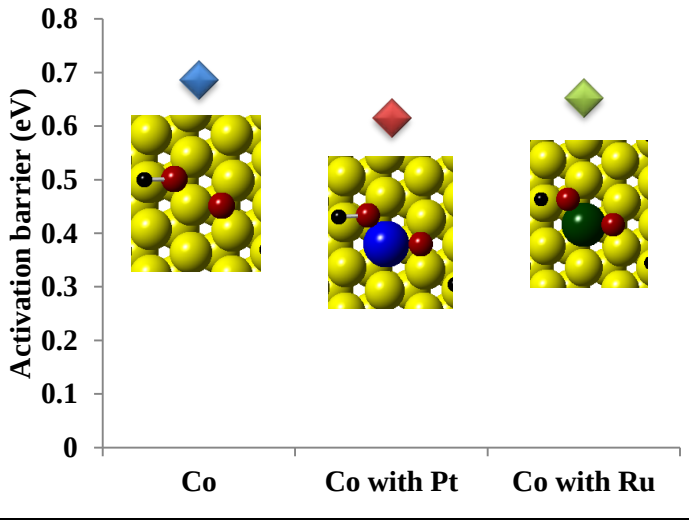	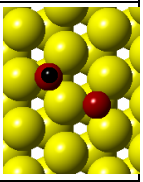
Co with Pt	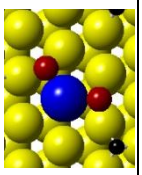		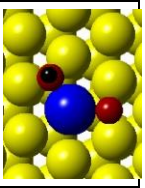
Co with Ru	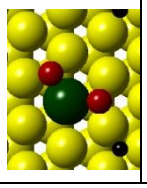		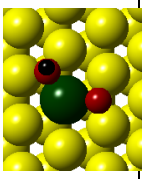
H + C + C → CC + H			
Co	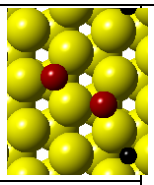	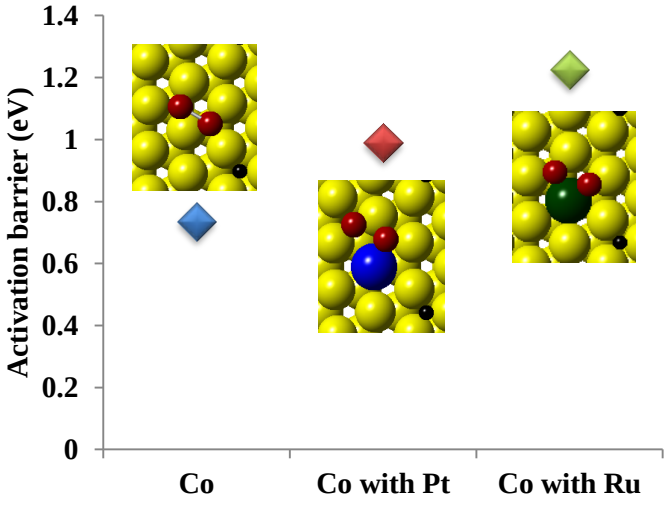	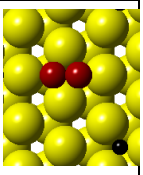
Co with Pt	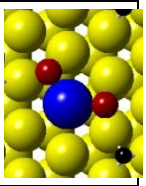		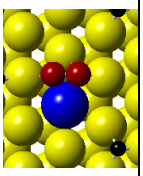
Co with Ru	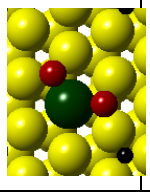		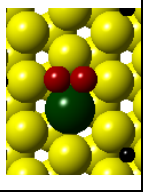

Table 4.2. Initial, transition, final states and activation barriers for forward and backward reactions for C-C-C coupling on unpromoted, Pt promoted and Ru promoted Co surface (Yellow – Co atom, Blue – Pt atom, Red – C atom).

Surface	Initial State	Activation barriers and transition State	Final State
CC + H + C → CCH + C			
Co	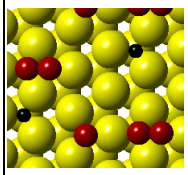	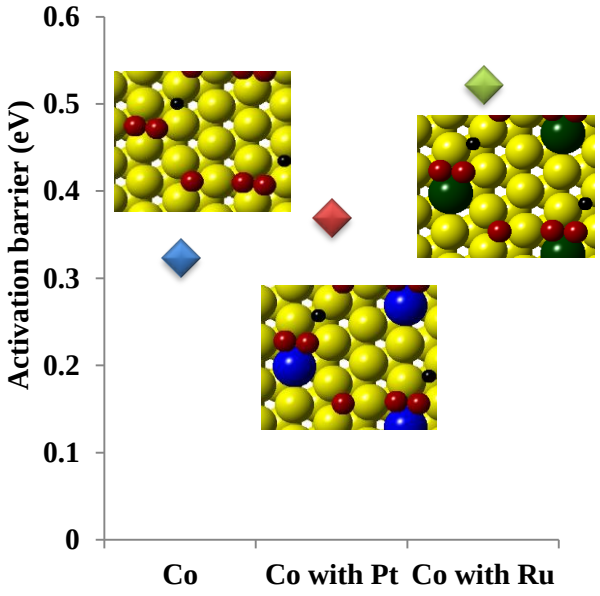	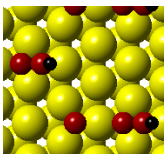
Co with Pt	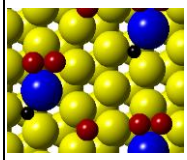		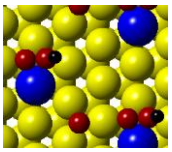
Co with Ru	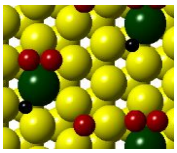		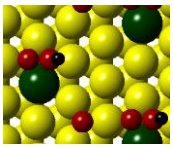
CC + H + C → CCC + H			
Co	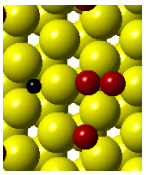	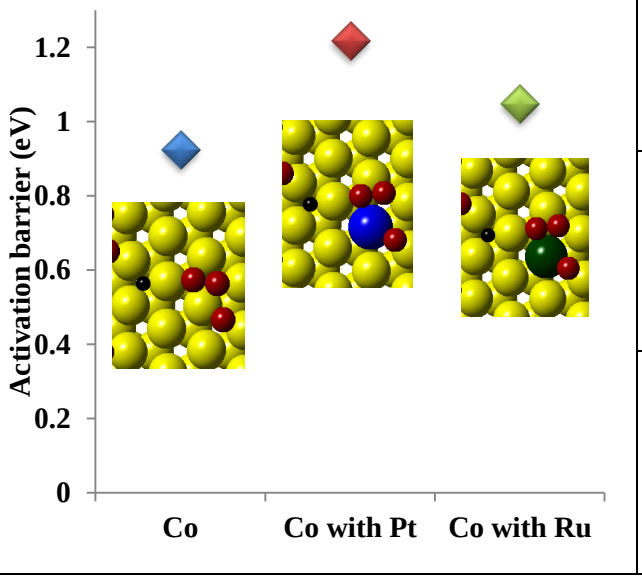	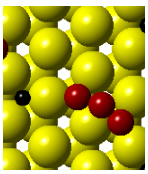
Co with Pt	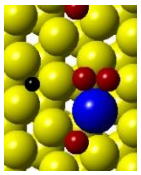		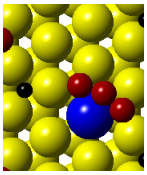
Co with Ru	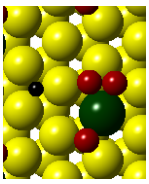		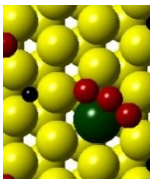

Table 4.3. The d-band center for the atoms involved in bonding for C in hcp position.

Surface	Co	Pt promoted Co	Ru promoted Co
d-band center	-1.055 eV	-1.577 eV	-1.028 eV

CHAPTER 5:

THEORETICAL INVESTIGATION OF THE INFLUENCE OF PLATINUM PROMOTER ON CO ACTIVATION PATHWAYS OF COBALT CATALYST

In this chapter, the influence of Pt promoter on FTS initiation pathway is investigated using DFT. CO activation is the first step in Fischer-Tropsch Synthesis (FTS). CO activation pathways for unassisted CO dissociation and hydrogenation of CO were determined on unpromoted and Pt promoted Co surfaces to determine the effect of promoter on the activation barriers and reaction pathways.

5.1. Introduction

FTS (Fischer-Tropsch Synthesis) is a process for the production of liquid fuel which includes CO activation, hydrogenation of carbon-containing species and oxygen, hydrocarbon chain growth and termination processes.[136] CO activation is the first step towards the production of FTS products. CO activation could occur either by unassisted CO dissociation or by H assisted CO dissociation.[6] The C formed by unassisted CO dissociation or CH formed by H assisted CO dissociation will couple with other C and H to form various hydrocarbons which then desorb from the catalyst surface via chain termination.

CO dissociation was widely accepted as the first step towards CO activation. Recently, H assisted CO dissociation was shown to be favored on Co catalysts.[6, 56] H_2 and

CO kinetic effects on FTS rates and density functional theory estimates of activation barriers and binding energies are consistent with H-assisted CO dissociation, but not with the previously accepted kinetic relevance of direct CO dissociation and chemisorbed carbon hydrogenation elementary steps.[56] Extensive density function theory calculations performed to study the mechanism of the formation of aldehyde and alcohol on Co surfaces showed that the preferred mechanism is pathway via CHO and also suggested that the CO-insertion mechanism may be responsible for the production of long-chain oxygenates.[6]

Promoters can affect the selectivity and activity of catalysts.[8, 137-139] Pt promotion of Co catalysts increased the CO hydrogenation rates[75, 77] and higher methane selectivity.[80, 108] Pt promoters also exhibit lower selectivity towards higher hydrocarbons.[70, 108] DFT studies on the influence of twelve transition metals (Zr, Mn, Re, Ru, Rh, Ir, Ni, Pd, Pt, Cu, Ag and Au) on Co showed that late transition metals (e.g. Pd and Cu) improved α-olefin selectivity.[8] Schanke *et al.*[75] found that Pt promoted Co had higher apparent turn-over numbers due to the increased coverage of reaction intermediates. Chu *et al.*[70] found that promotion of alumina supported Co catalyst with small amounts of Pt resulted in increased FT reaction rate and reduced selectivity towards C5+ hydrocarbons.

Promoters influence the activity and selectivity of catalyst by altering the energetics of a particular pathway and providing alternate routes for the reaction mechanism.[140-142] Promoters can alter the activation barrier of the reaction steps making a promoted surface more or less favorable for the formation of certain products. Promotion of precipitated Fe/Cu/SiO_2 catalyst with Ca, Mg and La promoters were shown to have

significant influences on the pathways of CO_2 and H_2O formation during the FTS reaction.[140] Kinetic studies on the effect of La, V and/or Fe promoters on Rh based catalysts showed that the addition of different promoters resulted in different rate-limiting steps influencing the activity and selectivity of CO hydrogenation.[141] K promoted Fe catalysts affected the reaction pathway for the formation of CH_4 while the pathway for formation of long chain hydrocarbons was unaffected.[142]

In this work, the influence of Pt promoters on the CO activation pathways of Co catalysts was studied. Plausible reactions for the CO activation pathways were studied to determine the barriers and pathway followed by a Pt promoted surface. These barriers and pathways would explain the impact of Pt promoter on activity or CO hydrogenation rate of Co catalysts.

5.2. Computational Details

In this work, VASP (Vienna Ab Initio Simulation package) code[30-32] was used with Perdew–Burke–Ernzerhof (PBE) form of the generalized gradient approximation (GGA)[86] for the exchange and correlation functional. Projector-augmented wave (PAW)[48] method was used to model the electron-ion interaction. Spin polarized calculations were done with a plane-wave cutoff energy of 500 eV. The convergence criterion for structure optimization and transition state search was set to an energy tolerance of about 0.01 eV/ Å and 0.05 eV/ Å respectively except for transition state search for H_2 dissociation where 0.01 eV/ Å was used. The accuracy of the settings was tested earlier.[121]

Stepped Co(0001) surface was modeled by removing two of the four rows of cobalt atoms on the top layer. The simulations were done using a slab supercell approach with periodic boundary conditions. Calculations were carried out on a 4x2 surface of stepped Co(0001) with 4 layers of atoms consisting of 28 atoms. Among the 4 layers of metal atoms, the bottom two layers were frozen and top 2 metal layers and the adsorbates were allowed to relax. Our previous results showed that the energy difference between 5 layers of atoms and 4 layers of atoms on stepped surface were found to be less than 0.02 eV and hence 4 layers of atoms were studied. [121] One of the atoms on the slab surface was replaced by platinum as shown in Figure 5.1. Surface Monkhorst[89] Pack meshes of 5x2x1 k-point sampling in the surface Brillouin zone was used. The vacuum region between the slabs was set to about 10 Å to reduce interactions. We used a one-sided slab approach in our calculations. The activation barriers and the transition states were determined using the CI-NEB method developed by Jonsson and co-workers and the minimum energy path (MEP) was identified. Normal mode harmonic frequencies were calculated to confirm the transition states.

5.3. Results

5.3.1. CO Dissociation

Dissociation of CO into C and O was studied on stepped Co and Pt promoted Co surface. In the initial state of the lowest energy pathway for CO dissociation, CO prefers a step-corner site and after dissociation C occupies an fcc site in the lower terrace and O occupies an hcp site the upper terrace on both unpromoted and Pt promoted surface. In the transition state, CO occupies an edge bridge site on both the surfaces and C occupies

an hcp site and an fcc site in the lower terrace on unpromoted and Pt promoted surface respectively. The barriers and transition states for CO dissociation on both the surfaces are given in Table 5.1. The C-O distance in the initial state was found to be 1.307 Å (1.284 Å)[91] and 1.311 Å on unpromoted and Pt promoted surfaces respectively. The C-O distance in the transition state was found to be 2.164 Å (2.170 Å)[91] and 3.163 Å on unpromoted and Pt promoted surface respectively. The transition states and distances on Co(0001) surface are similar to the results of Gong *et al.*[91] Pt promoter slightly increased the activation barrier for CO dissociation on the Co surface.

5.3.2. H_2 Dissociation

H_2 dissociates on adsorbtion on both the unpromoted and Pt promoted Co surface. After dissociation, both the H adsorb on fcc sites in the upper terrace on the unpromoted surface and on edge bridge sites on the Pt promoted surface. The distance between H atoms in the gaseous phase, transition state and after dissociation are 0.754 Å, 0.760 Å and 2.506 Å respectively on unpromoted Co surface and 0.755 Å, 0.764 Å and 2.706 Å respectively on Pt promoted Co surface. The barriers and transition states are given in Table 5.2. The barrier is very small suggesting that H_2 dissociation takes place very easily on both the surfaces and due to the very small barrier Pt promoter does not have any effect on the reaction.

5.3.3. Hydrogenation of CO

The barriers and transition states for the formation of HCO (formyl) and COH (hydroxymethylidyne) from CO and H on unpromoted and Pt promoted Co surface were calculated and are given in Table 5.3. The initial state of the lowest energy pathway for

the formation of HCO has CO and H on a step-corner site and an fcc site in the lower terrace respectively on both the promoted and unpromoted surfaces. The transition state has CO on a step-corner site and H on a top site on both the surfaces. The distance between CO and H was about 1.497 Å (1.55 Å)[143] and 1.527 Å in the transition state on unpromoted and Pt promoted surfaces respectively. HCO adsorbs on a corner site with C in the lower terrace hcp site and O near an edge bridge site on both the surfaces. Pt promoter lowers the activation barrier for the formation of HCO but the reverse barrier is similar on both the surfaces.

The lowest energy pathway for the formation of COH has CO and H on a step-corner site and hcp site in the upper terrace in the initial state on both the surfaces. The transition state has CO on an hcp site in the lower terrace and H on the edge bridge site on both the surfaces. The distances between CO and H were about 1.238 Å (1.23 Å)[143] and 1.245 Å in the transition state on the unpromoted and Pt promoted surfaces respectively. COH adsorbs on a step-corner site with C on the step-corner site on both the surfaces. Pt promoter lowers the activation barrier for the formation of COH and the reverse barrier is larger on the Pt promoted surface.

5.3.4. Hydrogenation of HCO and COH

COH can hydrogenate to form HCOH (hydroxymethylene) and HCO can hydrogenate to form CH_2O (formaldehyde). The barriers and transition states for the lowest energy pathways are given in Table 5.4. COH on a step-corner site reacts with H on an hcp site on the upper terrace to form HCOH on an edge bridge site with C on the edge bridge on both promoted and unpromoted CO surfaces. COH stays in the step-

corner site and H occupies an edge bridge site in the transition state. The distance between C and H in the transition state is 1.259 Å (1.32 Å)[143] and 1.255 Å on the unpromoted and Pt promoted surface respectively. Pt promoter lowers the activation barrier for the formation of HCOH and the reverse barrier is also lower on the promoted surface.

HCO on a corner site reacts with H on an hcp site in the upper terrace to form CH_2O on an edge bridge site with C on the edge-bridge and O on a Co top site on both the surfaces. The distance between C and H in the transition state is 1.708 Å (1.59 Å)[143] and 1.832 Å on the unpromoted and Pt promoted Co surfaces respectively. In the transition state, HCO occupies and edge bridge site and H occupies a top site on both the surfaces. Pt promoter decreases the activation barrier for the formation of CH_2O on the Co surface and the reverse barrier is also decreased on the promoted surface.

5.4. Discussion

The activation barriers for unassisted CO dissociation on both unpromoted and promoted Co surfaces are high compared to the barriers for H-assisted CO dissociation via HCO/COH formation. Hence, on both the stepped surfaces H-assisted CO dissociation would be preferred over unassisted CO dissociation. Ojeda *et al*.[56] suggested H-assisted CO dissociation to be the primary CO activation pathway on flat Co surface. According to their kinetic studies,[56] the first hydrogenation step is quasi equilibrated and the second hydrogenation step is kinetically relevant during CO activation. Hydrogenation of CO is highly likely to occur on Co stepped surfaces even in the presence of Pt promoter and Pt promoter increases the activation barrier for unassisted or

direct CO dissociation. The barrier for H_2 dissociation on unpromoted and Pt promoted CO surface was found to be very small. Hence H_2 molecule would readily dissociate to form H which then reacts with CO to form FTS products. Pt promoter did not have influence on H_2 dissociation barrier as the reaction could readily happen even on unpromoted Co surface.

Hydrogenation of CO on Co surface could occur via the formation of HCO or COH. HCO and COH can also hydrogenate to form CH_2O and HCOH as shown in Figures 5.2-5.3. Various FTS products could then be formed by dissociation, coupling, hydrogenation or oxidation of previously formed products. The barrier for the formation of HCO was found to be lower than the barrier for COH formation on both the unpromoted and Pt promoted Co surfaces. In addition, the barrier for formation of COH and HCO were lowered on Pt promoted CO surface. The barrier for the second hydrogenation reaction was again found to be lower in the pathway via HCO on both unpromoted and Pt promoted surface. Pt promoter also decreased the barrier for the second hydrogenation step for the pathway via HCO and the barrier for the second hydrogenation step via COH was also reduced. But the barrier for the formation of CH_2O was still lower than the barrier for the formation of HCOH. Hence, both the Pt promoted and unpromoted CO surface would follow the same CO activation pathway via HCO.

The lower activation barrier for the formation of HCO and CH_2O on Pt promoted Co surface compared to the unpromoted Co surface shows that hydrogenation of CO could occur on Pt promoted Co surface faster than that on unpromoted Co surface accounting for the faster CO hydrogenation rates observed on Pt promoted Co catalyst.[75,

[77] Thus, the activity of Pt promoted catalyst would be higher than unpromoted Co catalyst.

5.5. Conclusions

Direct CO dissociation was found to have high barriers on stepped Co surface and Pt promoted stepped Co surface. The dissociation of H_2 was found to occur with very lower barriers on both the unpromoted and Pt promoted surfaces suggesting that hydrogenation of CO would most likely occur than direct CO dissociation. CO hydrogenation was found to occur via HCO formation on both the surfaces. Pt promoter lowered the barrier for both the hydrogenation steps suggesting that Pt promoter would increase the CO hydrogenation rate of Co catalyst.

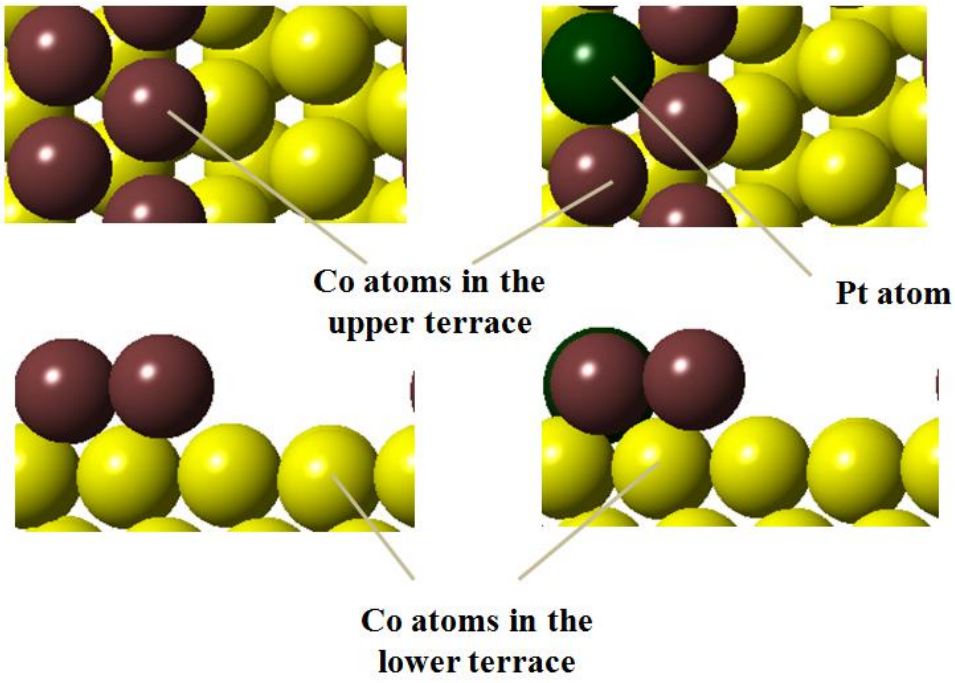

Figure 5.1. Models showing the stepped Co surface and stepped Pt promoted Co surface.

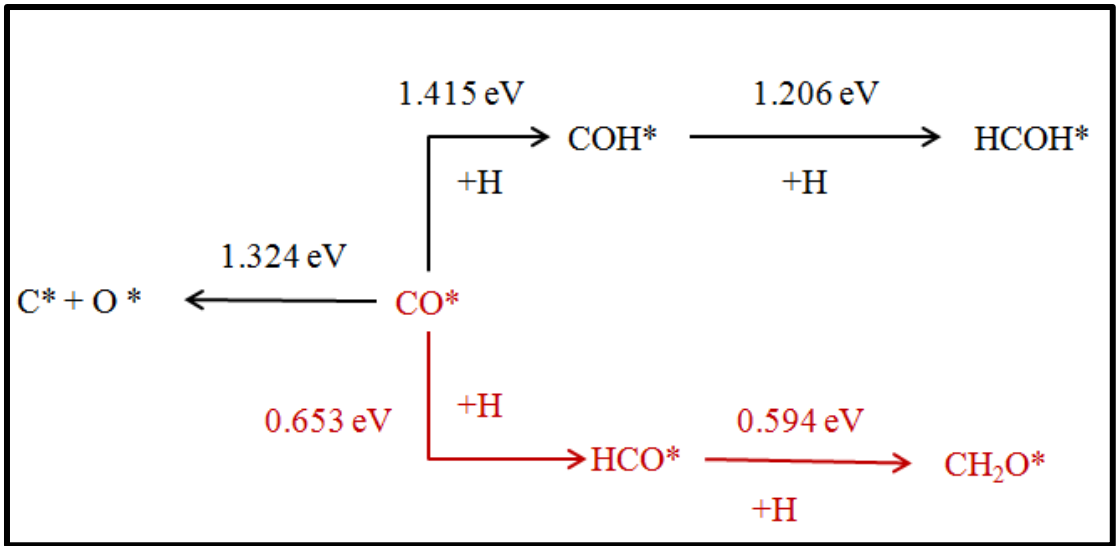

Figure 5.2. Pathways and activation barriers for unassisted and H-assisted CO dissociation on stepped Co surface. The most feasible pathway is given in red.

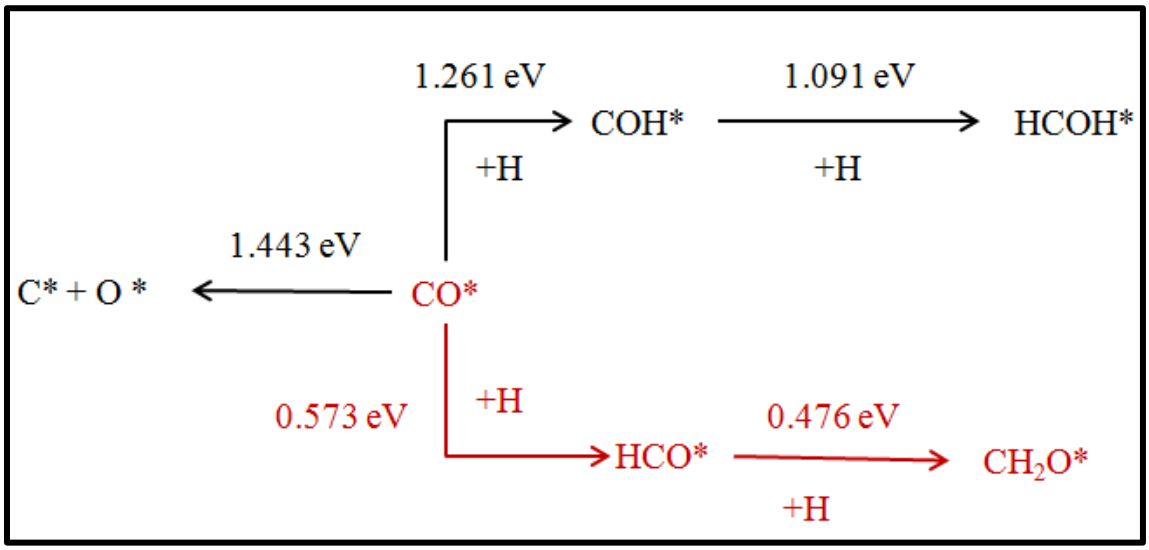

Figure 5.3. Pathways and activation barriers for unassisted and H-assisted CO dissociation on Pt promoted stepped Co surface. The most feasible pathway is given in red.

Table 5.1. Initial, transition, final state and forward and reverse barriers for CO dissociation on unpromoted and Pt promoted surfaces. (Yellow-Co atom, Brown-Co atom in the upper terrace, Green- Pt atom, Red- O atom, Black- C atom).

Surface	**Initial state**	**Barriers and Transition state**	**Final state**	**Forward barrier (eV)**	**Reverse barrier (eV)**
Co	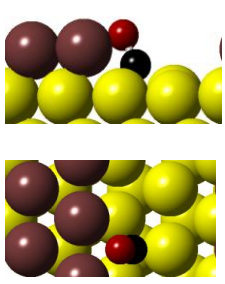	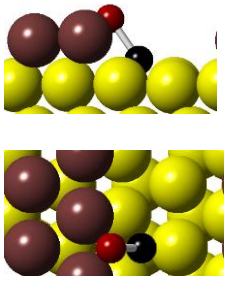	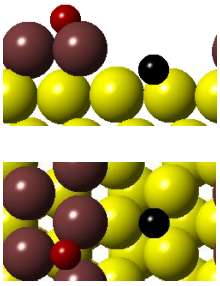	1.324 (1.61) [91]	0.424 (1.4) [91]
Pt promoted Co	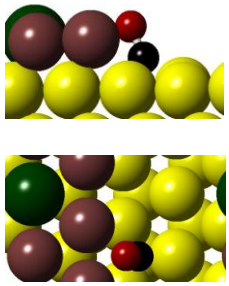	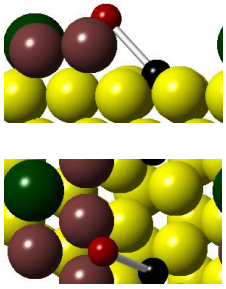	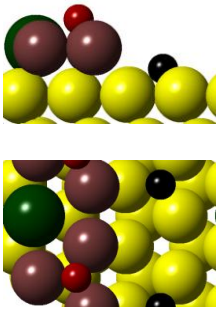	1.443	0.274

Table 5.2. Initial, transition, final state and barriers for forward and reverse reactions for H_2 dissociation on unpromoted and Pt promoted surfaces. (Yellow-Co atom, Brown-Co atom in the upper terrace, Green- Pt atom, Grey- H atom).

Surface	**Initial state**	**Transition state**	**Final state**	**Forward barrier (eV)**	**Reverse barrier (eV)**
Co	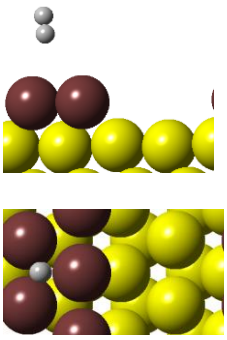	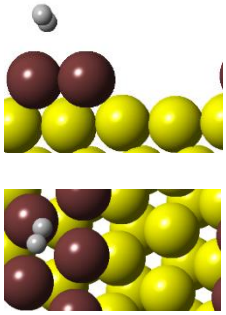	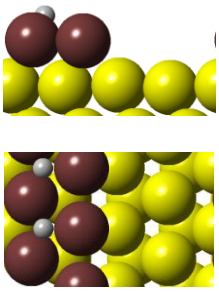	0.029	1.135
Pt promoted Co	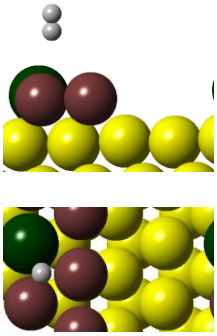	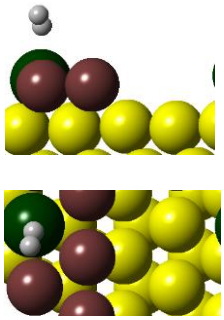	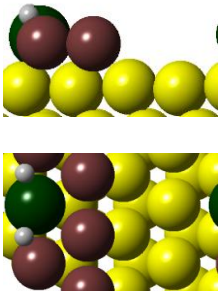	0.023	0.989

Table 5.3. Initial, transition, final state and barriers for forward and reverse reactions for first hydrogenation on unpromoted and Pt promoted surfaces. (Yellow-Co atom, Brown-Co atom in the upper terrace, Green- Pt atom, Red- O atom, Black- C atom, Grey- H atom).

Surface	**Initial state**	**Barriers and Transition state**	**Final state**	**Forward barrier (eV)**	**Reverse barrier (eV)**
CO+H → HCO					
Co	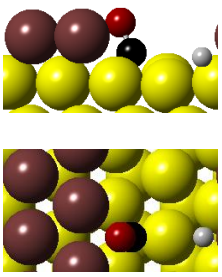	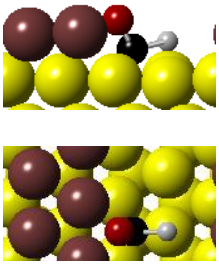	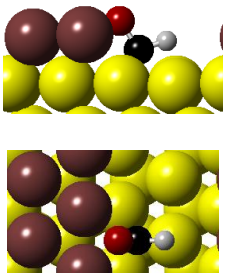	0.653 (0.77)[143]	0.089 (0.12)[143]
Pt promoted Co	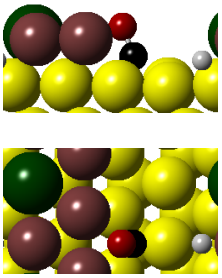	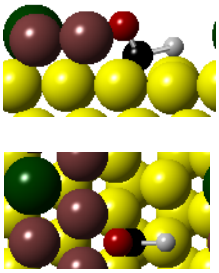	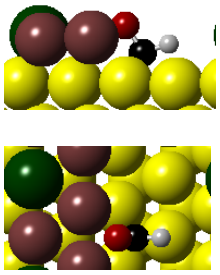	0.573	0.088
CO+H→COH					
Co	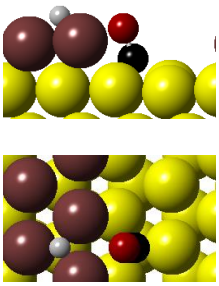	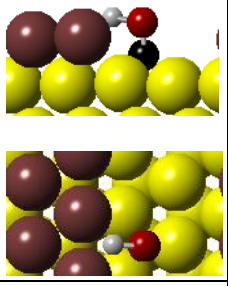	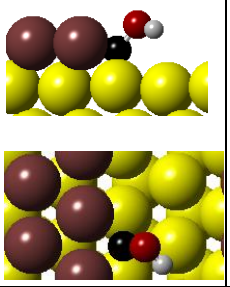	1.415 (1.46)[143]	0.676 (0.51)[143]
Pt promoted Co	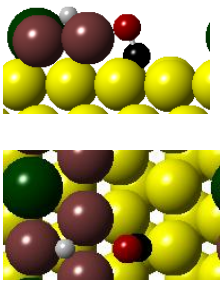	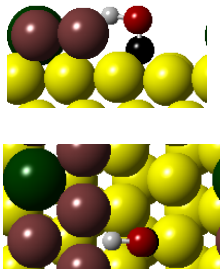	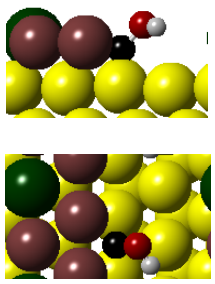	1.261	0.747

Table 5.4. Initial, transition, final state and barriers for forward and reverse reactions for second hydrogenation on unpromoted and Pt promoted surfaces. (Yellow-Co atom, Brown-Co atom in the upper terrace, Green- Pt atom, Red- O atom, Black- C atom, Grey- H atom).

Surface	**Initial state**	**Barriers and Transition state**	**Final state**	**Forward barrier (eV)**	**Reverse barrier (eV)**
COH+H → HCOH					
Co	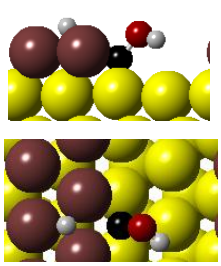	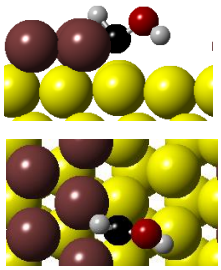	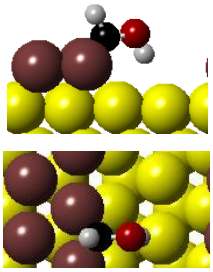	1.206 (0.77)[143]	0.607 (0.51)[143]
Pt promoted Co	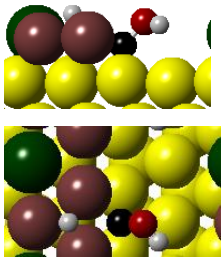	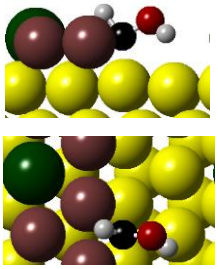	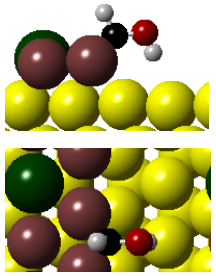	1.091	0.552
HCO+H →CH_2O						
Co	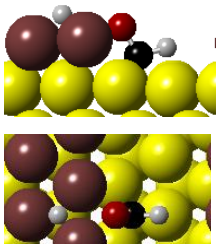	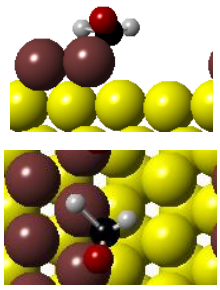	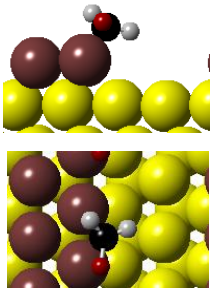	0.594 (0.71)[143]	0.441 (0.34)[143]
Pt promoted Co	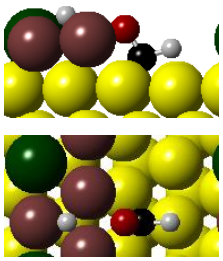	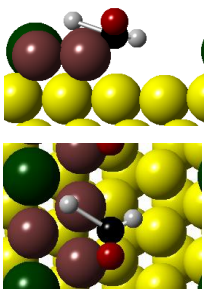	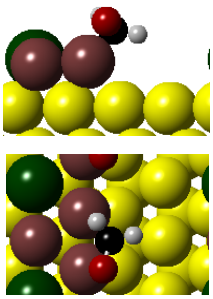	0.476	0.397

CHAPTER 6:

CARBON MONOXIDE OXIDATION BY COBALT OXIDE: A THEORETICAL STUDY ON REACTION KINETICS

This chapter discusses the mechanism of CO oxidation on CoO catalyst using first principle calculations. DFT calculations were done to find the transition states and the activation barriers for CO oxidation reaction on CoO(100) with the objective of finding the reaction pathways. Four possible mechanisms of CO oxidation were explored to determine the activation barriers for each step of the reaction mechanism. The mechanism with the lowest activation energy will be the most feasible pathway for CO oxidation on CoO. The computed activation barriers were then compared to the barriers determined experimentally.

6.1. Introduction

Considerable interest has grown towards CO oxidation owing to the increasing air pollution from exhausts gases of industry and automobiles as well as to remove CO from the reformer gas to avoid poisoning of fuel cell catalysts.[9-13] Precious metals like Pd,[16] Pt,[16] Rh,[144] Ru[145] and metal oxides[17-18, 146-148] have been widely used for CO oxidation and CO oxidation mechanism has been well established on such metals and metal oxides. Metal oxides were found to be more efficient than their unoxidized metals with lower

activation energies for CO oxidation.[19-21] Inexpensive catalysts are being explored for CO oxidation to replace the traditional noble metal catalyst.[147, 149-157]

Understanding the reaction mechanism of CO oxidation at the molecular level is the first step towards designing catalyst with better efficiency. During CO oxidation, CO can combine with O in the lattice to form CO_2 *via* Mars–van Krevelen mechanism or O_2 can dissociate to react with CO to form an intermediate and then form CO_2 *via* Langmuir Hinshelwood mechanism or O_2 can directly combine with CO to form an intermediate and then form CO_2. On Pd,[16] Pt[16] and Fe_2O_3,[17] CO oxidation follows Langmuir Hinshelwood mechanism where CO and dissociated O_2 gets adsorbed on the surface which then reacts to form CO_2. On PtO, CO reacts with O_2 adsorbed at a bridge site to form OO-CO intermediate which then forms CO_2.[18] On $Cu_2O(111)$,[146] two pathways were found to be viable: (i) where CO in the gas phase reacts with adsorbed O_2 to form CO_2 and (ii) where the adsorbed CO and adsorbed O_2 molecule react to form an intermediate OO-CO which then produces CO_2.

DFT calculations on Co_3O_4 nanorods[147] and $Co_3O_4(110)$[158] surface showed that CO molecule extracts the two fold coordinate oxygen from the lattice to form CO_2 and an oxygen molecule dissociates to fill the oxygen vacancy. Co_3O_4 nanorods exposing (101) facets were found to be efficient for CO oxidation even at temperatures as low as -77°C owing to the presence active Co^{3+} ions on the (101) facets.[147] On crude cobalt oxide (CoO_x) with high valence cobalt, adsorbed CO and adsorbed O_2 molecule react to form CO_2.[159] CO oxidation studies on CoO are limited and the mechanism is not yet clear.

DFT+U calculations were applied to calculate activation energies for postulated reaction mechanisms of CO oxidation reaction on CoO(100). DFT does not accurately treat the localized electrons of CoO and predicts CoO to be a metal.[160] Adding the Hubbard U correction to the DFT would describe the strongly correlated 3d electrons of CoO more accurately and predict the correct band gap of CoO. To the best of our knowledge, studies on mechanistic pathways of CO oxidation on CoO(100) are not available.

The results from our DFT calculations were compared with the experiments done by Mankidy.[29] Mankidy synthesized CoO nanoparticles of various sizes (1, 2, 6 and 14 nm) using thermal decomposition technique. The CoO nanoparticles were then immobilized on the surface of Stober SiO_2 support by surface functionalization methods. Temperature programmed in-situ surface IR experiments were done to determine the activation energies for CO oxidation on these nanoparticles. The IR spectra showed bands at 2058 cm^{-1} corresponding to adsorbed CO, 2140 cm^{-1} and 2170 cm^{-1} corresponding to CO in bulk gaseous phase as CO was introduced into the reactor. As the temperature was ramped from 475ºC at various heating rates, the peaks at 2058 cm^{-1}, 2140 cm^{-1} and 2170 cm^{-1} had a disappearing trend and new peaks appeared at 2350 cm^{-1} and 2342 cm^{-1} corresponding to the formation of CO_2 gas. Two activation energies were calculated based on the disappearance of peak for adsorbed CO (step-1) and appearance of CO_2 gas (step-2) peak. The activation energies were found to be small for the first step and larger for the second step. In addition, the activation energies for both the steps were found to increase with the increase in nanoparticle size. However, the experiments did not provide any information about the reaction intermediates. DFT calculations were

done to determine the reaction intermediates and the activation barriers to validate the experimental results.

6.2. Methods

VASP (Vienna Ab initio Simulation Package) code[30-32] was used with Perdew–Burke–Ernzerhof (PBE) form of the generalized gradient approximation (GGA)[86] for the exchange and correlation functional. The electron-ion interaction was modeled by the projector-augmented wave (PAW)[48] method. A kinetic energy cutoff of 500 eV was used. DFT+U method by Dudarev *et al.*[161] was used in spin polarized DFT-PBE calculations which accurately treats the strongly localized d or f electrons. Spin-orbit coupling (SOC) was neglected in our calculations. The convergence criterions for structure optimization and transition state search were set to an energy tolerance of 0.01 eV/Å and 0.05 eV/Å respectively. A U value of 10 eV was optimized with a J value of 1.0 giving a U_{eff} value of 9 eV (U_{eff} for CoO = 6.88 eV)[162] with a band gap of 2.523 eV close to the experimental value (2.53 eV)[163]. The bulk lattice parameter for rocksalt structure of CoO was found to be 4.253 Å (Exp. value = 4.258 Å)[164] and the magnetic moment on cobalt was determined to be 2.85 μB (Theoretical value of spin orbital moment = 2.69 μB).[165]

DFT + U method is well known to possess orbital degrees of freedom giving multiple meta stable states with energies varying by several eV per formula unit.[166] Two methods have been used to reach the ground state within the DFT+U formulation, namely: 1. Monitoring of the occupation matrix of the correlated orbitals[166] 2. U-ramping method.[167] In the first method, the ground state is reached by imposing different

occupation matrices for the valence d or f level during the first 10 iterations of calculation. Each occupation matrix leads to different final state and the ground state is the lowest energy state. In the second method, the value of U is increased after iteratively applying the occupation matrices (wavefunctions and charge density in VASP) from the previous calculations until all bands are integrally occupied. The ground state can then be confirmed by monitoring the occupation matrix. This method was proved to be efficient for a number of compounds like CoO, NiO, UO_2, CeO_2.[167] U-ramping method is easier to apply to a calculation in VASP where initializing an occupation matrix is not straightforward. We used U-ramping method on the CoO(100) surface with various adsorbants from Ueff = 0 eV for DFT calculations to Ueff = 9 eV with increments of 1 eV.

CoO(100) surface was chosen for our study since it is the most stable surface for the rocksalt structure that has the lowest surface energy with one broken bond per surface atom. The CoO(100) surface has both Co^{2+} and O^{2-} ions. CoO(100) surface was simulated using a slab supercell approach with periodic boundary conditions. For this purpose, a (2x2) supercell of CoO (100) surface with 4 layers of atoms consisting of 64 atoms was considered. Among the 4 layers of metal atoms, the bottom two layers were frozen and top 2 metal layers and the adsorbates were allowed to relax. Surface Monkhorst[89] Pack meshes of 3x3x1 k-point sampling in the surface Brillouin zone were used. The vacuum region between the slabs was set to about 10 Å to reduce interactions. We used a one-sided slab approach in our calculations. The adsorption energy of an adsorbant A on the surface is given by $E_{ads} = E_{slab} + E_A - E_{tot}$, where E_A is the energy of isolated adsorbate A, E_{slab} is the energy of the clean metal surface and E_{tot} is the total

energy of the slab with adsorbate A. After determining the ground state of various possible adsorbants on the surface, the transition state for each reaction pathway was located using the climbing-image nudged elastic band (CI-NEB) method developed by Jonsson and co-workers [49-51] and the minimum energy path (MEP) was identified.

6.3. Results and Discussion

Four possible mechanisms were considered for CO oxidation on CoO based on, previously determined mechanisms on various metals and metal oxides[146, 168-170] as shown in Schemes 6.1 – 6.4.

In mechanism I, CO adsorbed on the surface reacts with the lattice oxygen O_L on the CoO(100) surface to form CO_2 and leaves a vacant oxygen site (O_V) on the surface.[168] In mechanism II, CO adsorbed on the surface reacts with adsorbed oxygen to form an intermediate OOCO which later forms CO_2 leaving an oxygen atom behind on the surface.[169] In mechanism III, CO adsorbed on the surface reacts with molecular oxygen to form an intermediate OCO and O on the surface.[170] In mechanism IV, O_2 dissociates to form 2 O atoms on the surface which then reacts with CO adsorbed on the surface to form an intermediate OCO which then desorbs as CO_2.[146] OCO intermediate then desorbs to form CO_2 in the gaseous phase. Only pathways with the lowest activation barriers are reported here. For the three proposed mechanisms, CO adsorption at 3 different sites was considered: cobalt top, oxygen top and bridge site between cobalt and oxygen. It was found that CO initially placed on an oxygen atom relaxed to the bridge site. Therefore, among all the configurations, cobalt top and bridge positions were found to be the most

stable configurations where CO adsorbs vertically with C atom directed towards the surface.

6.3.1. CO Reacting with Lattice Oxygen

The bridge site was found to be the most stable configuration with CO adsorbing at an angle with C atom at the bridge and O close to a surface O atom. The activation barrier for the adsorbed CO to react with lattice oxygen to form CO_2 was found to be 289.5 kJ/mol. The transition states and barriers are given in Figure 6.1. Mechanism I was ruled out due to the high activation energy required for the adsorbed CO to react with O_L to form CO_2.

6.3.2. CO Reacting with O_2 in the Gas Phase

In mechanism II, CO_2 formation followed two steps. In the first step, adsorbed CO combines with adsorbed O_2 to form an OOCO intermediate. In the second step, the OOCO dissociates into CO_2 gas leaving an adsorbed O atom on the surface. The lowest activation barriers for these two steps were found to be 80.1 kJ/mol and 154.4 kJ/mol respectively. Similarly, the CO_2 formation is a two-step process in the case of mechanism III. The activation barrier for the first step was found to be 51.2 kJ/mol for reaction between O_2 and CO that was adsorbed on the bridge site to form an OCO intermediate on an O_L top site. The activation energy for the second step was 95.5 kJ/mol. The activation barriers for the reaction where the oxygen dissociates before the formation of the intermediate OCO as in mechanism IV was also calculated. The dissociated oxygen formed a bond with CO which was similar to the OCO intermediate. The transition states and the reaction barriers for mechanism IV were also found to be similar to mechanism

III. Comparing both mechanisms, mechanism III is more likely due to the lower energy barriers obtained. Figure 6.1 – 6.4 depicts the activation barriers and transition states for the reactions occurring on CoO(100). This leaves us finally to find the activation barriers for an adsorbed CO to react with the O atom that was retained from previous reaction which can be written as follows:

$$CO + O \rightarrow OCO \rightarrow CO_2 \quad (6.1)$$

The O atom on top of a cobalt site combines with another CO on top site of cobalt to form a CO_2 molecule. The activation barriers and the transition states for this reaction are shown in Figure 6.5. In this case, there was no energy barrier for the formation of OCO on an oxygen top site as it was a downhill process. The barrier for dissociation of CO_2 was 84.9 kJ/mol. Therefore, from these calculations, the overall mechanism for CO oxidation on a CoO(100) can be written as:

$$CO + O_2 \rightarrow OCO + O \rightarrow CO_2 + O \quad (6.2)$$

$$CO + O \rightarrow OCO \rightarrow CO_2 \quad (6.3)$$

Experimental results of Mankidy[29] showed that the activation energies varied from 9.4 kJ/mol to 21.3 kJ/mol for step-1 and from 63.6 kJ/mol to 95.4 kJ/mol for step-2 as the size of CoO nanoparticle increases. The activation energies for both the steps increased with the increase in nanoparticle size. There is agreement between the DFT results and the experiments in predicting the activation barrier for step-2 to be larger than the barrier for step-1 and the activation barrier for step-2 was found to be in agreement with the activation barrier from the experiments. The experimental results are shown in Figure 6.6.

To determine the effect of size using DFT, the optimized lattice constant of CoO cell was reduced by 1% to represent a smaller size particle as the average lattice constant would be smaller for a small size particle.[171-173] The activation barrier for step-2 in mechanism III was re-calculated for the surface with modified lattice constant and was found to be 60.1 kJ/mol. Thus, both experiments and DFT calculations show that activation barriers increase with particle size.

6.4. Conclusions

Four possible mechanisms for CO oxidation on CoO(100) were explored to determine the most feasible mechanism. DFT+U calculations show that CO oxidation on CoO occurs via a 2-step mechanism where adsorbed CO reacts with O_2 molecule to form an intermediate OCO which then desorbs to form CO_2 gas. The activation barriers were found to be 51.2 kJ/mol and 95.5 kJ/mol for steps one and two respectively for bulk CoO(100). The results are in agreement with experiments where the activation energy for step-2 was found to be larger than step-1. The activation barrier was also found to decrease with the decrease in lattice spacing of bulk CoO(100) surface suggesting that activation energy would decrease with decrease in particle size in agreement with experiments.[29]

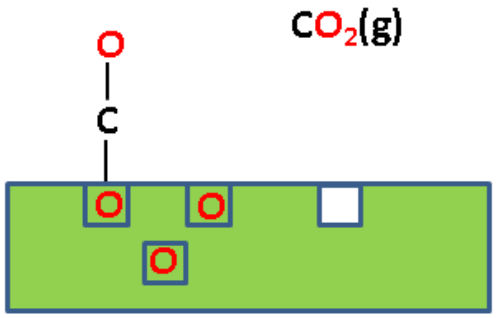

Scheme 6.1. Pathway for mechanism I.

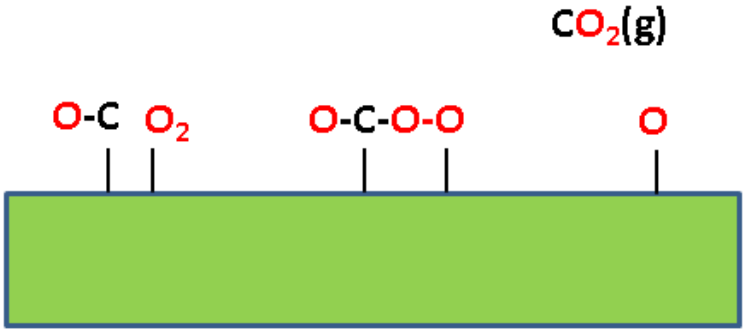

Scheme 6.2. Pathway for mechanism II.

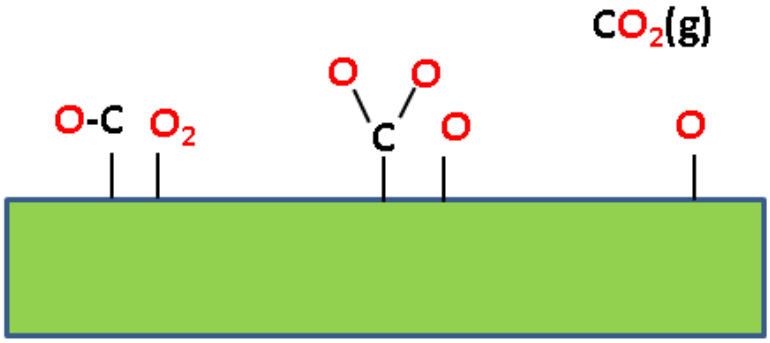

Scheme 6.3. Pathway for mechanism III.

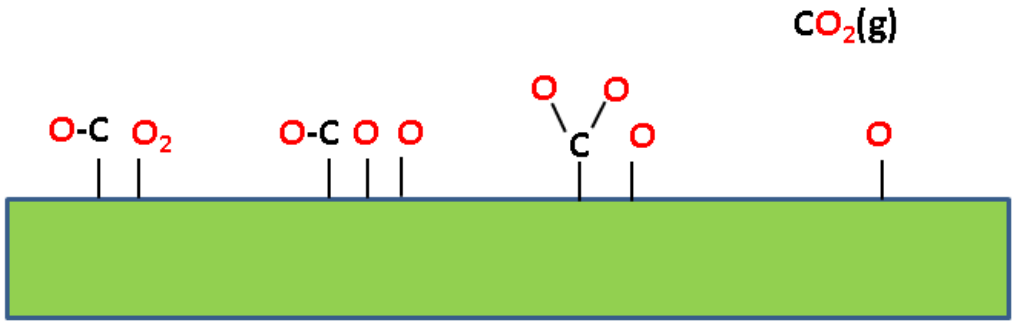

Scheme 6.4. Pathway for mechanism IV.

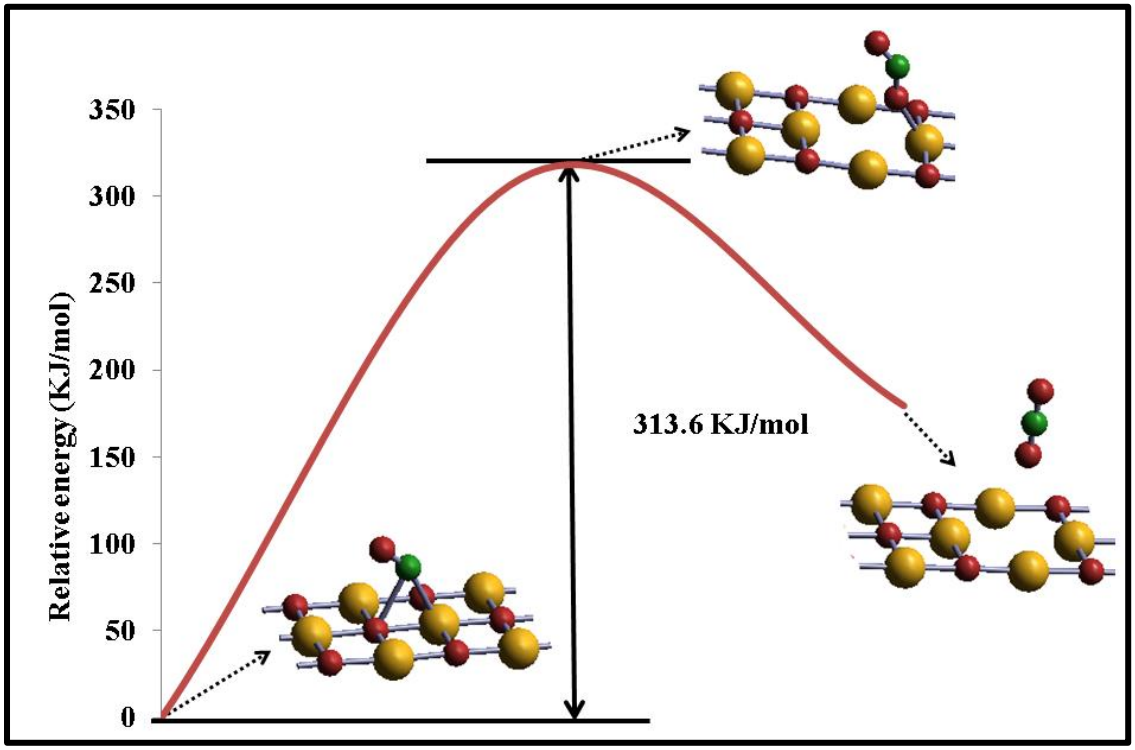

Figure 6.1. Activation barriers and transition states for the reactions CO + O_L → CO_2 + O_V. (Yellow-Co atom, Red- O atom, Green- C atom).

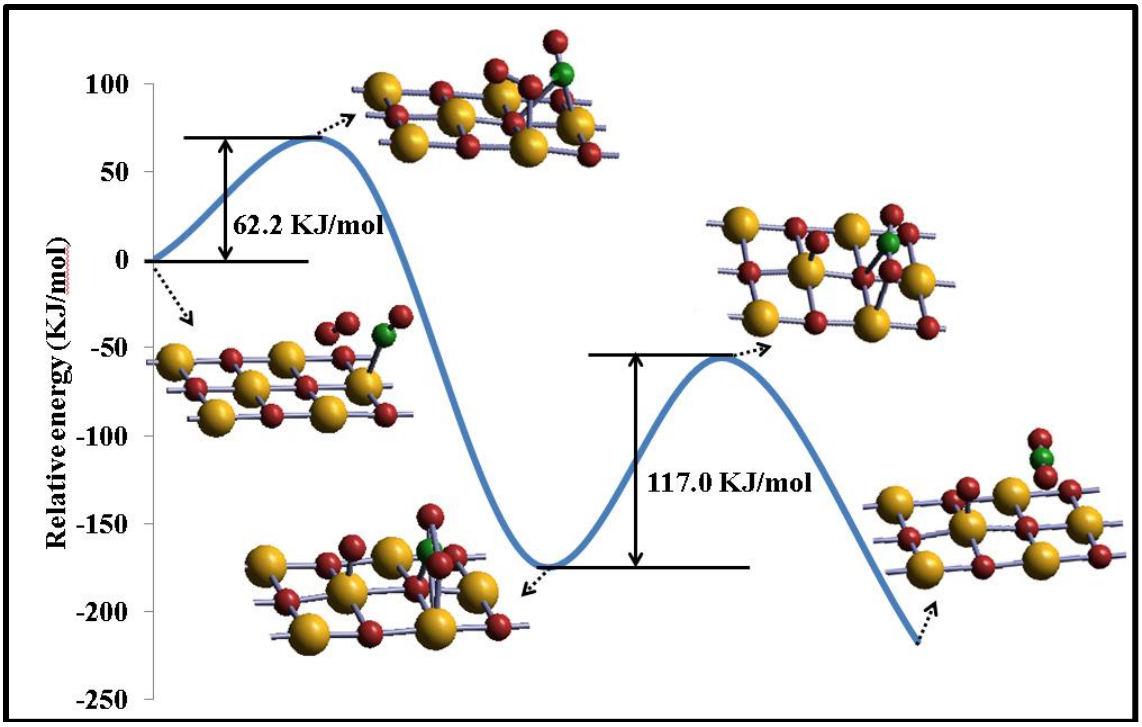

Figure 6.2. Activation barriers and transition states for the reactions CO + O_2 → CO + O + O → OCO + O → CO_2 + O. (Yellow-Co atom, Red- O atom, Green- C atom).

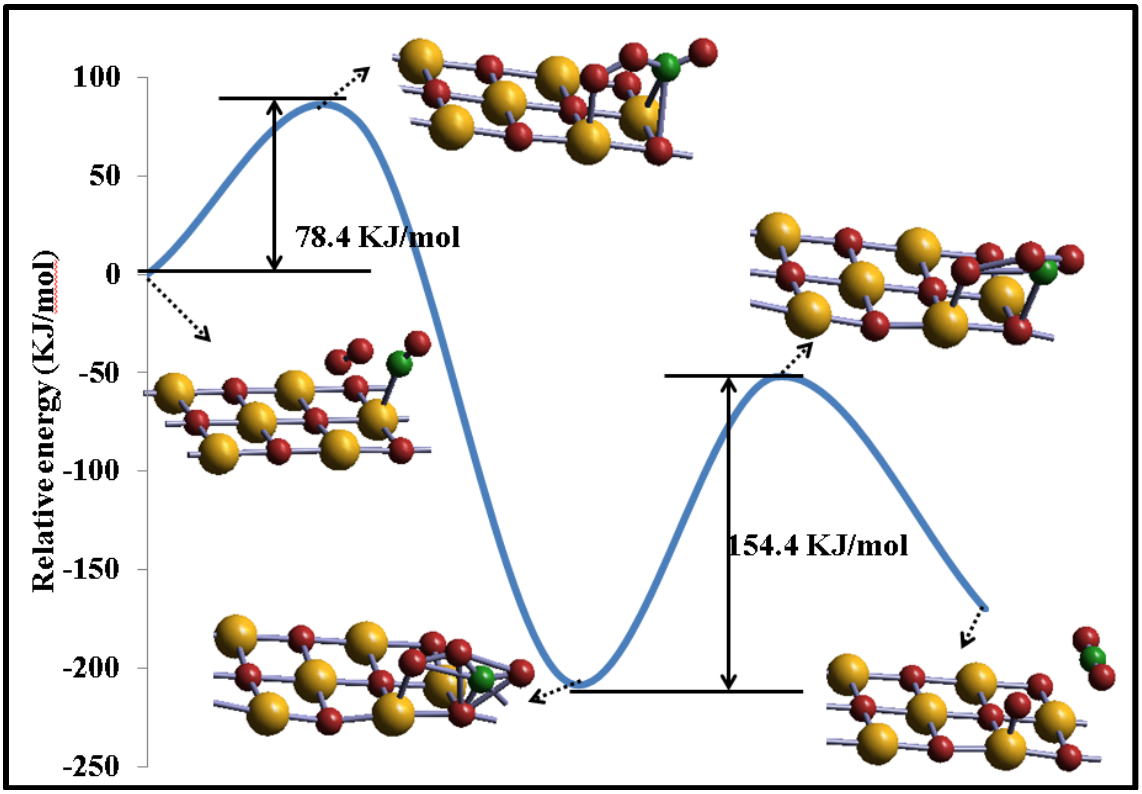

Figure 6.3. Activation barriers and transition states for the reactions CO + O_2 → OOCO + O → CO_2 + O. (Yellow-Co atom, Red- O atom, Green- C atom).

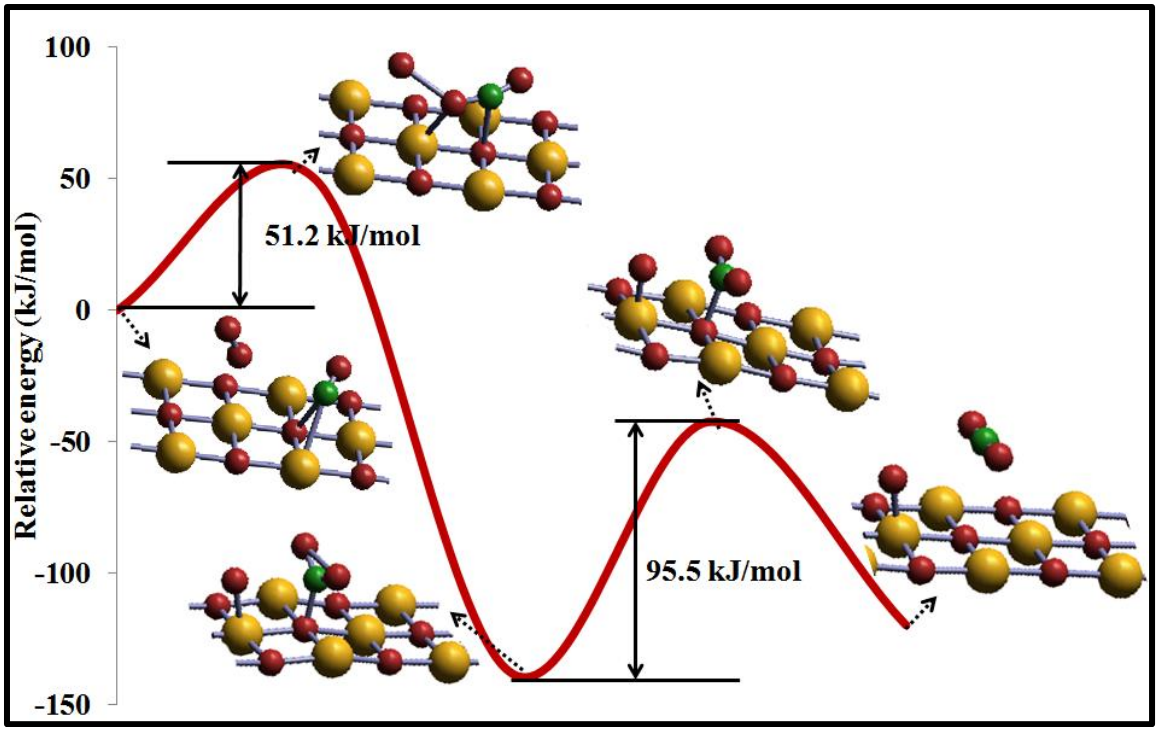

Figure 6.4. Activation barriers and transition states for the reactions CO + O_2 → OCO + O → CO_2 + O. (Yellow-Co atom, Red- O atom, Green- C atom).

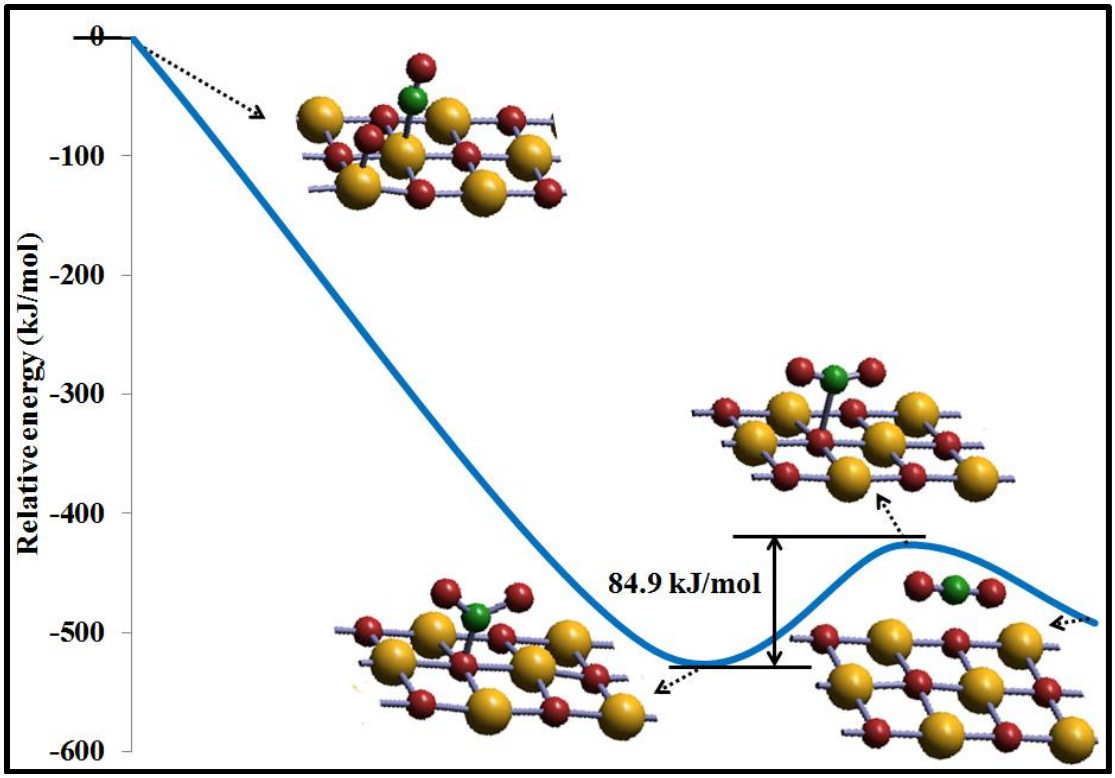

Figure 6.5. Activation barriers and transition states for the reactions CO + O → OCO → CO_2. (Yellow-Co atom, Red- O atom, Green- C atom).

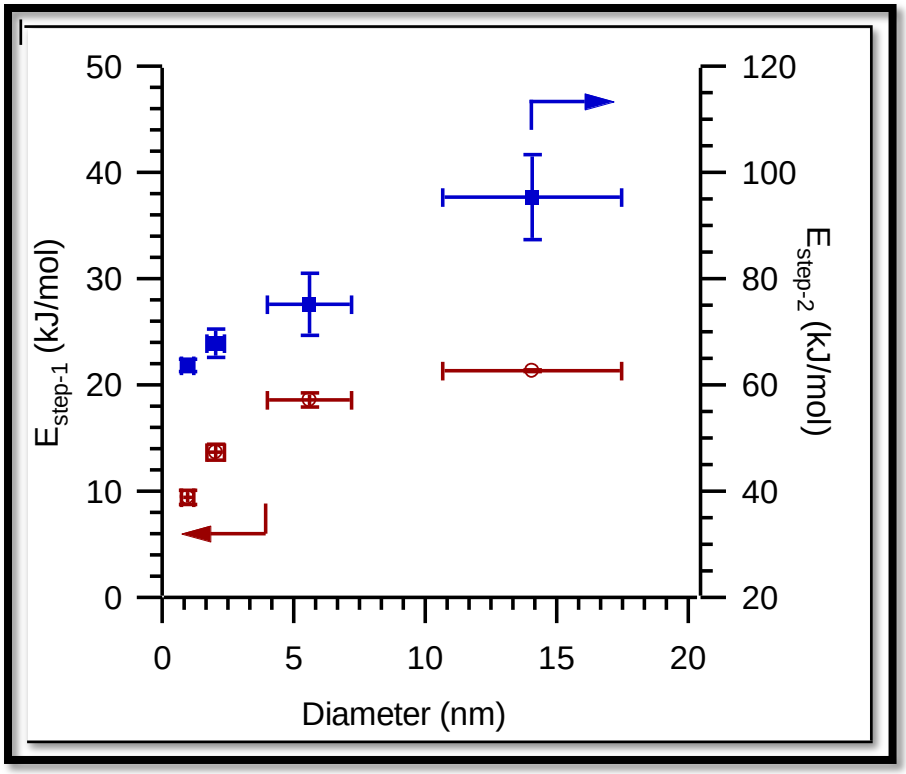

Figure 6.6. Experimental activation energies of step-1 and step-2 plotted as a function of CoO nanoparticle size.[2]

[2] Reproduced with the permission of the copyright holder. Copyright © 2012 Bijith. D. Mankidy. Refer to Appendix B-2.

CHAPTER 7:

SUMMARY, CONCLUSIONS AND FUTURE WORK

7.1. Summary and Conclusions

In this doctoral research, DFT was used as a tool to study the various aspects of CO oxidation and reduction on promoted and unpromoted cobalt based catalyst surfaces. The overall goal of this research was to obtain a fundamental understanding of the reaction mechanisms which is essential to identify the nature of the catalyst.

We studied the influence of promoters on the deactivation of Co catalysts which would help in designing catalysts with higher resistance to deactivation and higher activity. Catalysts deactivation could occur by reoxidation, C deposition, sintering, formation of Cobalt-support compounds and poisons like nitrogen, sulphur etc. Promoters can also influence various activation pathways affecting the activity and selectivity of catalysts. The influence of promoters on O removal and C deposition on Co catalysts was investigated. The effect of promoters on CO activation pathways of Co catalysts was also investigated. We also studied the CO oxidation mechanism on CoO catalyst to compare the barriers with experimental results reported by Mankidy.[29]

Oxygen removal is an important step in FTS reaction. The role of Pt promoters in the removal of O from the Co catalyst surface was studied. The activation barriers for the removal of O on flat and stepped Co(0001) was compared to that on $Co_3Pt(0001)$. The

barriers were reduced on the promoted surface. On the flat surface, the lowest barrier pathway is the one with OH on a bridge site on Co(0001) and on a hcp hollow site on $Co_3Pt(0001)$. Whereas, on the stepped surface, the lowest barrier pathway is the one with OH on an edge bridge site on both Co(0001) and $Co_3Pt(0001)$. The removal of O to form H_2O was easier on the Pt promoted Co surface compared to the unpromoted Co surface. The lower activation barrier was attributed to the change in the electronic structure of CO surface by Pt promoter which changes the favorable adsorption sites on the surface. An approximate micro-kinetic model was developed for the reaction and turn-over frequency was calculated based on the activation barriers for the lowest energy pathway for the stepped Co surface. A volcano plot was also developed based on the micro-kinetic model and the turn-over frequency on the stepped Co surface suggested that Pt promoter increased the rate of the reaction aiding the easy removal of O from the surface.

The influence of Pt and Ru promoters on C deposition on Co surface was explored in detail. Different pathways for the formation of carbon compounds on unpromoted and Pt and Ru promoted Co surfaces were studied using DFT to gain a mechanistic understanding of the effect of promoters on these reactions. The barriers for C-C and C-C-C coupling reactions were increased on both the promoted surfaces suggesting that C chain formation will be reduced by the promoters. The promoters did not have a significant effect on the subsurface C diffusion. However, the barriers for C-C/C-C-C formation was lower than the barrier for subsurface C diffusion suggesting that subsurface diffusion could occur at low C coverages. The promoters also had lower barriers for C-H formation indicating that the formation of other FTS products could also be affected by promoters. The stability of the finite and infinite C structures on Pt

promoted surface and the larger C structures on Ru promoted surface were lower than on the unpromoted surface. Also, C structures on the Pt promoted surface were less stable than the C structures on the Ru promoted surface suggesting that Pt promoter would be better than Ru promoter to prevent C deposition on Co catalyst. These results indicate that Pt and Ru promoted Co surfaces would decrease C formation and C compound formation on the Co surface.

The effect of Pt promoter on CO activation pathway of FTS was studied on stepped Co surface. Stepped Co surface and Pt promoted stepped Co surface have high barriers for direct CO dissociation. H_2 dissociation has lower barrier on both the unpromoted and Pt promoted surfaces suggesting that hydrogenation of CO would occur more easily than direct CO dissociation. CO hydrogenation was found to occur via HCO formation on both the surfaces. Pt promoter lowered the barrier for both the hydrogenation steps suggesting that Pt promoter would increase the CO hydrogenation rate of Co catalyst.

Various mechanisms of CO oxidation on bulk CoO(100) surface was explored to determine the most plausible one. DFT+U calculations indicated that CO oxidation on CoO takes place via a 2-step mechanism with barriers of 51.2 kJ/mol and 95.5 kJ/mol for steps one and two respectively. In step-1 of the most plausible mechanism, CO reacts with O_2 molecule to form an intermediate OCO. In step-2, the intermediate desorbs to form CO_2 gas. The results were fund to be in agreement with the experiments with the activation energy for step-2 larger than the energy for step-1. The activation barrier for the CoO surface with the decreased lattice spacing was found to be lower than the activation barrier for the surface with the normal lattice spacing. This suggested that

activation energy would decrease with decrease in particle size in agreement with experiments.

7.2. Future Work

This doctoral research discussed only a few aspects of the effect of promoters on deactivation of Co catalyst. Preventing deactivation of catalysts could be beneficial for extending the life of catalyst given the high cost of Co catalyst used for FTS. There are still other deactivation modes which were not explored in this research like cobalt-support interaction, sintering and poisoning. Future DFT studies on other deactivation modes would help in designing a catalyst which would be resistant to all modes of deactivation. This would help in reducing the overall cost of catalyst. Furthermore, this research focused on Pt and Ru promoters. Studies on other transition metal promoters and cheaper promoters like alkali can be done to test the resistance of such promoters to various forms of deactivation.

To fully understand the effect of promoters on a catalyst it is necessary to determine how it impacts various steps in the reaction mechanism. Promoters are known to influence the catalytic pathways by altering the energetics of a particular pathway and providing alternate routes for the reaction mechanism.[140-142] Promoters alter the activation barrier of various reaction steps making a promoted surface more or less favorable for the formation of certain products. This could be beneficial in designing catalysts with better activity and catalyst life. The research can be extended to study the selectivity of catalyst in the presence of promoter which can aid in fine tuning of catalyst properties to produce desired products. This research also provides a base to further study the use of other

cheaper promoters like alkali metals to increase the catalyst activity, better selectivity and catalyst life. A volcano type plot can be created with different promoters that can help experimentalist to design an efficient catalyst according to the requirements.

FTS processes occur at high H_2 coverages and DFT studies at high H_2 coverages are limited.[174-176] The surface stable species was found to vary with the coverages of H_2 and CO.[174] The repulsions due to presence of high H_2 coverage could affect the barriers for FTS reactions. DFT studies of FTS mechanism at high H_2 coverages can shed light into the actual barriers observed in experiments. New pathways for FTS mechanism could also be observed. In addition, FTS mechanism in the presence of different promoters could also be studied at such high coverages.

CO oxidation mechanism studies on CoO surface paves the path for exploring other catalysts for CO oxidation. Activation barriers of less than 100 kJ/mol were observed on CoO surface. Surface modification of CoO like kinks or steps could lower the activation barrier for CO oxidation. Also, addition of promoters to CoO or bimetallic catalysts can also be explored. Such mechanistic studies could complement experiments in searching for alternate catalysts to the expensive Pt catalyst widely used for CO oxidation.

REFERENCES

1. Bligaard, T.; Norskov, J. K.; Dahl, S.; Matthiesen, J.; Christensen, C. H.; Sehested, J., *J. Catal.* **2004,** *224*, 206-217.

2. Lischka, M.; Mosch, C.; Gross, A., *Electrochim. Acta* **2007,** *52*, 2219-2228.

3. Zhang, J.; Jin, H. M.; Sullivan, M. B.; Chiang, F.; Lim, H.; Wu, P., *Phys. Chem. Chem. Phys.* **2009,** *11*, 1441-1446.

4. Tavasoli, A.; Trepanier, M.; Abbaslou, R. M. M.; Dalai, A. K.; Abatzoglou, N., *Fuel Process. Technol.* **2009,** *90*, 1486-1494.

5. An, W.; Zeng, X. C.; Turner, C. H., *J. Chem. Phys.* **2009,** *131*.

6. Cheng, J.; Hu, P.; Ellis, P.; French, S.; Kelly, G.; Lok, C. M., *J. Phys. Chem. C* **2008,** *112*, 9464-9473.

7. Cheng, J.; Hu, P.; Ellis, P.; French, S.; Kelly, G.; Lok, C. M., *J. Phys. Chem. C* **2008,** *112*, 6082-6086.

8. Cheng, J.; Hu, P.; Ellis, P.; French, S.; Kelly, G.; Lok, C. M., *Surf. Sci.* **2009,** *603*, 2752-2758.

9. Daté, M.; Haruta, M., *J. Catal.* **2001,** *201*, 221-224.

10. Schubert, M. M.; Hackenberg, S.; van Veen, A. C.; Muhler, M.; Plzak, V.; Behm, R. J., *J. Catal.* **2001,** *197*, 113-122.

11. Haruta, M.; Tsubota, S.; Kobayashi, T.; Kageyama, H.; Genet, M. J.; Delmon, B., *J. Catal.* **1993,** *144*, 175-192.

12. Herzing, A. A.; Kiely, C. J.; Carley, A. F.; Landon, P.; Hutchings, G. J., *Science* **2008,** *321*, 1331-1335.

13. Oh, S. H.; Sinkevitch, R. M., *J. Catal.* **1993,** *142*, 254-262.

14. Freund, H.-J.; Meijer, G.; Scheffler, M.; Schlçgl, R.; Wolf, M., *Angew. Chem. Int. Ed.* **2011,** *50*, 10064-10094.

15. McClure, S. M.; Lundwall, M.; Yang, F.; Zhou, Z.; Goodman, D. W., *J. Phys. Chem. C* **2009,** *113*, 9688-9697.

16. Santra, A. K.; Goodman, D. W., *Electrochim. Acta* **2002,** *47*, 3595-3609.

17. Khedr, M. H.; Halim, K. S. A.; Nasr, M. I.; El-Mansy, A. M., *Mater. Sci. Eng., A* **2006,** *430*, 40-45.

18. Gong, X.-Q.; Raval, R.; Hu, P., *Phys. Rev. Lett.* **2004,** *93*, 106104-1-4.

19. Over, H.; Kim, Y. D.; Seitsonen, A. P.; Wendt, S.; Lundgren, E.; M., S.; Varga, P.; Morgante, A.; Ertl, G., *Science* **2000,** *287*, 1474.

20. Hendriksen, B. L. M.; Frenken, J. W. M., *Phys. Rev. Lett.* **2002,** *89*, 046101.

21. Gong, X.-Q.; Liu, Z.-P.; Raval, R.; Hu, P., *J. Am. Chem. Soc.* **2004,** *126*, 8-9.

22. Greeley, J.; Stephens, I. E. L.; Bondarenko, A. S.; Johansson, T. P.; Hansen, H. A.; Jaramillo, T. F.; Rossmeisl, J.; Chorkendorff, I.; Nørskov, J. K., *Nat. Chem.* **2009,** *1*, 552-556.

23. Jóhannesson, G. H.; Bligaard, T.; Ruban, A. V.; Skriver, H. L.; Jacobsen, K. W.; Nørskov, J. K., *88* **2002,** *Phys. Rev. Lett.*, 255506-1 - 255506-5.

24. Hansgen, D. A.; Vlachos, D. G.; Chen, J. G., *Nat. Chem.* **2010,** *2*, 484-489.

25. Nørskov, J. K.; Bligaard, T.; Rossmeisl, J.; Christensen, C. H., *Nat. Chem.* **2009,** *1*, 37-46.

26. Studt, F.; Abild-Pedersen, F.; Bligaard, T.; Sørensen, R. Z.; Christensen, C. H.; Nørskov, J. K., *Science* **2008,** *320*, 1320-1322.

27. Das, T. K.; Jacobs, G.; Davis, B. H., *Catal. Lett.* **2005,** *101*, 187-190.

28. Jacobs, G.; Chaney, J. A.; Patterson, P. M.; Das, T. K.; Maillot, J. C.; Davis, B. H., *J. Synchrotron Radiat.* **2004,** *11*, 414-422.

29. Mankidy, B. D., *PhD dissertation* **2012**.

30. Kresse, G.; Furthmuller, J., *Comp. Mater. Sci.* **1996,** *6*, 15-50.

31. Kresse, G.; Furthmuller, J., *Phys. Rev. B: Condens. Matter Mater. Phys.* **1996,** *54*, 11169-11186.

32. Kresse, G.; Hafner, J., *Phys. Rev. B: Condens. Matter Mater. Phys.* **1993,** *47*, 558-561.

33. Hohenberg, P.; Kohn, W., *Phys. Rev.* **1964,** *136*, B864-B871.

34. Kohn, W.; Sham, L. J., *Phys. Rev.* **1965,** *140*, A1133-A1138.

35. Jones, R. O.; Gunnarsson, O., *Rev. Mod. Phys.* **1989,** *61*, 689-746.

36. Perdew, J. P.; Wang, Y., *Phys. Rev. B* **1991,** *44*, 13298-13307.

37. Burke, K.; Ernzerhof, M.; Perdew, J. P., *Chem. Phys. Lett.* **1997,** *265*, 115-120.

38. Thomas, L. H., *Math. Proc. Cambridge* **1927,** *23*, 542-548.

39. Fermi, E., *Rend. Accad. Naz. Lincei* **1927,** *6*, 602-607.

40. Dirac, P. A. M., *Math. Proc. Cambridge* **1930,** *26*, 376-385.

41. Ceperley, D. M., *Phys. Rev. B* **1978,** *18*, 3126-3138.

42. Ceperley, D. M.; Alder, B. J., *Phys. Rev. Lett.* **1980,** *45*, 566-569.

43. Becke, A. D., *J. Chem. Phys.* **1993,** *98*, 5648-5652.

44. Lee, C.; Yang, W.; Parr, R. G., *Phys. Rev. B* **1988,** *37*, 785-789.

45. Phillips, J. C., *Phys. Rev.* **1958,** *1*, 685-695.

46. Antoncik, E., *J. Phys. Chem. Solids* **1959,** *10*, 314-320.

47. Vanderbilt, D., *Phys. Rev. B* **1990,** *41*, 7892-7895.

48. Blochl, P. E., *Phys. Rev. B: Condens. Matter Mater. Phys.* **1994,** *50*, 17953-17979.

49. Sheppard, D.; Terrell, R.; Henkelman, G., *J. Chem. Phys.* **2008,** *128*, 134106.

50. Henkelman, G.; Jonsson, H., *J. Chem. Phys.* **2000,** *113*, 9978-9985.

51. Henkelman, G.; Uberuaga, B. P.; Jonsson, H., *J. Chem. Phys.* **2000,** *113*, 9901-9904.

52. Tang, W.; Sanville, E.; Henkelman, G., *J. Phys.: Condens. Matter* **2009,** *21*, 084204.

53. Sanville, E.; Kenny, S. D.; Smith, R.; Henkelman, G., *J. Comput. Chem.* **2007,** *28*, 899-908.

54. Henkelman, G.; Arnaldsson, A.; Jónsson, H., *Comput. Mater. Sci.* **2006,** *36*, 254-360.

55. Khodakov, A. Y.; Chu, W.; Fongarland, P., *Chem. Rev.* **2007,** *107*, 1692-1744.

56. Ojeda, M.; Nabar, R.; Nilekar, A. U.; Ishikawa, A.; Mavrikakis, M.; Iglesia, E., *J. Catal.* **2010,** *272*, 287-297.

57. Saeys, M.; Tan, K. F.; Chang, J.; Borgna, A., *Ind. Eng. Chem. Res.* **2010,** *49*, 11098-11100.

58. Huo, C. F.; Li, Y. W.; Wang, J. G.; Jiao, H. J., *J. Phys. Chem. C* **2008,** *112*, 3840-3848.

59. Schanke, D.; Hilmen, A. M.; Bergene, E.; Kinnari, K.; Rytter, E.; Adnanes, E.; Holmen, A., *Energy Fuels* **1996,** *10*, 867-872.

60. van Berge, P. J.; van de Loosdrecht, J.; Barradas, S.; van der Kraan, A. M., *Catal. Today* **2000,** *58*, 321-334.

61. Jacobs, G.; Patterson, P. M.; Zhang, Y. Q.; Das, T.; Li, J. L.; Davis, B. H., *Appl. Catal., A* **2002,** *233*, 215-226.

62. van Steen, E.; Claeys, M.; Dry, M. E.; van de Loosdrecht, J.; Viljoen, E. L.; Visagie, J. L., *J. Phys. Chem. B* **2005,** *109*, 3575-3577.

63. Saib, A. M.; Moodley, D. J.; Ciobica, I. M.; Hauman, M. M.; Sigwebela, B. H.; Weststrate, C. J.; Niemantsverdriet, J. W.; van de Loosdrecht, J., *Catal. Today* **2010,** *154*, 271-282.

64. Saib, A. M.; Borgna, A.; van de Loosdrecht, J.; van Berge, P. J.; Geus, J. W.; Niemantsverdriet, J. W., *J. Catal.* **2006,** *239*, 326-339.

65. Iglesia, E.; Soled, S. L.; Fiato, R. A.; Via, G. H., *J. Catal.* **1993,** *143*, 345-368.

66. Ma, X. D.; Sun, Q. W.; Ying, W. Y.; Fang, D. Y., *J. Nat. Gas Chem.* **2009,** *18*, 232-236.

67. Escalona, N.; Medina, C.; Garcia, R.; Reyes, P., *Catal. Today* **2009,** *143*.

68. Gaube, J.; Klein, H. F., *Appl. Catal., A* **2008,** *350*.

69. Borg, Ø.; Hammera, N.; Eri, S.; Lindva, O. A.; Myrstad, R.; Blekkan, E. A.; Rønning, M.; Rytter, E.; Holmen, A., *Catal. Today* **2009,** *142*, 70-77.

70. Chu, W.; Chernavskii, P. A.; Gengembre, L.; Pankina, G. A.; Fongarland, P.; Khodakov, A. Y., *J. Catal.* **2007,** *252*, 215-230.

71. Bae, J. W.; Kim, S.-M.; Park, S.-J.; Prasad, P. S. S.; Lee, Y.-J.; Jun, K.-W., *Ind. Eng. Chem. Res.* **2009,** *48*, 3228-3233.

72. Park, S.-J.; Bae, J. W.; Lee, Y.-J.; Ha, K.-S.; Jun, K.-W.; Karandikar, P., *Catal. Commun.* **2011,** *12*.

73. Pour, A. N.; Housaindokht, M. R.; Zarkesh, J.; Tayyari, S. F., *J. Ind. Eng. Chem.* **2010,** *16*.

74. Diehl, F.; Khodakov, A. Y., *Oil Gas Sci. Technol.* **2009,** *64*, 11-24.

75. Schanke, D.; Vada, S.; Blekkan, E. A.; Hilmen, A. M.; Hoff, A.; Holmen, A., *J. Catal.* **1995,** *156*, 85-95.

76. Morales, F.; Smit, E. d.; Groot, F. M. F. d.; Visser, T.; Weckhuysen, B. M., *J. Catal.* **2007,** *246*, 91-99.

77. Jacobs, G.; Das, T. K.; Zhang, Y. Q.; Li, J. L.; Racoillet, G.; Davis, B. H., *Appl. Catal., A* **2002,** *233*, 263-281.

78. Bao, A.; Liew, K.; Li, J., *J. Mol. Catal. A: Chem.* **2009,** *304*, 47-51.

79. Jacobs, G.; Ribeiro, M. C.; Ma, W. P.; Ji, Y. Y.; Khalid, S.; Sumodjo, P. T. A.; Davis, B. H., *Appl. Catal., A* **2009,** *361*, 137-151.

80. Tsubaki, N.; Sun, S. L.; Fujimoto, K., *J. Catal.* **2001,** *199*, 236-246.

81. Xu, D.; Li, W.; Duan, H.; Ge, Q.; Xu, H., *Catal. Lett.* **2005,** *102*, 229-235.

82. Fenske, D.; Yim, W. L.; Neuendorf, S.; Hoogestraat, D.; Greshnykh, D.; Borchert, H.; Kluner, T.; Al Shamery, K., *ChemPhysChem* **2007,** *8*, 654-656.

83. Baudoing-Savois, R.; Dolle, P.; Gauthier, Y.; Saint-Lager, M. C.; De Santis, M.; Jahns, V., *J. Phys.: Condens. Matter* **1999,** *11*, 8355-8375.

84. C.Saint-Lager, M.; Baudoing-Savois, R.; Santis, M. D.; Dolle, P.; Gauthier, Y., *Surf. Sci.* **1998,** *418*, 485-492.

85. Chui, Y. H.; Chan, K. Y., *Chem. Phys. Lett.* **2005,** *408*, 49-53.

86. Perdew, J. P.; Burke, K.; Ernzerhof, M., *Phys. Rev. Lett.* **1996,** *77*, 3865-3868.

87. Ducreux, O.; Rebours, B.; Lynch, J.; Roy-Auberger, M.; Bazin, D., *Oil Gas Sci. Technol.* **2009,** *64*, 49-62.

88. Kittel, C., *Introduction to Solid State Physics* Wiley: New York, 1976.

89. Monkhorst, H. J.; Pack, J. D., *Phys. Rev. B: Condens. Matter Mater. Phys.* **1976,** *13*, 5188-5192.

90. Viljoen, E. L.; van Steen, E., *Catal. Lett.* **2009,** *133*, 8-13.

91. Gong, X. Q.; Raval, R.; Hu, P., *Surf. Sci.* **2004,** *562*, 247-256.

92. Henkelman, G.; Arnaldsson, A.; Jónsson, H., *Comput. Mater. Sci.* **2006,** *36*, 254-360.

93. Wang, X.; Li, N.; Pfefferle, L. D.; Haller, G. L., *Catal. Today* **2009,** *146*, 160-165.

94. Tang, W.; Henkelman, G., *J. Chem. Phys.* **2009,** *130*, 194504.

95. Hammer, B.; Norskov, J. K., *Surf. Sci.* **1995,** *343*, 211-220.

96. Kitchin, J. R.; Nørskov, J. K.; Barteau, M. A.; Chen, J. G., *J. Chem. Phys.* **2004,** *120*, 10240.

97. Wilke, S.; Natoli, V.; Cohen, M. H., *J. Chem. Phys.* **2000,** *112*.

98. Lin, Y. C.; Fan, L. T.; Shafie, S.; Bertok, B.; Friedler, F., *Comput. Chem. Eng.* **2009,** *33*, 1182-1186.

99. Gladys, M. J.; Inderwildi, O. R.; Karakatsani, S.; Fiorin, V.; Held, G., *J. Phys. Chem. C* **2008,** *112*, 6422-6429.

100. Michaelides, A., *Surf. Sci.* **2007,** *601*, 3529-3531.

101. Cheng, J.; Hu, P.; Ellis, P.; French, S.; Kelly, G.; Lok, C. M., *J. Phys. Chem. C* **2008,** *112*, 1308-1311.

102. George A. Huff, J.; Satterfleld, C. N., *Ind. Eng. Chem. Proc. Des. Dev.* **1985,** *24*, 986-995.

103. Bartholomew, C. H.; Bowman, R. M., *Appl. Catal.* **1985,** *15*, 59-67.

104. Schanke, D.; Hilmen, A. M.; Bergene, E.; Kinnari, K.; Rytter, E.; Ådnanes, E.; Holmen, A., *Energy Fuels* **1996,** *10*, 867-872.

105. Bae, J. W.; Kim, S. M.; Park, S. J.; Prasad, P. S. S.; Lee, Y. J.; Jun, K. W., *Ind. Eng. Chem. Res.* **2009,** *48*, 3228-3233.

106. Tsakoumis, N. E.; Ronning, M.; Borg, O.; Rytter, E.; Holmen, A., *Catal. Today* **2010,** *154*, 162-182.

107. Karaca, H.; Hong, J.; Fongarland, P.; Roussel, P.; Griboval-Constant, A.; Lacroix, M.; Hortmann, K.; Safonova, O. V.; Khodakov, A. Y., *Chem. Commun.* **2010,** *46*, 788–790.

108. Park, S.-J.; Bae, J. W.; Lee, Y.-J.; Ha, K.-S.; Jun, K.-W.; Karandikar, P., *Catal. Commun.* **2011,** *12*, 539-543.

109. Shetty, S.; Santen, R. A. v., *Phys. Chem. Chem. Phys.* **2010,** *12*, 6330-6332.

110. Inderwildi, O. R.; Jenkins, S. J.; King, D. A., *J. Phys. Chem. C Lett.* **2008,** *112*, 1305-1307.

111. Ciobica, I. M.; Santen, R. A. v.; Berge, P. J. v.; Loosdrecht, J. v. d., *Surf. Sci.* **2008,** *602*, 17-27.

112. Bartholomew, C. H., *Appl. Catal., A* **2001,** *212*, 17-60.

113. Moodley, D. J.; van de Loosdrecht, J.; Saib, A. M.; Overett, M. J.; Datye, A. K.; Niemantsverdriet, J. W., *Appl. Catal., A* **2009,** *354*, 102-110.

114. Tan, K. F.; Xu, J.; Chang, J.; Borgna, A.; Saeys, M., *J. Catal.* **2010,** *274*, 121-129.

115. Rostrup-Nielsen, J. R., *J. Catal.* **1984,** *85*, 31-43.

116. Andersen, N. T.; F.Topsøe; Alstrup, I.; Rostrup-Nielsen, J., *J. Catal.* **1987,** *104*, 454-465.

117. Bengaard, H. S.; Nørskov, J. K.; Sehested, J.; Clausen, B. S.; Nielsen, L. P.; Molenbroek, A. M.; Rostrup-Nielsen, J. R., *J. Catal.* **2002,** *209*, 365-384.

118. Cheng, J.; Gong, X.-Q.; Hu, P.; Lok, C. M.; Ellis, P.; French, S., *J. Catal.* **2008,** *254*, 285-295.

119. Swart, J. C. W.; Ciobica, I. M.; Santen, R. A. v.; Steen, E. v., *J. Phys. Chem. C* **2008,** *112*, 12899-12904.

120. Escalona, N.; Medina, C.; Garcia, R.; Reyes, P., *Catal. Today* **2009,** *143*, 76-79.

121. Balakrishnan, N.; Joseph, B.; Bhethanabotla, V. R., *Surf. Sci.* **2012,** *606*, 634-643.

122. Gaube, J.; Klein, H. F., *Appl. Catal., A* **2008,** *350*, 126-132.

123. Pour, A. N.; Housaindokht, M. R.; Zarkesh, J.; Tayyari, S. F., *J. Ind. Eng. Chem.* **2010,** *16*, 1025-1032.

124. Besenbacher, F.; Chorkendorff, I.; Clausen, B. S.; Hammer, B.; Molenbroek, A. M.; Nørskov, J. K.; Stensgaard, I., *Science* **1998,** *279*, 1913-1915.

125. Saeys, M.; Tan, K. F.; Chang, J.; Borgna, A., *Ind. Eng. Chem. Res.* **2010,** *49*, 11098-11100.

126. Guo, J.; Xie, C.; Lee, K.; Guo, N.; Miller, J. T.; Janik, M. J.; Song, C., *ACS Catal.* **2011,** *1*, 574–582.

127. Sun, S.; Fujimoto, K.; Yoneyama, Y.; Tsubaki, N., *Fuel* **2002,** *81*, 1583-1591.

128. Lu, S. L.; Lonergan, W. W.; Zhu, Y. X.; Xie, Y. C.; Chen, J. G. G., *Appl. Catal., B* **2009,** *91*, 610-618.

129. Iglesia, E.; Soled, S. L.; Fiato, R. A.; Via, G. H., *J. Catal.* **1993,** *143*, 345-368.

130. Weller, S.; Hofer, L. J. E.; Anderson, R. B., *J. Am. Chem. Soc.* **1948,** *70*, 799-801.

131. Anderson, R. B.; Hall, W. K.; Krieg, A.; Seligman, B., *J. Am. Chem. Soc.* **1949,** *71*, 183-188.

132. Xiong, J. M.; Ding, Y. J.; Wang, T.; Yan, L.; Chen, W. M.; Zhu, H. J.; Lu, Y., *Catal. Lett.* **2005,** *102*, 265-269.

133. Bian, G.; Nanba, T.; Koizumi, N.; Yamada, M., *J. Mol. Catal. A: Chem.* **2002,** *178*, 219-228.

134. Cheng, J.; Hu, P.; Ellis, P.; French, S.; Kelly, G.; Lok, C. M., *J. Phys. Chem. C* **2010,** *114*, 1085-1093.

135. Nikolla, E.; Schwank, J.; Linic, S., *J. Catal.* **2007,** *250* 85–93.

136. Cheng, J.; Hu, P.; Ellis, P.; French, S.; Kelly, G.; Lok, C. M., *J. Phys. Chem. C* **2008,** *112*, 6082-6086.

137. Hussain, S. T.; Nadeem, M. A.; Mazhar, M., *Catal. Commun.* **2008,** *9*, 2048-2052.

138. Zhang, C. H.; Zhao, G. Y.; Liu, K. K.; Yang, Y.; Xiang, H. W.; Li, Y. W., *J. Mol. Catal. A: Chem.* **2010,** *328*, 35-43.

139. Jacobs, G.; Ribeiro, M. C.; Ma, W. P.; Ji, Y. Y.; Khalid, S.; Sumodjo, P. T. A.; Davis, B. H., *Appl. Catal. A: Gen.* **2009,** *361*, 137-151.

140. Pour, A. N.; Shahri, S. M. K.; Zamani, Y.; Zamanian, A., *J. Nat. Gas Chem.* **2008,** *19*, 193-197.

141. Jia Gao; Mo, X.; Jr., J. G. G., *J. Catal.* **2009,** *268*.

142. Graf, B.; Schulte, H.; Muhler, M., *J. Catal.* **2010,** *276*.

143. Cheng, J.; Hu, P.; Ellis, P.; French, S.; Kelly, G.; Lok, C. M., *J. Phys. Chem. C* **2008,** *112*, 9464-9473.

144. Abbott, H. L.; Harrison, I., *J. Phys. Chem. C* **2007,** *111*, 13137-13148.

145. Stampfl, C.; Scheffler, M., *Surf. Sci.* **1999,** *119*, 433-435.

146. Sun, B.-Z.; Chen, W.-K.; Xu, Y.-J., *J. Chem. Phys.* **2010,** *133*, 154502-1-7.

147. Xie, X.; Li, Y.; Liu, Z.-Q.; Haruta, M.; Shen, W., *Nature* **2009,** *458*, 746-749.

148. Martynova, Y.; Yang, B.; Yu, X.; Boscoboinik, J. A.; Shaikhutdinov, S.; Freund, H.-J., *Catal. Lett.* **2012,** *142*, 657-663.

149. Wang, X.; Song, L.; Yang, H.; Xing, W.; Lu, H.; Hu, Y., *J. Mater. Chem.* **2012,** *22*, 3426-3431.

150. Uddin, M. A.; Komatsu, T.; Yashima, T., *J. Catal.* **1994,** *146*, 468-475.

151. Li, P.; Miser, D. E.; Rabiei, S.; Yadav, R. T.; Hajaligol, M. R., *Appl. Catal. B: Environ.* **2003,** *43*, 151-162.

152. Xiong, Y.; Li, Z.; Li, X.; Hu, B.; Xie, Y., *Inorg. Chem.* **2004,** *43*, 6540-6542.

153. Khedr, M. H.; Halim, K. S. A.; Nasr, M. I.; El-Mansy, A. M., *Mater. Sci. Eng.: A* **2006,** *430*, 40-45.

154. Lin, H.-Y.; Chen, Y.-W.; Wang, W.-J., *J. Nanopart. Res.* **2005,** *7*, 249-263.

155. Kang, M.; Song, M. W.; Lee, C. H., *Appl. Catal. A: Gen.* **2003,** *251*, 143-156.

156. Ko, E.-Y.; Park, E. D.; Lee, H. C.; Lee, D.; Kim, S., *Angew. Chem. Int. Ed.* **2007,** *46*, 734-737.

157. Luo, J.-Y.; Meng, M.; Li, X.; Li, X.-G.; Zha, Y.-Q.; Hu, T.-D.; Xie, Y.-N.; Zhang, J., *J. Catal.* **2008,** *254*, 310-324.

158. Jiang, D.-e.; Dai, S., *Phys. Chem. Chem. Phys.* **2010,** *13*, 978-984.

159. Lin, H.-K.; Wang, C.-B.; Chiu, H.-C.; Chien, S.-H., *Catal. Lett.* **2003,** *86*, 63-68.

160. Wdowik, U. D.; Parlinski, K., *Phys. Rev. B: Condens. Matter Mater. Phys.* **2007,** *75*, 104306.

161. Dudarev, S. L.; Botton, G. A.; Savrasov, S. Y.; Humphreys, C. J.; Sutton, A. P., *Phys. Rev. B: Condens. Matter* **1998,** *57*, 1505-1509.

162. Anisimov, V. I.; Zaanen, J.; Andersen, O. K., *Phys. Rev. B: Condens. Matter* **1991,** *41*, 943-954.

163. Elp, J. v.; Wieland, J. L.; Eskes, H.; Kuiper, P.; Sawatzky, G. A.; Groot, F. M. F. d.; Turner, T. S., *Phys. Rev. B: Condens. Matter* **1991,** *44*, 6090-6103.

164. Wyckoff, R. W. G., *Crystal Structures*. Wiley: New york, 1963.

165. Feng, X., *Phys. Rev. B: Condens. Matter* **2004,** *69*, 155107.

166. Dorado, B.; Amadon, B.; Freyss, M.; Bertolus, M., *Phys. Rev. B: Condens. Matter* **2009,** *79*, 235125.

167. Meredig, B.; Thompson, A.; Hansen, H. A.; Wolverton, C., *Phys. Rev. B: Condens. Matter* **2010,** *82*, 195128-.

168. Xie, X.; Li, Y.; Liu, Z.-Q.; Haruta, M.; Shen, W., *Nature* **2009,** *458*, 746.

169. Gong, X.-Q.; Raval, R.; Hu, P., *Phys. Rev. Lett.* **2004,** *93*, 106104.

170. Derekaya, F. B.; Guldur, C., *Int. J. Chem. React. Eng.* **2010,** *8*, 1-18.

171. Vines, F.; Illas, F.; Neyman, K. M., *J. Phys. Chem. A* **2008,** *112*, 8911-8915.

172. Wang, L.; Roudgar, A.; Eikerling, M., *J. Phys. Chem. C* **2009,** *113*, 17989-17996.

173. Qi, W. H.; Wang, M. P., *J. Nanopart. Res.* **2005,** *7*, 51-57.

174. Cao, D.-B.; Zhang, F.-Q.; Li, Y.-W.; Wang, J.; Jiao, H., *J. Phys. Chem. B* **2005,** *109*, 10922-10935.

175. Helden, P. v.; Steen, E. v., *J. Phys. Chem. C* **2008,** *112*, 16505-16513.

176. Swart, I.; Fielicke, A.; Rayner, D. M.; Meijer, G.; Weckhuysen, B. M.; Groot, F. M. F. d., *Angew. Chem. Int. Ed.* **2007,** *46*, 5317-5320.

APPENDIX A:

NOMENCLATURE

DFT	Density Functional Theory
FTS	Fischer-Tropsch Synthesis
CI-NEB	Climbing Image Nudged Elastic Band
VASP	Vienna Ab Initio Simulation package
TOF	Turn-over frequency
LDA	Local density approximation
GGA	Generalized gradient approximation
PW91	Perdew-Wang functional
PBE	Perdew-Burke-Ernzerhof functional
B88	Becke
LYP	Lee-Yang-Parr
US-PP	Ultrasoft pseudopotentials
MEP	Minimum energy path
BEP	Bronsted- Evans – Polanyi
MT	Multiply-twined
WP	Wulff-polyhedrons
ΔH_R	Enthalpy change of reactant
ΔH	Overall enthalpy change for the reaction
P_{H_2}	Partial pressure of H_2

APPENDIX A (CONTINUED)

P_{H_2O}	Partial pressure of H_2O
$Rate_{des}$	Rate with desorption as rate determining step
$Rate_{ads}$	Rate with adsorption as rate determining step
k_1	Rate constant for adsorption
k_2	Rate constant for desorption
K_1	Standard equilibrium constant for adsorption
K_2	Standard equilibrium constant for desorption
K_{eq}	Overall standard equilibrium constant
K_B	Boltzmann constant
T	Temperature
h	Planck's constant
R	Gas constant
S_{H_2}	Entropy of H_2 in gaseous phase
S_{H_2O}	Entropy of H_2O in gaseous phase

APPENDIX B:

COPYRIGHT INFORMATION AND PERMISSION

B-1: Copyright Information to Use Published Manuscript in Dissertation

AUTHOR AND USER RIGHTS

INTRODUCTION

Elsevier requests transfers of copyright, or in some cases exclusive rights, from its journal authors in order to ensure that we have the rights necessary for the proper administration of electronic rights and online dissemination of journal articles, authors and their employers retain (or are granted/transferred back) significant scholarly rights in their work. We take seriously our responsibility as the steward of the online record to ensure the integrity of scholarly works and the sustainability of journal business models, and we actively monitor and pursue unauthorized and unsubscribed uses and re-distribution (for subscription models).

In addition to authors' scholarly rights, anyone who is affiliated with an institution with a journal subscription can use articles from subscribed content under the terms of their institution's license, while there are a number of other ways in which anyone (whether or not an author or subscriber) can make use of content published by Elsevier, which is free at the point of use or accessed under license.

Author Rights

As a journal author, you have rights for a large range of uses of your article, including use by your employing institute or company. These rights can be exercised without the need to obtain specific permission.

How authors can use their own journal articles

Authors publishing in Elsevier journals have wide rights to use their works for teaching and scholarly purposes without needing to seek permission.

APPENDIX B (CONTINUED)

Table of Author's Rights

	Preprint version (with a few exceptions- see below *)	Accepted Author Manuscript	Published Journal Articles
Use for classroom teaching by author or author's institution and presentation at a meeting or conference and distributing copies to attendees	Yes	Yes	Yes
Use for internal training by author's company	Yes	Yes	Yes
Distribution to colleagues for their research use	Yes	Yes	Yes
Use in a subsequent compilation of the author's works	Yes	Yes	Yes
Inclusion in a thesis or dissertation	Yes	Yes	Yes
Reuse of portions or extracts from the article in other works	Yes	Yes with full acknowledgement of final article	Yes with full acknowledgement of final article
Preparation of derivative works (other than for commercial purposes)	Yes	Yes with full acknowledgement of final article	Yes with full acknowledgement of final article
Preprint servers	Yes	Yes with the specific written permission of Elsevier	No
Voluntary posting on open web sites operated by author or author's institution for scholarly purposes	Yes (author may later add an appropriate bibliographic citation, indicating subsequent publication by Elsevier and journal title)	Yes, with appropriate bibliographic citation and a link to the article once published	Only with the specific written permission of Elsevier
Mandated deposit or deposit in or posting to subject-oriented or centralized repositories	Yes under specific agreement between Elsevier and the repository	Yes under specific agreement between Elsevier and the repository**	Yes under specific agreement between Elsevier and the repository
Use or posting for commercial gain or to substitute for services provided directly by journal	Only with the specific written permission of Elsevier	Only with the specific written permission of Elsevier	Only with the specific written permission of Elsevier

** Voluntary posting of Accepted Author Manuscripts in the arXiv subject repository is permitted.

APPENDIX B (CONTINUED)

B-2: Copyright Permission to Use Figure

02/20/2013
NianthriniBalakrishnan
PhD candidate
University of South Florida
Tampa, Florida 33620

Dear Dr. Bijith D. Mankidy:

I am completing a doctoral dissertation at University of South Florida entitled "Theoretical Studies of Co Based Catalysts on CO Hydrogenation and Oxidation". I would like your permission to reprint in my dissertation excerpts from the following:
PhD dissertation By Bijith D. Mankidy entitled "Design of Colloidal Composite Catalysts for CO_2Photoreduction and for CO Oxidation"

The excerpt to be reproducedis the following figure:

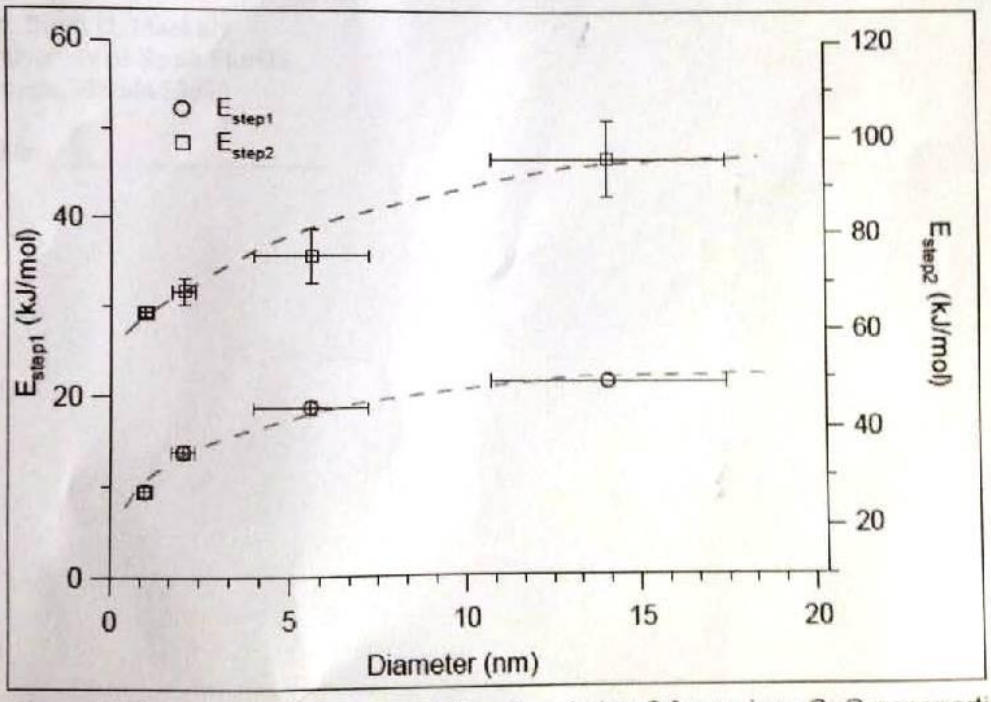

Figure 2.28. Activation energies of step-1 and step-2 for various CoO nanoparticle sizes

The requested permission extends to any future revisions and editions of my dissertation, including non-exclusive world rights in all languages, and to the prospective publication of my dissertation by ProQuest through its UMI® Dissertation Publishing business. ProQuest may produce and sell copies of my dissertation on demand and may make my dissertation available for free internet download at my request. These rights will in no way restrict republication of the

APPENDIX B (CONTINUED)

material in any other form by you or by others authorized by you. Your signing of this letter will also confirm that you own the copyright to the above-described material.
If these arrangements meet with your approval, please sign this letter where indicated below and return it to me. Thank you very much.
Sincerely,

[redacted]
Nianthrini Balakrishnan.

PERMISSION GRANTED FOR THE
USE REQUESTED ABOVE:

[redacted]

Dr. Bijith D. Mankidy
University of South Florida
Tampa, Florida 33620

Date: 02/22/2013

APPENDIX C:

ADDITIONAL INFORMATION AND DERIVATION

C-1: Test Calculations

Testing calculations for the k-point sampling were done for the adsorption energies of OH and H_2O on the stepped surfaces. The differences in the adsorption energies were found to be small. Thus, 5x2x1 k-point mesh would be sufficient enough for the stepped surface.

Surface	**Species**	**Adsorption energy for k-point sampling (eV)**	
		5x2x1	**5x3x1**
Co(0001)	OH	3.958	3.976
	H_2O	0.599	0.594
$Co_3Pt(0001)$	OH	3.816	3.917
	H_2O	0.586	0.583

C-2: Total d-Band Center

Total d-band center is the average d-band center of all the atoms in the supercell along with the adsorbates.

C-3: Average d-Band Center

This is the average d-band center of the atoms on which the adsorbates are adsorbed. For the Ohcp Hhcp Hhcp site, the d-band center is the average of the d-band centers of the atoms in the three hcp sites (O (hcp1, hcp2, hcp3), H (hcp1, hcp2, hcp3), H (hcp1, hcp2, hcp3)).

C-4: Adsorption Energy

Adsorption energies for the co-adsorbed species were calculated using the formula.

$$E_{O,\,H,\,H} = E_{Slab} + E_O + E_H + E_H - E_{O+H+H+Slab} \quad \text{(C.1)}$$

$$E_{OH,\,H} = E_{Slab} + E_{OH} + E_H - E_{OH+H+Slab} \quad \text{(C.2)}$$

C-5: Micro-Kinetic Model Derivation

C-5.1: Adsorption

$$H_2 + * \leftrightarrow 2H* \quad \text{(C.3)}$$

C-5.2: Multistep Desorption

$$O*(ads) + 2H*(ads) \leftrightarrow OH*(ads) + * \quad \text{(C.4)}$$

$$OH*(ads) + H*(ads) \leftrightarrow H_2O*(ads) + * \quad \text{(C.5)}$$

$$H_2O* \leftrightarrow H_2O + * \quad \text{(C.6)}$$

C-5.3: Single Desorption Step

$$O^*(ads) + 2H^*(ads) \leftrightarrow H_2O(g) + * \quad (C.7)$$

C-5.4: Assumption

Multistep desorption is considered as single step desorption. Reactions in equations C.4 to C.6 are considered as single step reaction as shown in equation C.7.

C-5.5: Rate Equation

Consider equilibrium coverage of oxygen and assuming it to be a constant for derivation purpose.

$$\theta_{O^*} = Constant = \frac{1}{4} \quad (C.8)$$

The reversibility of step i is defined by,

$$Z_i = \frac{\prod_j {a_j}^{v_{ij}}}{K_{ieq}} \quad (C.9)$$

where

v_{ij} is the stoichiometric coefficient for the reactant (or product) j of step i

a_j is the activity of the reactant (or product) j of step i

K_{ieq} is the standard equilibrium constant.

For the forward reaction, Z_i is between 0 and 1

For irreversible reaction, Z_i approaches 0 and for reaction at quasi-equilibrium Z_i approaches 1

APPENDIX C (CONTINUED)

The net reaction rate of step i is expressed as,

$$r_i = r_{+i} - r_{-i} = r_{+i}(1 - Z_i) \tag{C.10}$$

r_{+i} and r_{-i} are the forward and backward reaction rates of step i.

At steady state, r = r_1 = r_2 where r_1 and r_2 are the rates of adsorption and desorption respectively.

$$r_1 = 2k_1 P_{H_2} {\theta_*}^2 (1 - Z_1) \tag{C.11}$$

$$Z_1 = \frac{{\theta_{H^*}}^2}{P_{H_2} {\theta_*}^2 K_1} \tag{C.12}$$

$$r_2 = k_2 \theta_{O^*} {\theta_{H^*}}^2 (1 - Z_2) \tag{C.13}$$

$$Z_2 = \frac{P_{H_2O} {\theta_*}^2}{\theta_{O^*} {\theta_{H^*}}^2 K_2} \tag{C.14}$$

Z_1 and Z_2 are reversibilities, k_1 and k_2 are the rate constants of adsorption and desorption, K_1 and K_2 are the standard equilibrium constants of adsorption and desorption, P_{H_2} and P_{H_2O} are the partial pressures of H_2 and H_2O, θ_{O^*}, θ_{H^*}, θ_* are the coverages of O, intermediate H and free surface sites.

The overall reversibility is given by the product of reversibility of each step,

$$Z_{tot} = Z_1 Z_2 = \frac{4P_{H_2O}}{P_{H_2} K_1 K_2} \tag{C.15}$$

$$K_{eq} = K_1 K_2 \tag{C.16}$$

$$Z_{tot} = \frac{4P_{H_2O}}{P_{H_2} K_{eq}} \tag{C.17}$$

K_{eq} is the overall standard equilibrium constant.

The total surface coverage is equal to one,

$$\theta_{O^*} + \theta_{H^*} + \theta_* = 1 \tag{C.18}$$

If r_1 is rate limiting $Z_2 = 1$; $Z_1 \approx Z_{tot}$

$$1 - Z_2 = 0 \tag{C.19}$$

$$\theta_* = \theta_{H^*}\sqrt{\frac{K_2}{4P_{H_2O}}} \tag{C.20}$$

$$\theta_* = \frac{3}{4\left(1+\sqrt{\frac{4P_{H_2O}}{K_2}}\right)} \tag{C.21}$$

$$r_1 = \frac{\frac{9}{8}k_1 P_{H^2}\left(1-\frac{4P_{H_2O}}{P_{H_2}K_{eq}}\right)}{\left(1+\sqrt{\frac{4P_{H_2O}}{K_2}}\right)^2} \tag{C.22}$$

If r_2 is rate determining step $Z_1 = 1$; $Z_2 \approx Z_{tot}$

$$1 - Z_1 = 0 \tag{C.23}$$

$$\theta_{H^*} = \theta_*\sqrt{P_{H_2}K_1} \tag{C.24}$$

$$\theta_{H^*} = \frac{\frac{3}{4}}{\left(1+\frac{1}{\sqrt{P_{H_2}K_1}}\right)} \tag{C.25}$$

$$r_2 = \frac{\frac{9}{64}k_2\left(1-\frac{4P_{H_2O}}{P_{H_2}K_{eq}}\right)}{\left(1+\frac{1}{\sqrt{P_{H_2}K_1}}\right)^2} \tag{C.26}$$

$k_1 = \frac{K_B T}{h} e^{\frac{-S_{H_2}}{R}} e^{\frac{-E_1}{RT}}$ is the rate constant for adsorption

$k_{-1} = \frac{K_B T}{h} e^{\frac{-E_{-1}}{RT}}$ is the reverse rate constant for adsorption

$k_2 = \frac{K_B T}{h} e^{\frac{-E_2}{RT}}$ is the rate constant for desorption

$k_{-2} = \frac{K_B T}{h} e^{\frac{-S_{H_2O}}{R}} e^{\frac{-E_{-2}}{RT}}$ is the reverse rate constant for desorption

$K_1 = \frac{k_1}{k_{-1}} = e^{\frac{-S_{H_2}}{R}} e^{\frac{-(E_1 - E_{-1})}{RT}} = e^{\frac{-S_{H_2}}{R}} e^{\frac{-\Delta H_R}{RT}}$ is the standard equilibrium constant for adsorption

$K_2 = \frac{k_2}{k_{-2}} = e^{\frac{S_{H_2O}}{R}} e^{\frac{-(E_2 - E_{-2})}{RT}} = e^{\frac{S_{H_2O}}{R}} e^{\frac{\Delta H_P}{RT}}$ is the standard equilibrium constant for desorption

$K_{eq} = e^{\frac{-S_{H_2} + S_{H_2O}}{R}} e^{\frac{-\Delta H_R + \Delta H_P}{RT}} = e^{\frac{-S_{H_2} + S_{H_2O}}{R}} e^{\frac{-\Delta H}{RT}} = e^{\frac{\Delta G}{RT}}$ is the overall standard equilibrium constant

where S_{H_2} and $-S_{H_2O}$ are the entropies of H_2 and H_2O, $-\Delta H_R, \Delta H_P$, and ΔH are the enthalpies of H_2, H_2O and overall enthalpy, ΔG is the Gibbs free energy change and E_1, $-E_1$, E_2, $-E_2$ are the activation energies as described in Figure 3.8.

$$\Delta H = \Delta H_R - \Delta H_P \quad \text{(C.27)}$$

$$E_1 - E_{-1} = \Delta H_R \quad \text{(C.28)}$$

$$E_2 - E_{-2} = -\Delta H_P \quad \text{(C.29)}$$

$$\text{Rate of adsorption } r_1 = \frac{9K_BT\frac{-S_{H_2}}{R}e^{\frac{-E_1}{RT}}P_{H_2}\left(1-\frac{4P_{H_2O}}{P_{H_2}K_{eq}}\right)}{8h\left(1+\sqrt{\frac{4P_{H_2O}}{e^{\frac{S_{H_2O}}{R}}e^{\frac{\Delta H_P}{RT}}}}\right)^2} \quad \text{(C.30)}$$

$$\text{Rate of desorption } r_2 = \frac{9K_BTe^{\frac{-E_2}{RT}}\left(1-\frac{4P_{H_2O}}{P_{H_2}K_{eq}}\right)}{64h\left(1+\frac{1}{\sqrt{P_{H_2}e^{\frac{-S_{H_2}}{R}}e^{\frac{-\Delta H_R}{RT}}}}\right)^2} \quad \text{(C.31)}$$

APPENDIX D:

ADDITIONAL TABLE AND FIGURES

Table D-1. Supercell and K-point sampling for the various carbon clusters.

C compound	Supercell	K-point sampling
Clusters containing one C atom	2x2	7x7x1
Finite carbon clusters with the number of C atoms n = 2 to 8	3x3	5x5x1
Infinite carbon clusters like chain, branched, C5 ring, C6 ring and 1ring-top	2x3	7x5x1
1ring-bridge , 2ring-bridge	2x4	7x3x1
3ring-bridge, 4ring-bridge	1x6	7x3x1
Graphene	2x2	7x7x1
Diffusion barriers from hcp to fcc, to subsurface and Activation barriers for C-C, C-H, C-C-H and C-C-C formations	2x2	5x5x1

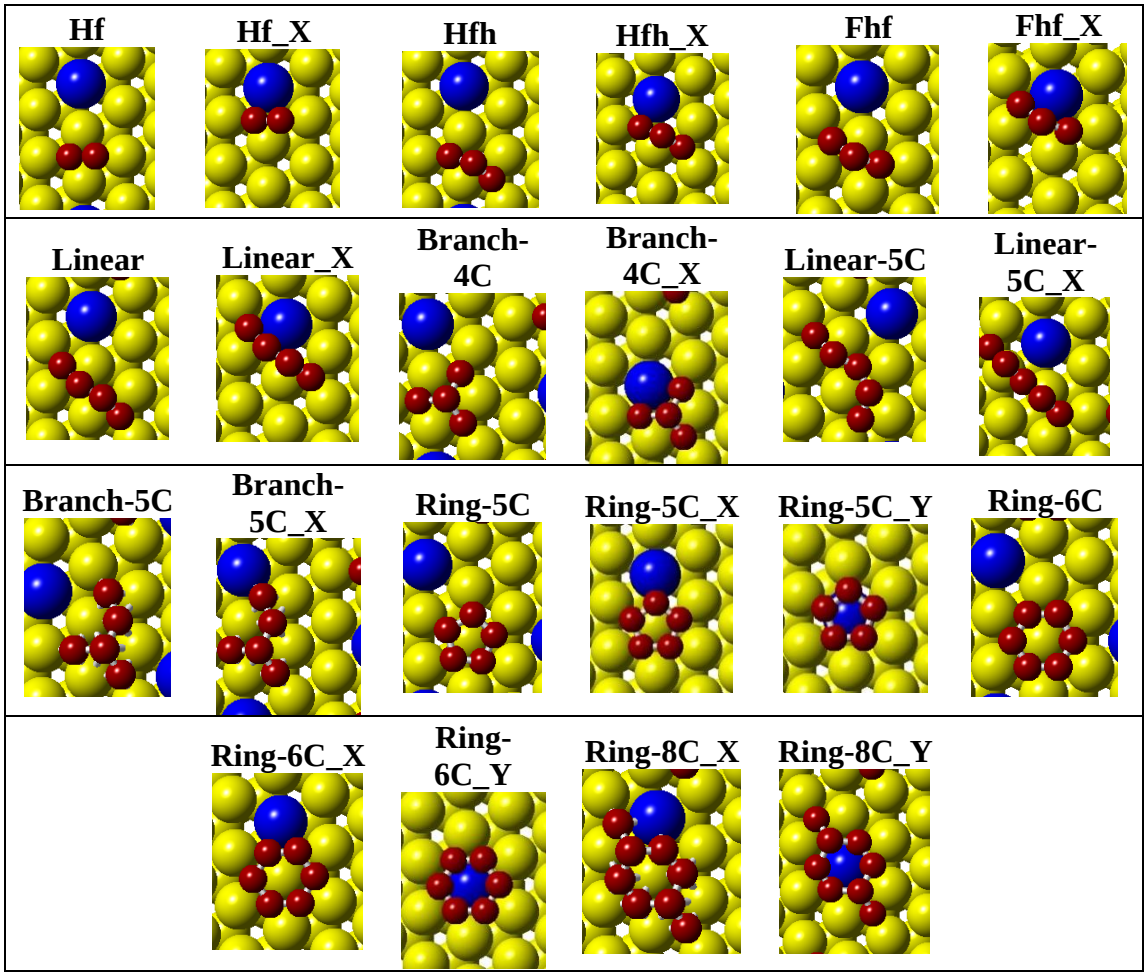

Figure D-1. Finite C clusters adsorbed on various sites on promoted Co surface (Yellow - Co atom, Blue – Pt or Ru atom, Red – C atom).

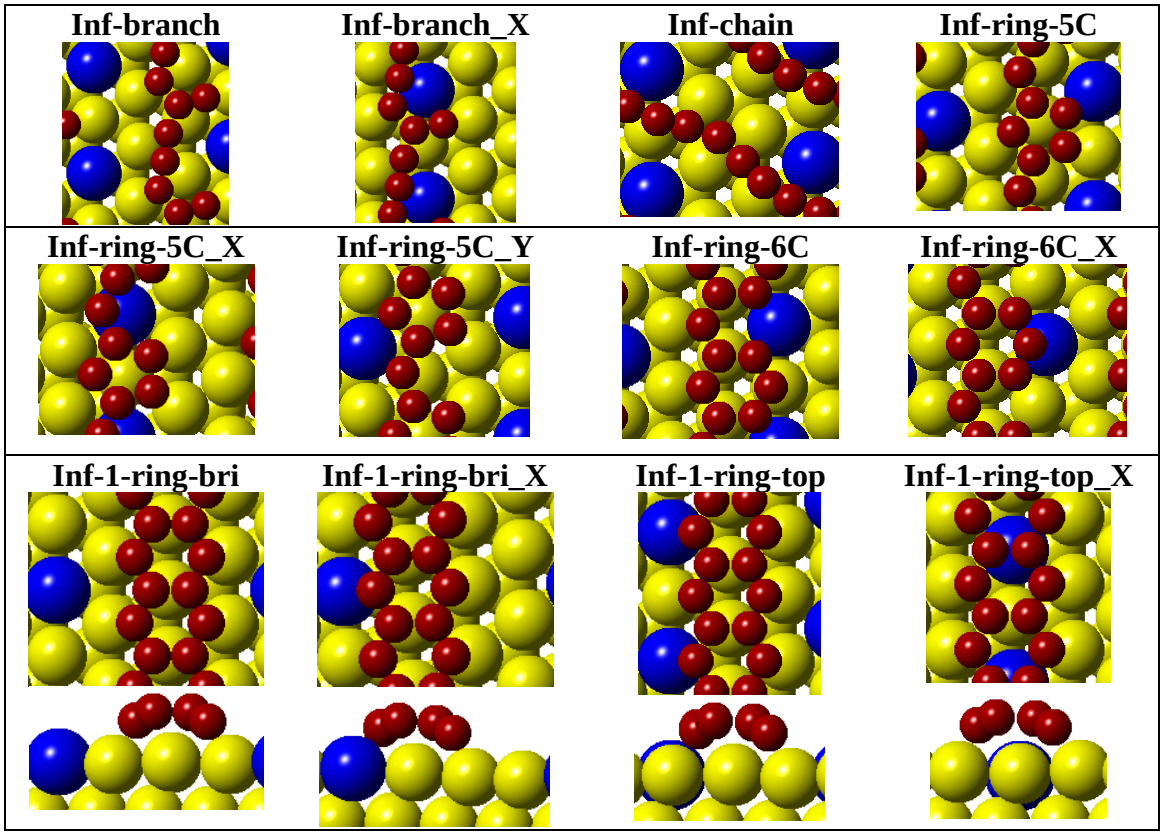

Figure D-2. Infinite C clusters adsorbed on various sites on promoted Co surface with up to 1 six C ring (Yellow - Co atom, Blue – Pt or Ru atom, Red – C atom).

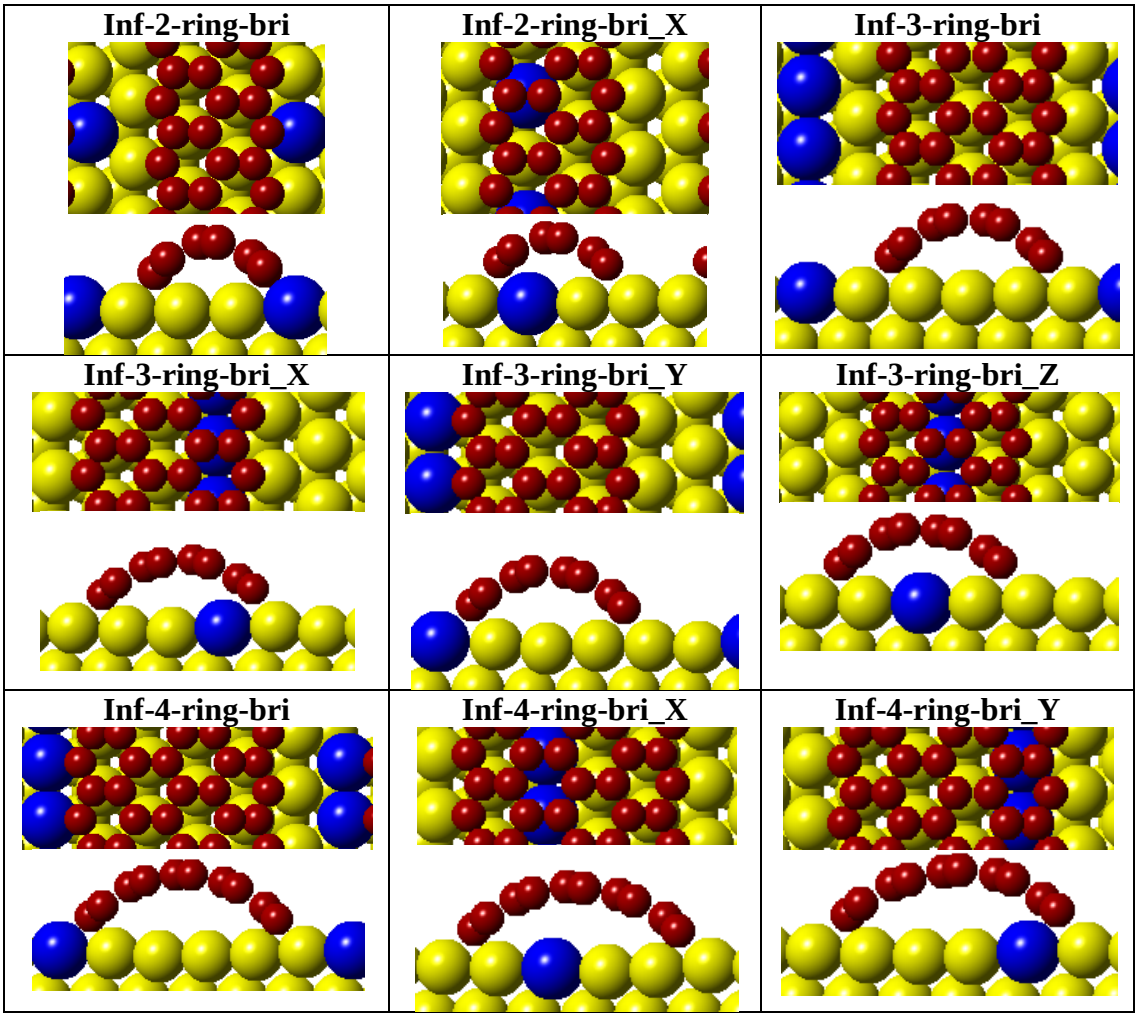

Figure D-3. Infinite C clusters adsorbed on various sites on promoted Co surface with 2, 3 and 4 – six C rings (Yellow - Co atom, Blue – Pt or Ru atom, Red – C atom).